

Bone Quality:

The Mechanical Effects of Microarchitecture and Matrix Properties

Thesis - Judd Day

Department of Orthopaedics, Erasmus MC, Rotterdam, Netherlands

Bone Quality: The Mechanical Effects of Microarchitecture and Matrix Properties

Copyright © by Judd S. Day

ISBN 90-9019339-1

Printed by: Optima Grafische Communicatie

This work was funded by EU Grant QLRT-1999-02024, Danish Health Research Council grant 9601833_lpa, and NIH grants AR39239, 2 PO1 AG05793-12, AR46225 and RR16631. Material used in this thesis was provided by the Gift of Hope Organ and Tissue Donor Network and the BIOMED I project. Computing time was provided by The National Computer Facilities of the Netherlands.

**Bone Quality:
The Mechanical Effects of Microarchitecture
and Matrix Properties**

**Botkwaliteit:
De mechanische effecten van microarchitectuur
en matrixeigenschappen**

Thesis

to obtain the degree of Doctor from the
Erasmus University Rotterdam
by command of the
rector magnificus

prof. dr. S.W.J. Lamberts

and according to the decision of the Doctorate Board.

The public defence shall be held on

Wednesday June 8, 2005 at 15.45 hrs

by

Judd Shamus Day
born at Chatham, Ontario, Canada

Doctoral Committee

Promoters: prof. dr. ir. H. Weinans
prof. dr. J.A.N. Verhaar
prof. dr. D.R. Sumner

Other Members: prof. dr. H.A.P. Pols
prof. dr. ir. A.M. Vossepoel
dr. ir. B. van Rietbergen

Contents

Chapter 1

Introduction

The anatomy of bone	11
Bone adaptation and remodeling	12
Trabecular bone mechanical properties and mechanical testing	14
Bone mass, bone quality and the mechanical properties of trabecular bone	16
Structure of this thesis.....	19

Chapter 2

A decreased subchondral trabecular bone tissue elastic modulus is associated with pre-arthritis cartilage damage

Abstract	23
Introduction.....	25
Methods.....	25
Results.....	28
Discussion	30
Acknowledgements.....	32

Chapter 3

Denatured collagen in osteoarthritic bone

Abstract	33
Introduction.....	35
Methods.....	35
Results.....	37
Discussion	40
Acknowledgements.....	41

Chapter 4

Adaptation of subchondral bone in osteoarthritis

Abstract	43
Introduction – The role of bone in osteoarthritis	45
Mechanical testing of arthritic bone: Scale effects	46
Bone mechanosensors, remodelling and adaptation	48
Simulation of bone adaptation in osteoarthritis	49

More on bone matrix properties in osteoarthritis..... 51
Discussion 52

Chapter 5

Bisphosphonate treatment affects trabecular bone apparent modulus through micro-architecture rather than matrix properties

Abstract..... 55
Introduction..... 57
Methods..... 58
 Experimental design..... 58
 Specimen preparation: MicroCT and mechanical testing 58
 Finite element models 59
 Simulation of increased mineralization 60
 Histomorphometry and microdamage..... 60
 Statistical analysis..... 60
Results..... 61
Discussion 64
Acknowledgements..... 66

Chapter 6

The parallel plate model for trabecular bone exhibits volume fraction dependant bias

Abstract..... 69
Introduction..... 71
Methods..... 72
Results..... 73
Discussion 75
Acknowledgements..... 79
Appendix: Formulas for morphometric parameters..... 80

Chapter 7

Inter-individual and inter-site variation in human trabecular bone morphometry

Abstract..... 81
Introduction..... 83
Materials and Methods..... 84
 Donor populations..... 84
 Micro-CT analysis 85
 Statistical analysis..... 85

Results.....	86
Discussion.....	94
Acknowledgements.....	99

Chapter 8

The effect of donor and skeletal site on morphology-elasticity constitutive models for trabecular bone

Abstract.....	101
Introduction.....	103
Materials and Methods.....	104
Donor populations.....	104
Micro-CT analysis.....	104
Finite element analysis.....	104
Morphology-elasticity relations.....	105
Statistical analysis.....	106
Results.....	107
Morphometric and mechanical data.....	107
General model fits.....	111
Site effects.....	111
Donor effects.....	113
Discussion.....	113
Acknowledgements.....	125

Chapter 9

Trabecular bone micro-architecture and orthotropic mechanical properties

Abstract.....	127
Introduction.....	129
Materials and Methods.....	130
Donor populations.....	130
Micro-CT analysis.....	131
Finite element analysis.....	131
Principal components analysis.....	131
Morphology-elasticity relations.....	131
Results.....	133
Principal components.....	133
Morphology-elasticity relations.....	133
Discussion.....	139
Acknowledgements.....	141

Chapter 10

Final Discussion	145
Morphometric parameters and bone micro-architecture.....	146
Structural anisotropy.....	147
Structural connectivity.....	149
Bone quality, micro-architecture and calcified tissue properties; implications for clinical treatment.....	150
Bone and the progression of osteoarthritis.....	151
Concluding remarks.....	153
Appendix A: Investigation of the effects of osteoarthritis on tissue properties in the GOH data set.....	154
Appendix B: A sub-study of donors with low bone density.....	156
Appendix C: A sub-study of donors with ‘fine’ and ‘coarse’ structures.....	158
Appendix D: Investigation of the relation between matrix properties and architecture in the GOH data set.....	160
Summary	161
Samenvatting	167
References	173
Acknowledgements	185
Publications	189
Curriculum Vitae	193

Chapter 1

Introduction

The anatomy of bone

An average adult human is approximately 20% bone by mass. The 206 bones of the human adult act to support the structure of the body, protect internal organs, facilitate movement, provide for storage of essential minerals, aid in calcium homeostasis, and act as a source for cell formation. As an organ, bone contains both calcified hard tissue and marrow. In the current body of work we shall focus on bone in its structural role as a hard tissue.

At the lowest level of organization, bone is a composite material composed mainly of fibrillar type I collagen stiffened by inorganic calcium phosphate crystals in the form of calcium hydroxyapatite with various substitutions. It is the mineralized phase of the material that provides its stiffness, especially in compression, while the collagen contributes to both toughness and tensile strength. Other constituents of bone include water, living cells and blood vessels and a number of noncollagenous proteins and polysaccharides.

In addition to the calcified matrix, there are various types of living cells of which the *bone lining cells*, *osteoblasts*, *osteocytes* and *osteoclasts* are most important for the maintenance of bone tissue. Bone lining cells cover all surfaces of bones and are believed to regulate the movement of ions between the plasma and bone. Osteoblasts are the cells that produce bone. They accomplish this by first laying down a collagenous matrix called osteoid. It is likely that mineralization of the osteoid matrix is facilitated by noncollagenous proteins (i.e. osteocalcin, bone sialoprotein) that are released by the osteoblasts. As new bone is created, a small number of osteoblasts are trapped within the newly formed matrix. These cells become osteocytes and are connected to each other and to the bone lining cells through a dense network of channels called canaliculi. It is believed that the osteocytes regulate the remodeling of bone, responding to the induction of microdamage or to mechanical signals. Osteoclasts are multinucleated cells from the monocyte/macrophage lineage that are responsible for the destruction (resorption) and replacement of old or damaged bone in a process called remodeling (1).

At the next level of organization we must distinguish between the multiple forms of bone in the human body. *Cortical* or *compact* bone makes up a large portion of skeletal mass providing the outer shell of most bones and the diaphysial ‘shaft’ of long bones. Cortical bone has a high volume fraction of mineralized material (90-95%) and a low surface area. *Cancellous* or *trabecular* bone forms approximately 20% of the mass of the skeleton, existing mainly at the epiphyses (ends) of long bones, within the spine, and within flat bones such as the skull and pelvis. Because of its spongy structure it provides an efficient lightweight structure to support the body’s articulating joints. It has a high surface area and a mineralized volume fraction that can range from below 5% to over 50%. The morphology of trabecular bone has been described by Singh (2) who classified the continuum of different structures into categories.

Singh noted that the structure varied from a delicate meshwork of tiny struts, usually found deep within bones and away from loaded surfaces to preferentially aligned sheets of plates nearer to loaded surfaces. In the current body of work, our focus is on trabecular bone.

Bone adaptation and remodeling

Although bone may appear to resemble a material somewhat like stone it is anything but inert and is a living, active material constantly renewing itself and capable of sensing and reacting to changes in its environment.

Over 100 years ago, Wolff described the relation between bone micro-architecture and loading (3). He noted that the overall orientation of trabecular bone was not random, but aligned to the directions of principal mechanical loading. He further speculated that loading was sensed by the bone, which then adapted accordingly. No doubt inspired by Darwin's theories of evolution, Roux suggested that this process was self-organizing and regulated locally by competition of individual cells for a limited resource, specifically mechanical stimulus (4, 5). These ideas were refined by various researchers such as Thompson, Powwels and Frost finally resulting in the concept of the mechanostat theory; that cells are regulated by local strain (6-8). Recent computer simulations support the idea that a self-organizing system will result in a structure similar to bone. Interestingly, these models tend to conflict with the previously held view that bone as a material is optimized overall to produce maximal stiffness with minimal mass (9-11).

Adaptation of bone is accomplished through the processes described as modeling and remodeling. While modeling is the process whereby the shape of bone is altered to facilitate growth, remodeling is a process where old bone is constantly 'turned over' and replaced by new bone. Remodeling is orchestrated in a tightly controlled process by a group of cells known as a bone multicellular unit (BMU). In the first stage, known as *origination* or *activation*, the bone lining cells change from their normal flat shape to a cuboidal shape and then secrete a substance called RANK ligand. When RANK ligand interacts with its receptor RANK on the pre-osteoclast (a macrophage type cell) it forms an osteoclast and begins to resorb bone. At any particular spot on the bone the resorption process takes about 2 weeks. Following osteoclast resorption, in a process known as *reversal*, osteoblasts are recruited to the site. After 1-2 weeks these cells begin to secrete osteoid in a process known as *formation*. When this osteoid is approximately 6 μm thick it begins to rapidly mineralize. Mineralization is facilitated by factors secreted by the osteoblasts and quickly reaches a density of about 1.4 g/cm^3 within a few days (primary mineralization). Mineralization then progresses slowly to a density of 1.8-2.0 g/cm^3 over the next six months, continuing to increase at an exponentially

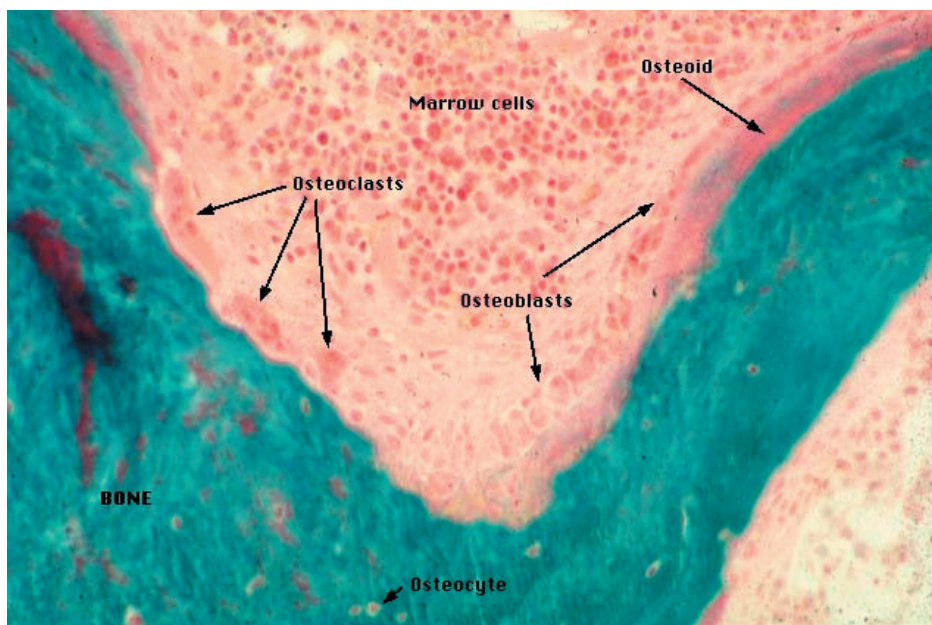


Figure 1.1: Histologic appearance of a bone modeling unit (from the University of Washington Department of Medicine <http://courses.washington.edu/bonephys/ophome.html>).

decreasing rate for several more years (secondary mineralization) (12). Figure 1.1 illustrates the histological appearance of a bone modeling unit.

In order for bone remodeling to preserve bone stock at a constant mass, it must proceed at equilibrium. In other words as much bone must be created during each formation period as was removed during resorption and new remodeling sites must be initiated at a steady state. Disrupting this balance can affect the bone in several ways. For example, humans reach a peak bone mass at 23-35 years, after which bone is slowly lost at a rate of about 0.3 to 0.5% per year due to a formation deficit. This happens because the osteoblasts do not completely refill the holes made by the osteoclasts resulting in a gradual loss of bone with age. Another way that the bone balance can be disrupted is by a sudden increase in the number of active remodeling sites. At equilibrium, the ratio of active sites of formation and resorption are balanced such that bone is created at the same rate that it is resorbed. This is disrupted at the onset of menopause when a sudden change in circulating estrogen levels leads to an increase in the number of active resorption sites. Because resorption occurs as the first phase in the bone remodeling cycle, there is a resulting period where there are temporarily more resorption pits and increased total resorption compared to formation. This results in a short period where there is an accelerated loss of bone stock. After this transient period, a new equilibrium is reached with an elevated remodeling rate.

The dynamics of the remodeling cycle affects not only the amount of bone in the body but also the density of the tissue itself. Because the process of remodeling occurs in discrete locations, regions of bone can contain packets of bone material with different levels of maturity and thus mineralization (Figure 1.2). When remodeling rates are high there tend to more packets of younger, less mineralized bone. When remodeling rates are low the converse is true and the overall density of the bone tissue increases. In the extreme case of osteopetrosis there is a failure of osteoclast function that results in hypermineralized bone that is very brittle.

Trabecular bone mechanical properties and mechanical testing

Trabecular bone, as a porous material, shares many characteristics of a class of materials called cellular solids. The single most important property of a cellular solid is its relative density. In the case of bone, this is a measure of how much mineralized material there is in

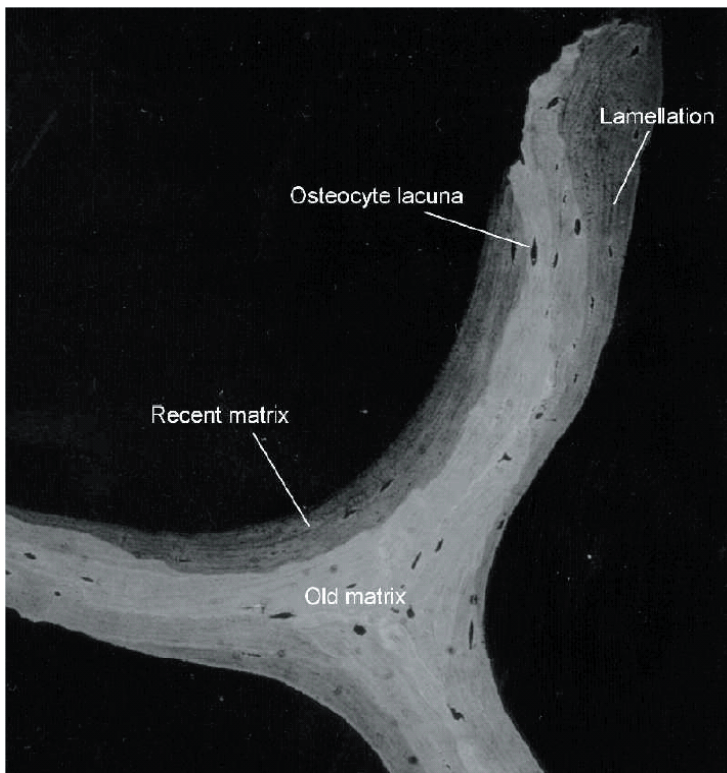


Figure 1.2: Backscattered scanning electron micrograph of trabecular bone illustrating packets of bone of various degrees of maturity (from Banse X, *Acta Orthop Scand Suppl.* 2002 73(303):1-57).

a unit of volume. Although the material properties of the actual bone matrix seem to depend both on the method used for measurement and the scale at which the measurement is made, it seems that the Young's modulus of bone matrix is between 5-20 GPa. The strength of this material is greater in compression than tension but the Young's modulus is invariant with respect to loading direction (tension or compression). As predicted from cellular solid theory, mechanical Young's modulus of trabecular bone can be predicted based on the density with a linear to cubic relation (13). The strength of trabecular bone is highly related to its Young's modulus but its failure strain seems to be unrelated to either the density or strength.

Trabecular bone is a difficult material to test mechanically. Because of its porous nature, clamping is not easily achieved for tensile testing. As a result, most studies have used compression testing of either cylindrical cores or block shaped specimens. This type of testing is not ideal, however, because frictional effects between the platens and the sample can have unpredictable effects upon the test results. Researchers have used lubricated polished platens, extensometers, or embedded samples in end-caps to try to reduce this effect (14-17). Another complicating factor when testing bone is its material anisotropy. As was mentioned in the section on adaptation and remodeling, the structure of trabecular bone tends to be aligned with the direction of loading in the material. In areas where the loading is highly directional the resulting trabecular structure is also highly directional. This means that the apparent Young's modulus can be very different depending on the testing direction (18, 19).

Recent advances in both three dimensional imaging and the ability to solve very large finite element models have led to the development of a powerful new tool for the investigation of the mechanical properties of bone. MicroCT scans of trabecular bone can now be converted directly into large-scale finite element (FE) models. By applying homogenization theory and an ingenious sequence of simulated mechanical tests, a complete three-dimensional description of the mechanical properties of a sample of bone can be derived. As it turns out, bone can be described as an orthotropic material (20-22). Loosely defined, this means that bone normally has three main directions and that these directions are perpendicular to each other. One disadvantage of the large-scale FE method is that it is necessary to assume that the material properties of the bone tissue are homogenous and isotropic and that the material Young's modulus must be specified by the researcher. This means that the properties of the micro-architecture are measured rather than the true properties of the bone specimen. However, this disadvantage can be turned into an advantage by combining FE modeling with mechanical testing. With this combination, the architectural stiffness can be fully characterized and the effective Young's modulus of the calcified tissue can be calculated as the scaling factor between the mechanical tests and finite element results (23-25).

Bone mass, bone quality and the mechanical properties of trabecular bone

The single most important determinant of bone strength, and thus the risk of fracture, is the amount of bone present. In the cortex this is determined by the overall size of the bone and the thickness and porosity of the cortex. In trabecular bone this is determined by the porosity, or the amount of bone present per volume of tissue. Clinically bone density can be measured using relatively cheap and reliable radiographic methods such as DEXA. Because of both the strong relation between fracture risk and bone mass coupled with the ability to reliably measure bone mass, standard definitions of osteopenia and osteoporosis have been proposed to identify individuals who are at risk of fracture. Osteopenia and osteoporosis, as defined by the World Health Organization, are the presence of a bone mineral density (BMD) of respectively 1.0 and 2.5 standard deviations below the population average for healthy young persons of the same gender. While fracture risk is increased by two to three times for each standard deviation below peak young adult mean bone mass, there is a large overlap in bone mass between patients who experience fractures and those who don't (26, 27). This observation has led to the concept that fracture risk is not only a function of bone mass alone but also *bone quality*. Bone quality is, in essence, a term that encompasses all of the properties of the bone that contribute to the mechanical properties with the exception of bone mass. This includes *micro-architecture*, quality and density of the *mineralized phase*, presence of *microdamage*, quality of the *collagen matrix*, and the degree of *turnover*.

Bone quality as a concept incorporates a number of different factors. We will first briefly examine the factors that affect bone at the matrix level before describing those that describe bone organization at the micro-architectural level.

As we have alluded to previously, the mechanical properties of the bone matrix are in part determined by the degree of *mineralization*. In an ideal world, bone would be mechanically stiff, incredibly tough, and have a high ultimate stress. Unfortunately, this is rare in the world of materials science as materials that are stiff are usually also brittle. In bone, the degree of stiffness as opposed to toughness is determined by the degree of mineralization of the matrix. From the highly mineralized and very stiff bones of the inner ear to the tough but compliant antlers of deer, the degree of mineralization can vary greatly between species and with the biological function of a particular bone (1). It can also be modulated by changes in the remodeling rate with disease and pharmaceutical intervention, as will be investigated in **chapter 5** of this thesis.

As we have mentioned previously, one of the functions of bone remodeling is to repair *microdamage* by replacing damaged bone. Microdamage is induced both during extreme exercise

and during daily activity, albeit at different rates. While detrimental towards both the stiffness and ultimate strength of the bone, it is the energy-related resistance to fracture (toughness) that is most sensitive to accumulation of microdamage (28). Although there is ample evidence to indicate that remodeling can be initiated preferentially in damaged areas, it is unlikely that the repair of microcracks is the only reason for bone remodeling (12, 29). Despite the reparative effects of remodeling, microdamage tends to accumulate with age, probably contributing to increased fracture risk (28, 30).

Considering that the formation of collagen rich osteoid is the first step in the creation of bone, it should not be surprising to learn that the quality of the *collagen matrix* can have profound effects upon the quality of the bone. An extreme example of this occurs in osteogenesis imperfecta, a genetic disorder, in which defects in either the amount or structure of type I collagen present as abnormally fragile bone. Collagen quality can also affect the overall bone properties in a more subtle manner. As bone ages the collagen can become denatured and/or accumulate mature cross-links. Collagen denaturation can result in reduced toughness of the bone while alteration of the cross-linking profile affects the stiffness (31, 32). In an intriguing study, it has even been suggested that the micro-architecture of the bone is related to the cross-link profile (33).

Recent clinical trials have suggested that the monitoring of bone *turnover* through biochemical markers of bone resorption may provide a powerful method of predicting fracture risk (34, 35). Elevated remodeling affects the level of mineralization of the matrix by reducing the mean age of the bone tissue. It has also been suggested that the increased number of resorption pits may act as stress risers within the trabecular structure (36).

Bone *micro-architecture* is thought to be another major determinant of bone quality. The study and quantification of form (in this case architecture) is known as morphometry and we will make use of multiple morphometric parameters in the current body of work. We will utilize morphometric measures that can be broadly classified into 3 groups; the measurement of orientation (or grain), scale (metric) and curvature (topology).

As we have previously noted, the grain of trabecular bone has a distinct *orientation* and can be very anisotropic. The degree of anisotropy varies widely between individuals and locations, even within a single skeletal site (37-42). Multiple methods have been proposed to quantify the morphometric anisotropy including surface based, volume based and fourier analyses (43). In the current work, we use the mean intercept length method (44). In three dimensions, the results of this kind of analysis can be transformed and represented as an ellipsoid (Figure 1.3).

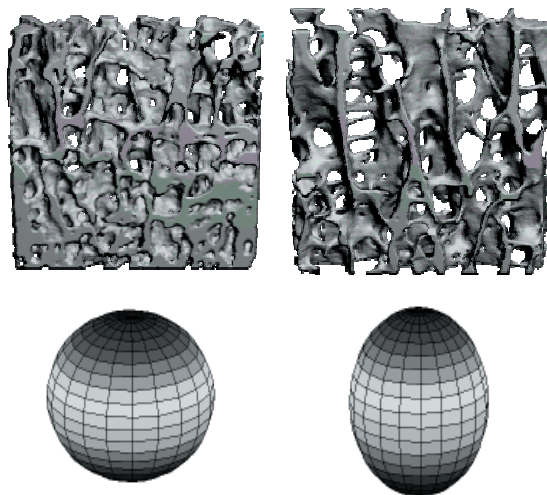


Figure 1.3: *Isotropic specimen (left) and an anisotropic specimen (right). Fabric can be represented as an ellipsoid (bottom) where the relative lengths of the radii represent the strength of anisotropy.*

In addition to the anisotropy, we also quantify the metric parameters of bone surface per unit of bone volume (BS/BV), trabecular thickness (tb.th), trabecular spacing (tb.sp) and trabecular number (tb.n). These parameters are often used in two-dimensional histological studies. Although much has been learned from these studies, we will see in **chapter 6** that two-dimensional methods have limitations and can produce biases. This is especially the case for model-based methods that require *a priori* assumptions regarding the structure of the bone. For this reason we use only three-dimensional methods in the current work (45).

The third group of morphometric measurements we will use in the current body of work are those based on curvature. Structure model index (SMI) is an index that describes the area averaged mean curvature (46, 47). This is used to assign a scale of how ‘rod-like’ or ‘plate-like’ a specimen is. SMI is defined in such a way that a structure composed of ideal plates would have a SMI of 0 and a structure composed of ideal rods would have a SMI of 3 (Figure 1.4). Connectivity is a topological parameter that is closely related to the Gaussian curvature of an object (48). In conceptual terms, the connectivity describes the number of redundant connections in a structure. In other words, if one were to choose carefully, the connectivity would represent the maximum number of trabecula that could be severed in a piece of bone before it actually broke into two pieces. In the current body of work we use a voxel-based method to quantify the connectivity (49).

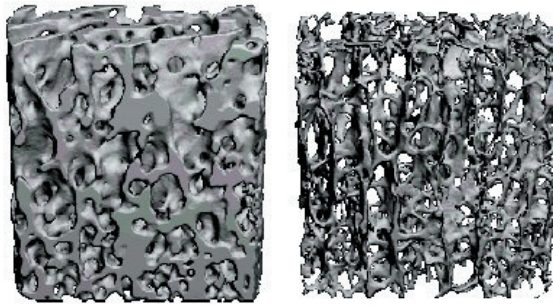


Figure 1.4: An illustration of a ‘plate-like’ structure (left) and a ‘rod-like’ structure (right)

Structure of this thesis

The objective of this body of work was to investigate how bone quality affects the mechanical properties of trabecular bone. In particular, we have examined the interaction between bone mass, matrix properties and trabecular micro-architecture. We have utilized advances in imaging by microCT, three-dimensional quantitative morphometry, finite element modeling and mechanical testing to examine each of these three contributing factors. Our investigations have focused on three main areas: the role of bone in human osteoarthritis, the mechanical implications of reduced bone remodeling after antiresorptive therapy, and how differences in trabecular bone micro-architecture between individuals and skeletal sites contribute to the mechanical properties. By examining a disease state that profoundly affects bone structure, a drug that alters the dynamics of bone remodeling, and variations within a large population we were able to investigate how variations in bone mass, matrix properties and micro-architecture interact to affect the mechanical properties.

Osteoarthritis is a chronic joint disease with pathological changes in all of the tissues of the affected joint including the bone. The extent of the involvement of bone in the disease’s etiology is currently a matter of debate (50, 51). We have performed a series of studies to quantify changes in the mechanical properties of subchondral trabecular bone, investigated possible causes, and explored the possible implications.

In the first study, reported in **chapter 2**, we have investigated changes in the mechanical properties of subchondral trabecular bone that occur in the earliest stages of human osteoarthritis. This was accomplished by studying a population of human donors who displayed mild damage to the cartilage on the medial side of the tibia and intact cartilage on the lateral side. A group of age and sex matched donors served as controls. Using a combination of microCT and mechanical testing we were able to quantify both the apparent modulus and tissue modulus of the subchondral trabecular bone.

In the second study (**chapter 3**) we investigated the hypothesis that degradation of the mechanical properties of bone observed in osteoarthritis was the result of mechanical damage inflicted upon the collagen network. We further investigated the hypothesis that the mechanism for the denaturation of bone collagen was mechanically induced. To investigate the first hypothesis, we used a novel digestion technique to quantify the amount of denatured collagen present in our population of donors with mild cartilage damage and compared the results to those from the donors with intact cartilage. In order to investigate the second hypothesis we performed a series of tests using bovine cortical bone. The amount of denatured collagen was measured after the induction of mechanical damage through fatigue testing, mechanical insult and pulverization.

Sclerotic stiffening of the subchondral bone plate is considered a hallmark of osteoarthritis. This presents an apparent paradox as it has been demonstrated that there is a degeneration of the mechanical properties of the bone tissue in osteoarthritis. In **chapter 4** we investigate whether an increased apparent modulus is consistent with the presence of a decreased tissue modulus under the assumption that bone adaptation is controlled at a local (cellular) level. We have used microCT scans of human trabecular bone and applied a simulation model where it was assumed that bone adaptation was controlled locally by strain. We assumed that the strain sensed at a local level was increased as the tissue modulus was decreased and that adaptation would occur until the median strain was normalized. We could then calculate the apparent modulus of the resulting structure.

Bisphosphonates are emerging as an important drug for the prevention of osteoporotic fractures. This class of drug acts as an osteoclast inhibitor and reduces the rate of bone remodeling. In addition to increasing the bone volume fraction, bisphosphonate treatment also results in an increased mean tissue age and therefore increased mineralization. In **chapter 5** we investigated the relative contributions of micro-architecture and increased mineralization after bisphosphonate treatment to the apparent Young's modulus of trabecular bone. Trabecular bone was harvested from the vertebral bodies of 36 beagles. These animals had been divided into two treatment groups and a control group. Animals in the treated groups received either high dose alendronate or risedronate for a one year period. As in chapter 2, we used a combination of microCT imaging, finite element modeling and mechanical testing to evaluate the relative contributions of trabecular micro-architecture and tissue properties to the overall mechanical properties.

It is well known that both the apparent Young's modulus and ultimate stress of trabecular bone are related to the bone volume fraction and/or apparent density (52, 53). It is also known that there is a strong relation between the bone volume fraction and other quantitative measures of bone morphometry such as the connectivity density, structure model index, trabecular

thickness, spacing and number. Further, it has been demonstrated that bone morphometry contributes to bone quality independent of the bone volume fraction. Clinically, DEXA is the most commonly used tool for the prediction of fracture risk. While this method has proved both effective and valuable for identifying at-risk individuals, there is a great deal of unexplained variation in the population that ends up with a fracture as opposed to those who don't. In our final series of studies we have used microCT scans to quantify various morphometric parameters and have investigated their influence on the bone mechanics. Because of our unique sample of human donor material we were able to make a detailed investigation of the influence of skeletal site and differences between multiple donors on both bone morphometry and mechanics.

Much of the work in this thesis utilizes morphometric parameters to quantify aspects of the micro-architecture of trabecular bone. We feel using unbiased three-dimensional morphometry with microCT data is essential. However, much of the literature is based on studies of two-dimensional histological sections. Many of these studies use the parallel plate model to quantify trabecular thickness, spacing and number (54). This requires the *a priori* assumption that the trabecular micro-architecture consists of plate-like structures. In **chapter 6** we, investigate the ramifications of using the plate model. We used microCT scans of bone specimens from a variety of species to compare results derived using the plate model to those that were measured using the direct thickness method.

While bone mass is a major predictor of the mechanical properties of trabecular bone, it is believed that trabecular micro-architecture is also important. In **chapter 7** we investigated the variation of trabecular micro-architecture between different people and different skeletal sites. Using a total of 813 biopsies from 105 donors we quantify the relation between between bone density and other morphometric parameters. We then examined whether this relation varied between donors and sites.

The mechanical properties of trabecular bone are highly dependant upon apparent density and anisotropy. Multiple predictive models have been described that can predict the orthotropic stiffness and/or compliance matrix for trabecular bone based on density in combination with a quantitative descriptor of anisotropy (55). In **chapter 8** we examined the performance of these models when applied to a subset of the data used in chapter 7. We specifically tested the hypothesis that these models were general with respect to individuals and skeletal site by comparing donor and site-specific fits to generalized fits. We also assessed the stability of the derived relations using a cross-validation procedure.

Although constitutive equations based on apparent density and anisotropy provide excellent predictions of the mechanical properties of trabecular bone, there is still room for improve-

ment. Relative errors of 20-60% are not uncommon depending on which model is used (55). Previous studies have demonstrated using multiple regression analysis that the prediction of uniaxial mechanical properties can be improved by adding other morphometric parameters. In **chapter 9** we extended the fabric-based model proposed by Cowin (56) using multiple parameters.

Finally, in **chapter 10** we discussed this body of work in a wider context. The methods, results and limitations of the studies are discussed and the clinical ramifications are considered. We also present results that relate to a number of subgroups of the data that were not included in the other chapters. Some of these subgroups were too small to warrant a full statistical analysis but did, however, assist us in the interpretations of the study results. We feel that their inclusion in the discussion of this thesis is justified in this context and helps to complete the full analysis of our data.

In this body of work we have investigated the relation between bone quality (architecture and matrix properties) and mechanical properties in three distinct contexts. In conjunction with the destruction of cartilage, sclerosis and pathological remodeling of the underlying bone is a hallmark of osteoarthritis. We investigate the alterations of both the matrix and apparent bone properties at the earliest stages of osteoarthritis as well as the bone's adaptive response. Bisphosphonates, a class of drugs commonly used for osteoporosis therapy, are a potent osteoclast inhibitor resulting in reduced bone remodeling, increased bone mass and increased matrix mineralization. Using an animal model, we examined the effect of a drastic reduction in bone remodeling on bone properties including mechanics. Finally, we examined the variation of bone architecture between individuals and skeletal sites in a human population. We then examined the relation between individual donors, trabecular architecture and the resulting mechanical properties. When viewed as a body of work, we have provided information that increases our understanding of how bone mass and bone quality affect the mechanical properties of trabecular bone.

Chapter 2

A decreased subchondral trabecular bone tissue elastic modulus is associated with pre-arthritic cartilage damage

JS Day, M Ding, JC van der Linden, I Hvid, DR Sumner, H Weinans

Abstract

In osteoarthritis, one postulate is that changes in the mechanical properties of the subchondral bone layer result in cartilage damage. The goal of this study was to examine changes in subchondral trabecular bone properties at the calcified tissue level in the early stages of cartilage damage. Finite element models were constructed from microCT scans of trabecular bone from the proximal tibia of donors with mild cartilage damage and from normal donors. In the donors with cartilage damage, macroscopic damage was present only in the medial compartment. The effective tissue elastic moduli were determined using a combination of finite element models and mechanical testing. The bone tissue modulus was reduced by 60% in the medial condyle of the cases with cartilage damage compared to the control specimens. Neither the presence of cartilage damage nor the anatomic site (medial vs. lateral) affected the elastic modulus at the apparent level. The volume fraction of trabecular bone was higher in the medial compartment compared to the lateral compartment of tibiae with cartilage damage (but not the controls), suggesting that mechanical properties were preserved in part at the apparent level by an increase in the bone volume fraction. It seems likely that the normal equilibrium between cartilage properties, bone tissue properties and bone volume fraction is disrupted early in the development of osteoarthritis.

Day JS, Ding M, van der Linden JC, Hvid I, Sumner DR, Weinans H. A decreased subchondral trabecular bone tissue elastic modulus is associated with pre-arthritic cartilage damage. *J Orthop Res* 19:914-8 (2001).

Introduction

Osteoarthritis has been described as an “organ failure” where pathological changes in the cartilage and bone interact, resulting in the failure of the joint. Progression of the disease is indicated by focal destruction of the cartilage and abnormal growth of the subchondral bone, producing both a thickened subchondral bone plate and osteophytes. There is evidence that suggests that the initiation and progression of osteoarthritis involves a disruption of the normal mechanical equilibrium between bone and cartilage. However, it is uncertain whether osteoarthritis is initiated in the cartilage layer, bone layer or both layers simultaneously (57-59).

Radin and Rose (51) proposed that cartilage lesions are created as a result of steep stiffness gradients within the underlying subchondral bone. The resulting stress gradients are propagated through the cartilage, and progression of cartilage lesions requires the presence of stiffened subchondral bone. Changes in bone density and mechanical properties late in the development of osteoarthritis suggest that stiffer subchondral bone may be present (58), and there are indications that bone density may be elevated and bone mechanical properties may be altered at the apparent level early in disease progression (60).

The mechanical properties of bone at the apparent level are affected by the amount of bone present (volume fraction), the architecture of this bone and the mechanical properties of this bone at the level of the calcified tissue matrix. In this study we used finite element models of the bone micro-architecture to separate the effects of bone volume and architecture from the tissue properties. By comparing the finite element models with mechanical tests we were able to estimate the calcified tissue matrix elastic modulus (hereafter referred to as the tissue modulus). We then used these results to test the hypothesis that bone mechanical properties at the level of the calcified tissue matrix are altered in the presence of (59) mild cartilage damage.

Methods

All of the bone material for this study was taken post mortem from the proximal tibiae of ten donors with mild cartilage damage and ten control donors. All donors were Caucasian and had died suddenly from trauma or acute disease. Donors in the control group were free from metabolic diseases, and the cartilage surfaces of the specimens were intact. Cartilage damage was defined as macroscopically degenerated fibrillated cartilage and was confirmed histologically. The cartilage-damaged tibiae showed visual degeneration with slight fissures in the superficial zone of the medial condyle cartilage whereas the surface of the lateral

	Age	Sex	Medial Mankin Score	Lateral Mankin Score
Damaged 1	71	M	5.0	1.5
Damaged 2	81	M	5.0	1.5
Damaged 3	77	F	4.0	1.5
Damaged 4	68	M	3.0	3.0
Damaged 5	72	M	4.0	1.5
Damaged 6	63	M	5.0	1.5
Damaged 7	78	F	6.0	1.5
Damaged 8	81	M	7.0	2.0
Damaged 9	63	M	5.0	1.5
Damaged10	78	F	5.0	1.5
<i>Average</i>	73		4.9	1.7
<i>St Dev</i>	7		1.1	0.5
Control 1	58	M	0.5	0.0
Control 2	66	M	1.0	1.0
Control 3	61	M	0.0	0.0
Control 4	62	M	1.5	1.0
Control 5	72	M	0.0	0.0
Control 6	80	F	0.0	0.0
Control 7	80	F	2.0	1.0
Control 8	85	F	1.0	1.0
Control 9	80	M	1.0	0.0
Control10	83	M	1.0	1.0
<i>Average</i>	73		0.8	0.5
<i>St Dev</i>	10		0.7	0.5

Table 2.1: Mankin scores for donor proximal tibial joint surfaces

condyle was intact. Cell clusters in the superficial zone and reduction of safranin O staining could be seen histologically in the damaged cartilage. Mankin scores (61) for normals were 2.0 or less and for tibiae with mild cartilage damage were between 3.0 and 7.0 (Table 2.1). No specimen with a Mankin score of greater than 8.0 (values depicting mild to moderate damage) was included.

Samples were chosen from a larger study of 6 sites on the lateral side and 7 sites on the medial side (62). One sample was chosen at random from the medial side and one from the lateral side. A post hoc analysis of the control specimens confirmed that calcified tissue modulus was not related to the sampling site within each compartment. One tibia was removed from

each donor and cylindrical trabecular bone specimens were selected from each of the medial and lateral condyles. The samples were cored from the proximal tibiae using a 7.5 mm trephine oriented perpendicular to the cartilage surface. Each sample was cut 1 mm below the subchondral bone plate and the distal edge was trimmed to create a cylindrical sample with both length and diameter of 7.5mm. All samples were stored in physiological saline in sealed plastic tubes at -20°C until testing.

A microCT scanner was used to scan the samples ($\mu\text{CT 20}$, Scanco Medical AgG., Zürich, Switzerland). The resulting edge length of the cubic voxels was $22\ \mu\text{m}$. The volume of each sample was measured using Archimedes' principle(63). Then the grey value which would produce a segmented image of the same volume was determined for each sample. Images were segmented using the average of the ten grey levels for each group.

Compressive mechanical tests were performed using a materials testing machine (MTS Systems Corporation, Minneapolis, Minnesota, USA) using a 1kN load cell and a static strain gauge extensometer (Model 632.11F-20, MTS) attached to the testing column. The platens were polished and lubricated with a low viscosity mineral oil to reduce the effect of friction (17). A preload of 3N was applied to the samples which were then preconditioned by applying 10 cycles of loading between the preload strain and $6000\ \mu\text{strain}$. Samples were then tested to failure with a strain rate of $2000\ \mu\text{strain/s}$. The apparent modulus of the sample was calculated as the tangent of the linear portion of the stress strain curve at $6000\ \mu\text{strain}$.

The tissue modulus was calculated using a combination of finite element modeling and mechanical testing (20). This method was used because it enables the tissue modulus to be evaluated separately from the trabecular architecture. All voxel μCT data were coarsened then converted to cubic elements with an edge length of $66\ \mu\text{m}$. Coarsening was performed using a bone volume preserving algorithm (64). After coarsening, the data were converted to a finite element mesh of 8 node cubic elements. All elements were assigned an arbitrary tissue Elastic modulus of 1 GPa and a Poisson ratio of 0.3.

Boundary values were assigned to simulate an unconstrained compressive test with no friction at the platens. Because the finite element analysis was linear elastic, the apparent modulus obtained from the finite element model could be simply scaled to match the apparent modulus from the mechanical tests. The resulting scaling factor can be considered the effective bone tissue modulus of the sample (20).

The statistical analyses included two-way analyses of variance for repeated measures for the experimental apparent modulus, bone volume fraction and tissue modulus. The group (i.e., normal vs. mild damage) was used as the between-subjects factor and compartment (medial

vs. lateral) as the within-subjects factor. When significant main effects or an interaction between the main effects was found, specific comparisons were made with student's t-tests and paired t-tests. In all cases, the exact p values are given and we considered $p < 0.05$ to represent significant effects. Statistical analysis was performed using SPSS version 8.0 (SPSS Inc., Chicago, IL, USA).

Inclusion of 10 control donors and 10 donors with mild cartilage damage insured 80% power for detecting an effect size of 1.325 (the ratio of the difference between the population means to the population standard deviation), based on a two-sided independent-sample t test with a 0.05 significance level. The two-sided paired t tests that were done separately for the control group and the group with mild cartilage damage had 80% power for detecting an effect size of 0.996 (the ratio of the mean differences to the standard deviation of the mean differences), based on a 0.05 significance level. Power calculations were done with nQuery Advisor software, Version 2 (Boston, MA).

Results

The tissue modulus was higher in the normal samples than in the samples from the cases with cartilage damage ($p = 0.004$ for the group effect in the analysis of variance). Neither compartment ($p = 0.684$) nor the compartment by group interaction ($p = 0.288$) were significant. Specifically with regard to the group effect, on the medial side the samples with cartilage damage had a nearly 60% reduction in tissue level modulus ($p = 0.013$, for the student's t-test with the variances not assumed to be equal). Laterally, although the mean for the normal samples was higher than for the cartilage damaged samples, the difference was not significant ($p = 0.169$; Figure 2.1 Top). While there was not an overall effect of compartment, the tissue modulus of the medial compartment was reduced compared to the lateral compartment in the damaged group ($p=0.009$).

The analysis of variance for the apparent modulus indicated that neither compartment ($p = 0.287$), group ($p = 0.242$) nor the interaction between compartment and group ($p = 0.152$) were significant (Figure 2.1 Middle).

In general, the volume fraction was greater medially than laterally ($p = 0.009$ for the effect of compartment in the analysis of variance), but group was not significant ($p = 0.140$), nor was the interaction between compartment and group significant ($p = 0.633$). Specifically, the medial-lateral difference was significant in the sample with cartilage damage ($p = 0.023$, paired t-test), but did not reach significance in the normal sample ($p = 0.155$; see Figure 2.1 Bottom).

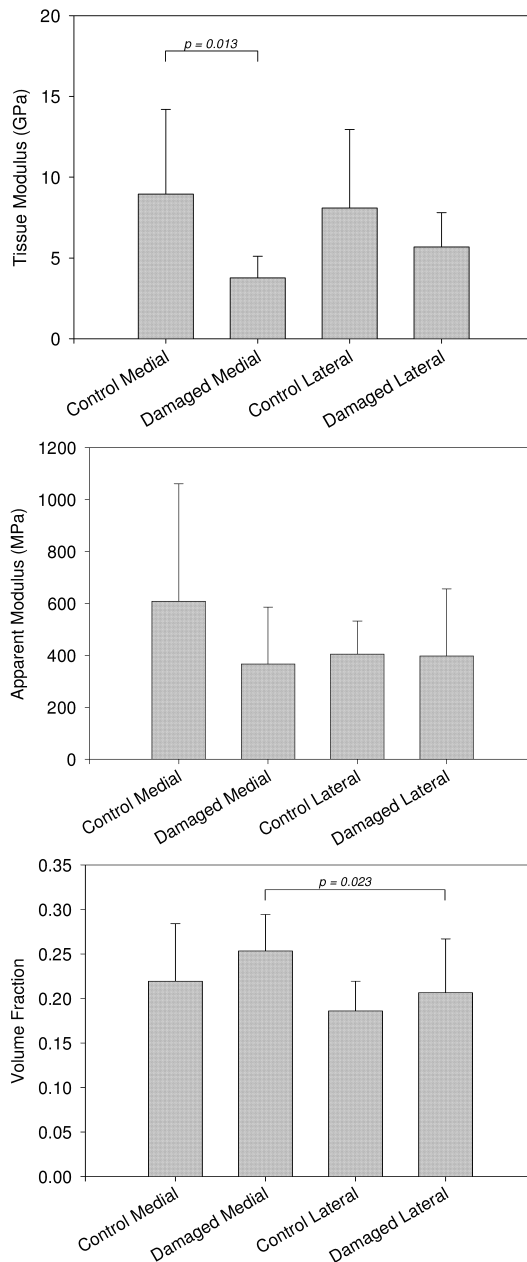


Figure 2.1: Results by group (control vs. damaged) and compartment (medial vs. lateral). The *p* values indicated are the result of post hoc *t*-tests. Only results that were significant in both the ANOVA and post hoc *t*-tests are indicated. Results displayed as mean \pm SD: Tissue modulus (Top), Apparent modulus (Middle), Average volume fraction (Bottom).

Discussion

Using a combination of finite element modeling, μ CT scanning and mechanical testing, we were able to determine the effective tissue elastic modulus for trabecular bone samples from the proximal tibia. This modulus can be considered as the effective tissue modulus for a homogeneous isotropic material. The apparent modulus and volume fraction were not significantly different between the damaged samples and controls. The variance in these measures was relatively large, and it is possible that there was an effect that was not detectable in this study. However, the goal of the present study was to examine changes in the properties of the material at the tissue matrix level. By using microFE modeling we were able to adjust the results of the mechanical testing to correct for differences in both volume fraction and tissue architecture. We found that there was a significant decrease in the tissue modulus in the group which exhibited mild cartilage damage.

The tissue modulus in this study varied from 3-20 GPa in the normal donors and from 2-9 GPa in the donors with cartilage damage. These values were within the range of those found by nanoindentation (65), acoustic microscopy (66) and micromechanical testing (67). Moduli which varied from 2 to 10 GPa were found in studies of human vertebrae using the finite element method (24, 68). The difference between our results and those of previous studies which used the finite element method may be due to anatomic location, disease state, or differences in mechanical testing protocol.

The voxels from the μ CT data set were coarsened to elements with an edge length of 66 μ m. The algorithm used ensured that the bone volume fraction was the same before and after coarsening, as previous research indicates that it is preferable to conserve volume (64). The voxel meshes were slightly coarser than recommended (16, 69), but the element size was constrained by limitations in computing time. Coarsening to 44 μ m and 66 μ m resulted in computing times of approximately 30,000 s and 4,000 s CPU time respectively on a Cray C90 supercomputer. Boundary conditions at the platens were simulated as frictionless to approximate the polished lubricated platens. This remains only an approximation which leads to an error of approximately 15% to 30% (15, 70). We assumed that the errors incurred by the modeling assumptions had a similar magnitude in all groups.

Assuming isotropic and homogeneous material properties for the elements, we calculated the effective stiffness of the trabecular tissue. In late stage osteoarthritis bone tissue is sclerotic, hypomineralized, and contains an increased fraction of water (71-74). The presence of large amounts of osteoid may implicate irregularities in bone turnover (75). Additionally, a possible relation between microcrack density and failure stress has been noted in osteoarthritic bone (58, 76). In the present study, it was impossible to determine whether the differences

observed were due to a disruption of tissue continuity (i.e., increased microcrack density or inclusion of defects) or to degeneration of the actual matrix (i.e., reduced mineralization or abnormal collagen properties).

The apparent properties of bone are determined by both bone architecture and tissue modulus. In normal bone, a large percentage of the variance in the apparent properties can be explained by the apparent density alone (77). In the present data set we found that there was a non-significant increase in the volume fraction and a non-significant decrease of the apparent stiffness of the bone in the damaged medial condyle. In a larger dataset where we measured volume fraction and apparent stiffness in 3 locations in each condyle these differences were significant. The fact that a general increase in volume fraction was not accompanied by an increase in the apparent modulus indicates that the normal relation between apparent stiffness and volume fraction is disrupted. This is not surprising considering the 60% reduction of the tissue modulus in the medial compartment of the group with cartilage damage. A change in the relation between volume fraction and apparent modulus has been noted previously in late stage osteoarthritis (72, 78).

The finding of reduced tissue stiffness associated with mild cartilage damage necessitates a change to the previous models of osteoarthritis progression. Radin proposed that cartilage degeneration occurred due to localized stiffening of the subchondral layer (51). In light of the present data, it seems that abnormal stress gradients in the subchondral layer may be the result of local degeneration of bone tissue properties. This may lead to local softening as the bone degenerates resulting in the disruption of the normal equilibrium between bone and cartilage stiffness. As well, the normal relation between volume fraction and apparent stiffness is disrupted. The disruption of the normally coupled relation between cartilage stiffness and bone apparent stiffness has been recently presented within the same donor group (62). Perhaps, as the bone remodels in response to its new mechanical environment, the subchondral bone plate thickens and the volume fraction in the underlying trabecular bone increases. Eventually, the remodeling process may even 'overshoot' the original equilibrium, resulting in stiffened subchondral bone at the apparent level. This hypothesis is supported by a previous study of late stage osteoarthritis where osteoarthritic bone from the femoral head was stiffer than bone from control donors at the apparent level but softer at the tissue level (62, 72, 79).

In conclusion, we have demonstrated that effective bone tissue stiffness is decreased and bone quantity is increased in the presence of mild cartilage damage. The reduction of tissue stiffness caused greater tissue deformation than was compensated for by increased bone volume. It is likely that this process leads to a loss of the normal mechanical equilibrium between cartilage and bone mechanical properties.

Acknowledgements

Support for this work was received from NIH grants AR46225 and AR39239 and the Danish Health Research Council grant 9601833_lpa. Computing time was provided by The Netherlands Computing Facility. The research of Harrie Weinans has been made possible by the Netherlands Royal Academy of Arts and Sciences. Jaqueline van der Linden was supported by the Dutch Foundation for Research (NOW/MW).

Chapter 3

Denatured collagen in osteoarthritic bone

Day JS, Manintveld O, Bank RA, Ding M, Verhaar JAN, Sumner DR, Hvid I, van Osch GJVM, Weinans H

Abstract

Osteoarthritic bone tissue is mechanically inferior to normal bone. In the current study we investigate a possible role of collagen denaturation. Denatured collagen was measured in early and late stage osteoarthritic donors and compared to controls. While the proportion of denatured collagen was increased by approximately 20% in early stage osteoarthritics, there were no obvious effects in late stage donors. We did, however, find that the proportion of denatured collagen was higher in deep trabecular bone than in the subchondral plate. We further proceeded to investigate mechanical insult as a possible mechanism for collagen denaturation. Using bovine cortical bone we used multiple methods to produce damage including, fatigue testing, crushing and pulverizing samples. Pulverizing samples to a fine powder only doubled the denatured collagen content. Crushing and fatiguing the samples had no measurable effect. We therefore conclude that while an elevated level of denatured collagen has been observed in early osteoarthritis, this does not seem to be caused by mechanical trauma (i.e. microdamage).

Introduction

The mechanical properties of connective tissue are influenced by quality of the collagen matrix. In aging, accumulation of advanced glycation end products results in wrinkled skin, stiffened joints and stiffening of the vascular system. In osteoarthritis, affected cartilage is mechanically inferior and contains 4 times as much denatured collagen as intact cartilage (80). It is not known if the breakdown of articular collagen is due to mechanical damage or enzymatic degradation.

Alterations of the collagen matrix can also affect the properties of bone. In osteoporosis there is increased lysine hydroxylation as well as increased collagen synthesis and degradation. Over-hydroxylation of the collagen leads to finer fibrils, modified cross-links and reduced calcification resulting in increased bone fragility (81). In normal aging, there is a decrease in bone collagen content accompanied by an increased concentration of denatured collagen (personal communication with Dr. R.A. Bank). The toughness, strength and stiffness of bone are all degraded as the collagen is denatured(31, 82, 83).

It has been demonstrated that osteoarthritic bone matrix is mechanically inferior to normal bone (23, 73). Turnover is increased sevenfold in the subchondral bone and there is a 25% decrease in mineralization. Phenotypic expression of the osteoblasts is modified to produce increasing proportions of type I homotrimer in addition to the normal type I heterotrimer. This homotrimer is associated with inferior mechanical quality (84).

It has previously been suggested that the onset of osteoarthritis is associated with mechanical micro-trauma in the subchondral bone (50, 51, 85, 86). In the current study, we investigate the hypothesis that there is an elevated level of mechanical damage in bone at the earliest stages of osteoarthritis. This damage should begin at a molecular level and thus be heralded by denaturation (unwinding) of the collagen matrix. In order to test our hypothesis, we have examined the content of denatured collagen in subchondral trabecular bone from donors with early stage osteoarthritis. These assays have been contrasted with those from donors with advanced osteoarthritis. Finally, to understand possible mechanical mechanisms, we have performed experiments to test the ability of mechanical damage to induce collagen denaturation in mineralized bone samples.

Methods

as This study consisted of three experiments, one involving material from donors with no or mild cartilage damage, one involving material from patients undergoing joint replacement

for end stage osteoarthritis, and one assessing the ability to induce collagen denaturation mechanically in bovine cortical bone. All of the experiments utilized a previously described assay for denatured collagen (80). Briefly, samples were decalcified in EDTA before selectively digesting denatured collagen using alpha-chymotrypsin. The supernatant (containing the digested denatured collagen) was separated from the remaining insoluble matrix. Next, the two pools were hydrolyzed in 6M HCl and the amount of hydroxyproline in each sample was measured using either reverse phase high performance liquid chromatography (Experiment 1) or a colorimetric assay (Experiments 2 & 3). Thus, the ratio of hydroxyproline in the two pools was used to quantify the amount of damaged collagen with respect to intact collagen in each sample.

Experiment 1: Human trabecular bone was harvested post mortem from the subchondral region of the proximal tibiae. All donors had died suddenly from trauma or acute disease. Donors in the control group were free from metabolic diseases and the cartilage surfaces of the specimens were intact. Cartilage damage was defined as macroscopically degenerated fibrillated cartilage and was confirmed histologically. The cartilage-damaged tibiae showed visual degeneration with slight fissures in the superficial zone of the medial condyle cartilage whereas the surface of the lateral condyle was intact. Cell clusters in the superficial zone and reduction of safranin O staining could be seen in the damaged cartilage. Mankin scores for control donors were 2.0 or less and for tibiae with mild cartilage damage (i.e. early OA) were between 3.0 and 7.0. No specimen with a Mankin score of greater than 8.0 was included. Nine trabecular bone specimens were obtained from either the medial and/or lateral compartment of 11 early-stage OA donors (average age: 75, range 63 – 87) and 13 normal controls (average age: 70, range 61-85). One 7.5 mm diameter cylindrical sample was drilled out from each condyle, orientated such that the axis of the cylinder was aligned with longitudinal axis of the tibia. Samples of approximately 7.5mm length were cut 1mm distal to the subchondral bone plate. These samples were then cut longitudinally into 4 quarters, one of which was used to quantify collagen denaturation. The groups were compared using two-way ANOVA before using *t*-tests for post-hoc analysis.

Experiment 2: Bone cores were obtained from the patients undergoing joint arthroplasty. Samples were cored using a water-cooled diamond trephine and split longitudinally into 4 quarters one of which was used to quantify denatured collagen. This sample was split into the subchondral bone plate (SP), the trabecular bone immediately underneath the subchondral plate (TB1) and one deep piece of trabecular bone from approximately 1 cm under the subchondral plate (TB4). Assays for denatured collagen were performed in triplo for each sample. The donors in this study could be divided into two sub-experiments:

- *Experiment 2A*

Femoral heads with internal control

Two core samples were harvested from the femoral head of patients undergoing total hip arthroplasty for osteoarthritis ($n_{\text{subjects}} = 2$). One core sample was taken from a region with intact cartilage (C+) and one was taken from a region with extreme cartilage damage as assessed visually (C-).

- *Experiment 2B*

Tibial plateau with external control

Two core samples were harvested from the proximal tibia of four patients undergoing total knee arthroplasty osteoarthritis, one from the medial and one on the lateral condyle. These were compared to cores from four donor tibias with visually intact cartilage.

Experiment 2 was performed as a pilot test and for this reason the analysis will be descriptive only.

Experiment 3: Fresh bovine tibiae were obtained from the slaughterhouse. Plank shaped samples of diaphysal compact bone (60 x 5 x 2 mm) were cut using a water-cooled diamond saw. Specimens were then subjected to one of the following treatments:

- *Experiment 3A*

i) untreated controls ($n = 10$)

ii) fatigue loading of a 50 mm span in 3-point bending for 170000 cycles with a maximum stress of 80 MPa ($n = 10$) and cross head velocity of 1.0 mm/s.

- *Experiment 3B*

i) untreated controls ($n = 10$)

ii) crushing by hand with a mortar and pestle to produce particles of approximately 2-3 mm ($n = 10$)

iii) pulverization to a fine powder in liquid nitrogen using a Mikro-Dismembrator ($n = 5$)

iv) submersion liquid nitrogen as a control for part of the pulverization procedure ($n = 5$)

In experiment 3, a Kruskal Wallis test was used to compare the groups overall. For *post hoc* testing, each treated group was compared to the relevant control group using a Mann Whitney test.

Results

Experiment 1: In human subchondral trabecular bone there was a difference between early arthritics and controls (ANOVA $p=0.04$). There was a 22% increase in denatured collagen in the medial condyle ($p=0.02$) and a similar non-significant increase of 18% on the lateral side ($p=0.11$). There were no significant differences between the medial and lateral condyles of either group (Figure 3.1).

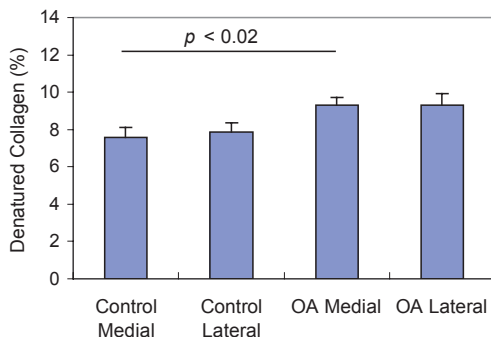


Figure 3.1: Denatured collagen in the proximal tibia of early osteoarthritic donors (Mean + SEM; n = 9 donors per group).

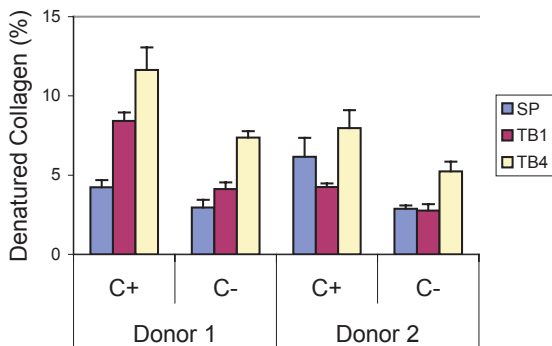


Figure 3.2: Denatured collagen from the femoral head of advanced arthritics (Mean + SEM; n = 3 assays per group). SP indicates the subchondral plate, TB1 indicates trabecular bone just distal to the plate and TB4 indicates deep trabecular bone. C+ and C- respectively denote areas with intact and damaged cartilage.

Experiment 2A: In the samples from the femoral head of two donors there seemed to be a slight elevation of the levels of denatured collagen in the areas with intact cartilage as opposed to the damaged areas. In all four locations the deep trabecular bone contained more denatured collagen than the subchondral plate (Figure 3.2).

Experiment 2B: In the samples from the proximal tibia of osteoarthritic and control donors there were no obvious differences between osteoarthritics or controls on either the medial or lateral side. One arthritic donor had extremely high amounts of denatured collagen on both the medial and lateral sides (3x the other donors). When this donor was removed from the analysis it was apparent that the deep trabecular bone once again contained more denatured collagen than the subchondral plate (Figure 3.3).

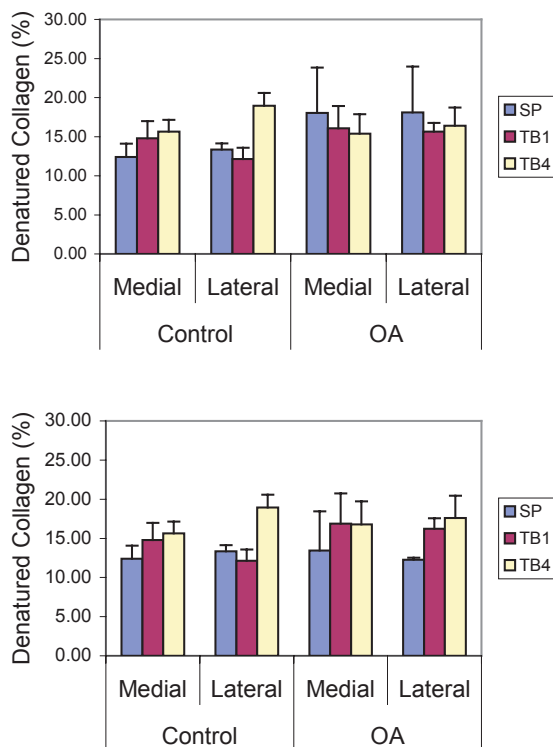


Figure 3.3: Denatured collagen in the medial and lateral tibia of advanced arthritis and controls (Mean + SEM; $n = 4$ donors per group). One of the subjects in the OA group had very high amounts of denatured collagen in the subchondral plate. Because of the small number of donors in this sub-study we have displayed the results with this donor included (Top) and with this donor removed from the results (Bottom).

Experiment 3A: Many fatigue specimens broke before 170000 cycles. One sample in the control group was destroyed during the assay procedure. After fatigue loading, there was no significant change in the amount of denatured collagen

Experiment 3B: One sample in the crushed group was destroyed during the assay procedure. ANOVA testing revealed that there were differences between groups (Kruskal Wallis $p = 0.006$). Crushing bovine cortical bone in a mortar and pestle did not significantly increase the amount of denatured collagen. However, pulverization doubled the denatured collagen content (Mann Whitney $p = 0.004$). Submersing the sample in liquid nitrogen did not affect the denatured collagen content (Figure 3.4).

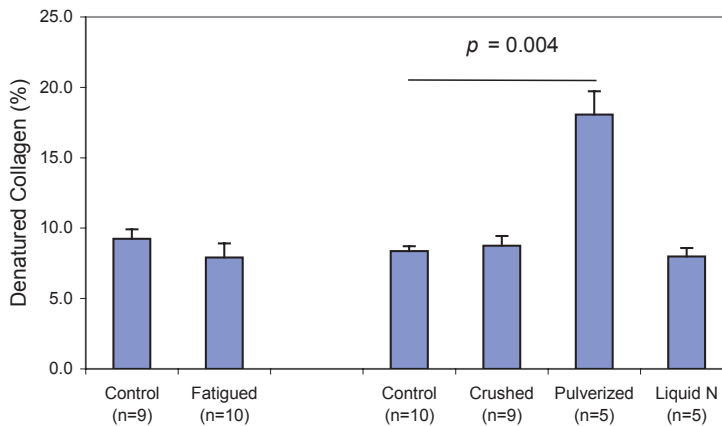


Figure 3.4: Mechanical induction of collagen damage (Mean + SEM). Samples were fatigued in 3 point bending, crushed in a mortar and pestle, pulverized to a powder in a Mikro-dismembrator, and submerged in liquid nitrogen. Only pulverization of the samples could induce significant denaturation of the collagen.

Discussion

In the first part of this study we examined the amount of denatured collagen in subchondral trabecular bone of human donors. An increase in the denatured collagen content was noted in the presence of mild to moderate cartilage damage on the medial side. Surprisingly, there were indications that this increase may also be present on the lateral side where the cartilage was intact. In late stage osteoarthritis, the only area with increased denatured collagen was where there was still intact cartilage (Figure 3.2A: denatured collagen was increased in C+ areas). Interestingly, there was more denatured collagen in the deep trabecular bone than in the subchondral plate. This has been reported previously in a study of equine bone (87). This would seem to indicate that the increased expression of cytokines in arthritic cartilage does not directly degrade the collagen in the mineralized subchondral plate. At the present time, we do not feel that we have enough data regarding late-stage osteoarthritis to make definitive conclusions regarding the status of the collagen. However, the evidence that we do have seems to indicate that there is an elevation in collagen denaturation early in the disease process and that this eventually stabilizes and returns to normal levels.

In our original hypothesis, we proposed that increased collagen denaturation would be observed in arthritic bone. We felt that this disruption of the collagen matrix may partially explain the degraded quality of the bone matrix that is observed in osteoarthritic bone (23, 73). We further hypothesized that the denaturation of collagen would be a molecular level indicator of microdamage. Our *in vitro* experiments indicate that it is unlikely that the increase in

denatured collagen is induced mechanically. Neither fatiguing nor crushing the samples had a measurable effect on the denatured collagen. Pulverization to a fine powder only doubled the amount of denatured collagen.

Explanation for the observed increased content of denatured collagen requires revision of our previous hypothesis. It has previously been observed that bone turnover is increased in arthritics(86, 88, 89). This also results in a decreased level of mineralization of the matrix. Arthritic bone has been reported to contain substantial amounts of woven bone. It has also been reported that an abnormal form of type I collagen is produced in arthritic bone (90). This leaves us with multiple possible explanations for the increase in denatured collagen in arthritic bone: i) bone collagen is denatured after cleavage by elevated levels of cytokines. These cytokines may be produced locally or transported across the subchondral plate from the cartilage. ii) the abnormal type I homotrimer in osteoarthritic bone may be susceptible to spontaneous denaturation iii) increased denatured collagen may be the result of elevated remodeling.

In conclusion, we observed an increase in the amount of denatured collagen in the subchondral trabecular bone of donors with mild cartilage damage. This was not observed in advanced osteoarthritis. We were not able to induce collagen denaturation *in vitro* mechanically except for the extreme case of pulverization suggesting that other factors may be important.

Acknowledgements

Funding was received from NIH-AR39239, The Dutch League Against Rheumatism and The Danish Health Research Council-96.

Chapter 4

Adaptation of subchondral bone in osteoarthritis

Day JS, van der Linden JC, Bank RA, Ding M, Hvid I, Sumner DR, Weinans H.

Abstract

Osteoarthritis is a chronic joint disease with pathological changes in the articulating cartilage and all other tissues that occupy the joint. Radin and coworkers have suggested the involvement of subchondral bone in the disease process. However, evidence for an essential role in the etiology has never been proven. Recent studies showing reduced chemical and mechanical properties of subchondral bone in various stages of the disease have invigorated interest in the role of subchondral bone in the development and progression of the disease. The current study showed that the concept of bone adaptation might explain subchondral stiffening, a process where subchondral bone becomes typically sclerotic in osteoarthritis. In addition, we report reduced mechanical matrix tissue properties as well as an increase in denatured collagen content. In conclusion, although osteoarthritic bone tissue contains increased denatured collagen and has reduced matrix mechanical properties, the widely accepted concept of subchondral stiffening is compatible with the process of normal bone adaptation.

Day JS, Van Der Linden JC, Bank RA, Ding M, Hvid I, Sumner DR, Weinans H.
Adaptation of subchondral bone in osteoarthritis. *Biorheology* 41(3-4):359-68
(2004).

Introduction – The role of bone in osteoarthritis

Osteoarthritis has been described as an “organ failure” where pathological changes in the cartilage, bone, synovium and other soft tissues interact resulting in failure of the joint. Indications of disease progression include destruction of the cartilage in combination with abnormal growth of the subchondral bone resulting in thickened subchondral bone plate, osteophytes and deformation of the affected joint (Figure 4.1). Although little is known about the relation between bone and cartilage in the etiology of osteoarthritis, clinical management has focused mainly on chondroprotective strategies.

The role of bone in disease pathogenesis requires examination, as the subchondral bone plate provides a mechanical base for the cartilage while supplying a large proportion of its nutrient requirements(91, 92). Sclerosis of the subchondral plate can be observed on x-rays of osteoarthritic patients and increased stiffness and bone mineral density(BMD) of the subchondral plate is considered a hallmark of osteoarthritis. Subchondral bone is altered in the earliest stages of osteoarthritis (59, 93-96) as the subchondral plate thickens and bone volume fraction is increased in the weight bearing areas of trabecular bone (71, 72, 97, 98). The structure of the trabecular bone is also altered to consist of thick, widely spaced trabeculae (99, 100). Although osteoarthritis has been repeatedly associated with increased BMD, both in the affected joint and appendicular skeleton(59, 60, 93, 101-106), the relation between BMD and disease progression is not clear (60, 107, 108).

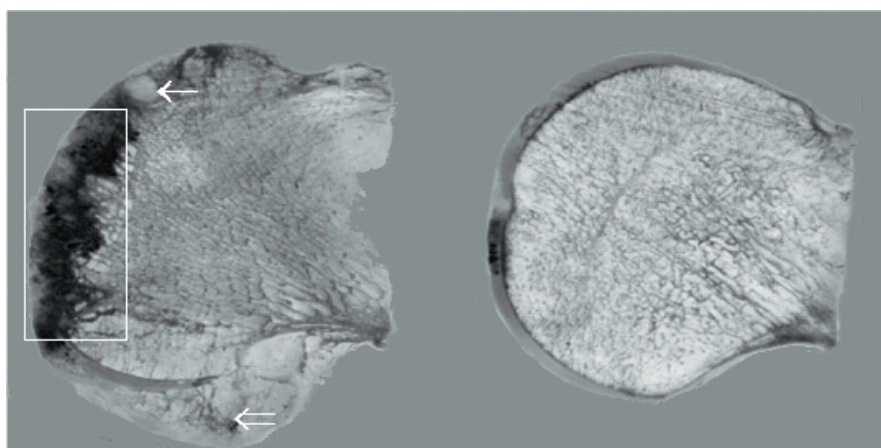


Figure 4.1: Pathological adaptation of an osteoarthritic femur head. A section through an osteoarthritic(left) and normal femur head(right). Prominent osteophytosis(⇔), cyst formation (←), and subchondral sclerosis(box) are indicated. Note the flattening of the osteoarthritic femur head and widening of the femoral neck.

Radin et al. (50, 51) were the first to propose a link between subchondral bone mechanics and disease progression. Based on observations of increased stiffness(109) and decreased energy absorbing capacity(110) of osteoarthritic bone they proposed that stiffening of the subchondral plate was an initiating factor in osteoarthritis. According to their hypothesis, trabecular microfracture due to impulsive loading initiates bone remodeling in the subchondral plate. This leads to localized stiffening that in turn produces increased shear stress in the cartilage, culminating in cartilage breakdown.

Mechanical testing of arthritic bone: Scale effects

In spite of evidence of the involvement of mechanical factors in the development of osteoarthritis, there is little data available regarding the mechanical properties of osteoarthritic bone. Upon examination of the available literature (summarized in Table 4.1), the concept of subchondral stiffening seems to present a paradox since arthritic bone has been reported to be both stiffer and more compliant than normal bone. However many of these studies fail to recognize that bone's mechanical properties can be altered at a minimum of two distinct levels of organization. Because bone is a cellular (i.e. foam-like) material its mechanical properties are influenced both by the material properties of the calcified matrix and the porosity of the structure as a whole. Matrix properties are measured at the micron scale and are commonly referred to as 'bone quality'. Apparent or functional level measurements are made at the millimeter to centimeter scale and reflect the matrix level properties combined with the effects of bone mass and trabecular architecture (Figure 4.2).

At this time, only two studies have measured both the apparent and matrix level properties of arthritic bone. Day et al.(23) used a combination of standard mechanical testing and micro finite element modeling to determine both the apparent and matrix Young's modulus

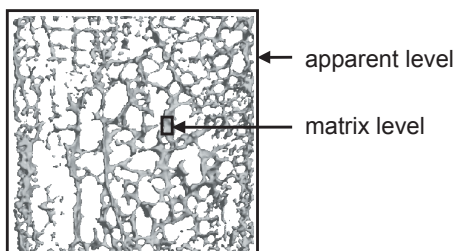


Figure 4.2: Definitions of the apparent level and the matrix level. The matrix modulus was defined as the modulus effective at the scale of tens to hundreds of microns. The apparent modulus was effective at the scale of millimeters to centimeters and includes both the influence of the matrix modulus and the influence of trabecular architecture.

Author	Type of Bone	Location	Disease Progression	Test Method	Finding	Comments
Radin et al. (1970)	subchondral plate	tibial plateau	early and late stage OA	drop test	65% reduction in impact energy in early OA	apparent properties
Lereim et al. (1974)	subchondral plate	tibial plateau	late stage OA	Brinell hardness (5 mm indenter)	50% reduction in hardness in OA	mixture of apparent and tissue properties
Pugh et al. (1974)	trabecular bone	femoral condyle	mild cartilage damage	dynamic apparent stiffness	40% increase in apparent modulus	apparent properties
Finlay et al. (1988)	trabecular bone	tibial plateau	late stage OA	4 mm indenter	result varied by location and disease progression	apparent properties
Hvid et al. (1988)	trabecular bone	tibial plateau	late stage OA	osteopenetrometer (2.5 mm indenter)	result varied by location and knee alignment	mixture of apparent and tissue properties
Li & Aspden (1997)	subchondral plate and trabecular bone	femoral head	late stage OA	standard compression testing ultrasound	15% increase in apparent modulus 15% decrease in matrix modulus	apparent properties tissue properties
Ding et al. (2001) Day et al. (2001)	trabecular bone	tibial plateau	mild cartilage damage	standard compression testing and finite element modeling	30% decrease in apparent modulus 45% decrease in matrix modulus	apparent properties tissue properties
Brown et al. (2002)	Trabecular bone	femoral head	late stage OA	standard compression testing	Arthritic apparent modulus was decreased compared to normal bone with equal bone mass	apparent properties (also with correction for BMD)

Table 4.1: A review of previously published mechanical testing results for osteoarthritis specimens. Although there have been multiple tests of osteoarthritic bone, many have used test methods that do not discriminate between matrix and apparent properties.

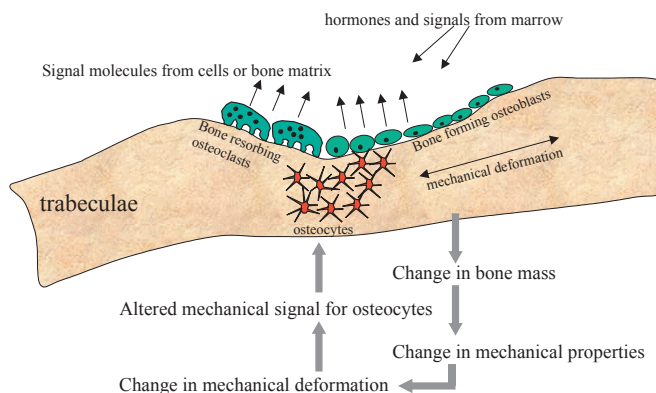


Figure 4.3: Illustration of a bone remodeling unit. Osteocytes and/or osteoblasts act to modulate the resorptive activity of osteoclasts. These cells are thought to be sensitive to both systemic signals and local mechanical stimulation.

of cadaveric specimens. Tibiae with mild cartilage damage in the medial compartment and intact cartilage on the lateral side were compared to intact controls. In these specimens, the matrix modulus was reduced by approximately 50% in the arthritic group with a larger reduction on the medial side. The apparent modulus was not significantly different from controls, but the ultimate stress was reduced on the medial side in the arthritic specimens(98). Li and Aspen(72, 73, 79) used a combination of standard compression and ultrasonic testing to measure the mechanical properties of bone taken from patients undergoing hip arthroplasty for osteoarthritis. They found a 15% increase in the apparent modulus of the trabecular bone and a 15% decrease in the matrix modulus of the subchondral bone plate compared to a control group. In common to both of these studies, one on early and the other on late-stage osteoarthritis, was a finding of increased bone volume fraction and decreased matrix properties in the arthritic groups.

Bone mechanosensors, remodelling and adaptation

It is important to note that bone remodeling and adaptation is driven by the cells and thus occurs at a scale that is closer to the tissue level than the apparent level. The cells that generate and resorb the bone matrix are the osteoblasts and osteoclasts respectively. Osteoclasts make resorption cavities on the surfaces of the trabeculae in the range of 20 to 60 microns deep. During normal turnover osteoblasts fill this cavity with collagen that slowly mineralizes thereafter. It has long been known that the osteoclastic resorption and osteoblastic apposition are a coupled mechanism, often referred to as a Bone Multicellular Unit or a BMU (Figure 4.3). It has been recently discovered that an important coupling mechanism

between osteoblasts and osteoclasts occurs due to cell binding molecules expressed on their cell membranes. Osteoblasts express a molecule called RANKL on the cell membrane and by physically making contact with the osteoclast they initiate osteoclast activity by binding to RANK at the osteoclast membrane(111-114). However many details on where osteoclasts start their activity, why they stop resorbing bone and what triggers the osteoblasts to express RANKL are unknown.

It is generally believed that mechanical loading or deformation of the bone matrix is an important aspect in bone remodeling regulation. During normal bone turnover there is often a small deficit in refilling the resorption cavity by the osteoblasts. Therefore each BMU cycle results in a small amount of net bone loss. Disuse (unloading the bone) stimulates this net bone loss while mechanical loading counteracts it. Although several hypotheses have been proposed in the literature, it is unclear how the hormonal, paracrine and autocrine factors interact with mechanical loading (113, 115-118).

An important consequence of turnover is the renewal of bone and repair of microdamage within the matrix. However, abnormally high turnover leads relatively bone with a relatively lower mean age. Since the mineralization of bone is a slow process there is also a resultant reduction in mean mineralization and a concomitant reduction of bone stiffness(12, 119).

Simulation of bone adaptation in osteoarthritis

Previously in this paper we have demonstrated that the calcified matrix stiffness is reduced and the bone volume fraction increased in osteoarthritis. We have also demonstrated that bone adaptation is most likely driven by either osteoblasts or the osteocyte network acting as mechanoreceptors at a local (matrix) level. It therefore seems plausible that the increase in bone volume fraction observed in osteoarthritis is an adaptive response to the increased bone strain that is experienced as the matrix becomes more compliant. In order to test whether this sequence of events is compatible with the concept of subchondral stiffening we have constructed a simulation of bone adaptation driven by matrix level strain. We have created models of the subchondral trabecular bone from high resolution microCT scans and simulated bone apposition in response to degeneration of the matrix. By analyzing the resulting apparent Young's modulus we could investigate the compatibility of the concept of subchondral stiffening with that of a reduced matrix modulus.

Cylindrical bone specimens of epiphyseal trabecular bone were obtained post mortem from the medial compartment of 4 donors (ages: 58, 61, 62, 80)(120). The donors had no record of musculoskeletal disease and the donor tibiae did not exhibit any macroscopic pathology.

The samples were taken 1mm distal to the subchondral bone plate, were 7.5mm in both diameter and length and were orientated such that the axes of the cylinders were parallel to the longitudinal axes of the tibiae. Specimens were scanned with a 3D voxel size of 20 μm using a microtomographic system ($\mu\text{CT}20$, Scanco Medical AG., Zurich, Switzerland).

Cubic data sets were extracted from the resulting image stacks. Each cube was taken from the centre of the sample and had an edge length of 4.3mm. The image data were converted into finite element models with 20 x 20 x 20 μm 8 node brick elements and isotropic material properties. A linear elastic modulus of 5 GPa and Poisson's ratio of 0.3 were assigned to all bone elements and confined compression tests were simulated(20, 23, 24, 68). The models were solved using in-house code that implemented the element-by-element method on a desktop computer(20). The apparent stiffness(quotient of applied stress and the applied strain at the scale of the entire sample) of each sample was then calculated from the output of the finite element models.

Degeneration of the calcified matrix and the subsequent adaptation process was simulated using an inverse approach. Instead of reducing the elastic modulus of the elements and then incrementally adding bone voxels, the adaptive response was first simulated by adding bone voxels to all surfaces using a dilation algorithm (Morph3D, R.A. Peters, Vanderbilt University). These bone voxels were assigned the same material properties as the existing matrix resulting in homogenous matrix properties. Next, the finite element models were solved and the maximal principal strain was calculated for each element. Because of their linear nature of

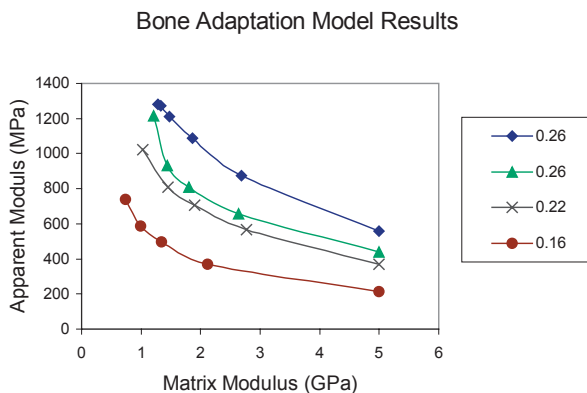


Figure 4.4: Results of the adaptive bone model. The matrix modulus(x axis) of each sample was initially assigned a value of 5Gpa and the apparent moduli of the 4 samples were calculated(y axis). The matrix modulus was then reduced for each specimen and the adaptive response was simulated. The new apparent modulus was then plotted. This was continued until the sample was a solid block. The initial bone volume fraction of each sample is indicated in the legend.

the finite element models, the matrix modulus could be scaled to a value that would normalize the median strain for the model. By repeating this process for a number of steps a tissue response curve could be generated.

As expected, an increase in the bone volume fraction was necessary to compensate for the decreased matrix modulus. In spite of the decline in the local matrix modulus, the increase in volume fraction resulted in an overall increase in the apparent modulus of the models (Figure 4.4). When the matrix modulus was reduced to 25% of its original value the adaptive response led to a solid block of bone with an apparent Young's modulus that was 4 times the original. A more moderate (and realistic) reduction of 20% for the matrix modulus resulted in a 25% increase in the apparent Young's modulus.

More on bone matrix properties in osteoarthritis

The reason for a reduced bone matrix modulus in osteoarthritis is unclear. Possible explanations include: lower mineralization levels due to increased bone remodeling, abnormal mineralization or defects in the collagen matrix.

While there is some debate on whether systemic breakdown of mature collagen is elevated in arthritic patients(121-125), there is considerable evidence that remodeling activity is increased in the subchondral bone of arthritic joints(57, 94). Increased remodeling activity results in a lower mean age of the bone matrix by reducing the time available for passive mineralization of the matrix(12). Thus increased remodeling activity results in a lower mean level of mineralization, and thus a reduced modulus in osteoarthritic bone(71, 93, 101, 126-128).

In addition to lower mineralization levels, there have also been observations of abnormalities in the collagenous matrix of osteoarthritis bone. Bailey et al.(90) have reported both increased collagen hydroxylation and the presence of an unusual type I homotrimer $[(\alpha 1)_3]$ as opposed to the normal heterotrimer $[(\alpha 1)_2(\alpha 2)_1]$ in osteoarthritic subchondral bone. Both increased hydroxylation and the formation of a type I homotrimer have been linked to a reduction in bone mechanical properties(129, 130).

We have reported an increase in the proportion of denatured collagen in the epiphyseal trabecular bone of donors with mild cartilage damage (i.e. early osteoarthritis)(131). In brief, trabecular bone samples were harvested from donors with early-stage osteoarthritis and normal controls. These samples were decalcified in EDTA before selectively digesting denatured collagen using α -chymotrypsin. By comparing the amount of hydroxyproline in the supernatant to that in the remaining insoluble matrix, the proportion of denatured collagen

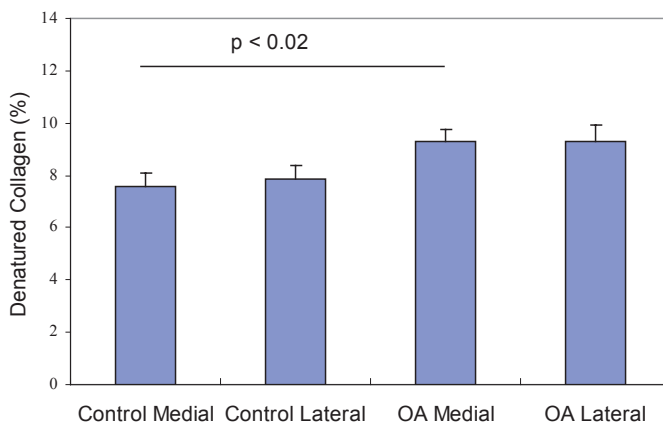


Figure 4.5: Denatured collagen content of subchondral trabecular bone in donors with early osteoarthritis. The amount of denatured collagen was measured for each sample using a selective digestion technique. Denatured collagen content was increased by approximately 22% in the arthritic medial condyle.

with respect to intact collagen could be measured in each specimen(80). We found a 22% increase in denatured collagen in the medial condyle of the arthritic donors with respect to controls(Figure 4.5). It has previously been demonstrated that mechanical toughness is inversely correlated to the denatured collagen content of bone(31). The presence of elevated levels of denatured collagen may be the result of increased levels of MMPs in osteoarthritic bone(74, 127).

Discussion

Recent advances have made it possible to examine the mechanical properties of bone matrix at multiple levels of organization. New methods such as high-resolution ultrasound and nanoindentation can be used to resolve the mechanical properties of bone osteons at the scale of single lamellae. Comparatively, the finite element derived matrix modulus is in fact the average effective matrix stiffness throughout the whole sample and includes effects such as trabecular architecture, matrix porosity, microdamage etc. In this paper we have described a reduction in the matrix Young's modulus in osteoarthritic bone as measured by multiple methods(23, 72, 73, 79). At this time, we are only beginning to understand the underlying chemical and/or physical explanation of this phenomenon. Reduced matrix properties may be, in part, due to hypomineralization of the bone matrix; a normal consequence of the increased remodeling activity in osteoarthritic joints. However, it is also likely that there is also a contribution due to degradation of the collagen network as evidenced by the presence

of increased collagen hydroxylation, an unusual collagen homotrimer and an increase in denatured collagen content.

We have applied a simulation model to investigate the apparent paradox of subchondral stiffening in the presence of reduced bone quality (matrix stiffness). We employed an equilibrium model constructed assuming homogenous tissue properties and neglecting the temporal aspects of the bone remodeling cycle (11, 132). The model demonstrates that, in an equilibrium state, the concept of subchondral stiffening at the apparent level is not incompatible with reduced calcified tissue stiffness when adaptation is driven by strain at the cell level. The model does not attempt to model the full remodeling cycle (i.e. resorption and formation phases) and does not examine the possibility of phase lags between tissue level degeneration and the adaptive response. The presence of a phase lag between degeneration of the matrix and the adaptive response may explain why an increased apparent modulus is reported in end-stage osteoarthritis(72, 73, 79, 133) and a decreased apparent modulus is reported in less severe osteoarthritis(23, 133).

In vivo it is likely that the driving factors behind the formation of pathological bone are more complex than the adaptive model proposed here. It is unlikely that such a model can explain the formation of subchondral cysts or osteophytes. However, a great deal of insight into the disease progress can be gained by applying such models. For example, we can apply this model to the original hypothesis proposed by Radin who suggested that subchondral sclerosis in osteoarthritis created stiffness gradients in the subchondral bone resulting in shearing of the overlying cartilage. From the model results we can see that it is possible for the reduced matrix modulus to result subchondral stiffening but from the experimental data it is likely that this is preceded by a period of increased compliance of the subchondral bone(23, 62, 133). It is of interest to note that the presence of a compliant region of subchondral bone would still, however, create stiffness gradients in the subchondral bone and thus shearing of the overlying cartilage.

Subchondral bone and overlying cartilage perform as a functional unit. Presently little is known about the interaction between the cartilage and bone in the etiology of osteoarthritis. Recent research indicates that bone is intimately involved in disease progression. While there is currently little evidence of a direct cause and effect relation between subchondral bone sclerosis and degeneration of the overlying cartilage, recent studies using bisphosphonates(bone antiresorptive compounds) have yielded interesting results with regard to both pain and cartilage degeneration(134-136). Thus, true understanding of the etiology of osteoarthritis will require study of all of the tissues of the joint.

Chapter 5

Bisphosphonate treatment affects trabecular bone apparent modulus through micro-architecture rather than matrix properties

JS Day, M Ding, P Bednarz, JC van der Linden, T Mashiba, T Hirano, CC Johnston, DB Burr, I Hvid, DR Sumner, H Weinans

Abstract

Bisphosphonates are emerging as an important treatment for osteoporosis. But whether the reduced fracture risk associated with bisphosphonate treatment is due to increased bone mass, improved trabecular architecture and/or increased secondary mineralization of the calcified matrix remains unclear. We examined the effects of bisphosphonates on both the trabecular architecture and matrix properties of canine trabecular bone. Thirty-six beagles were divided into a control group and 2 treatment groups, one receiving risedronate and the other alendronate at 5 to 6 times the clinical dose for osteoporosis treatment. After one year, the dogs were killed, and samples from the first lumbar vertebrae were examined using a combination of micro-computed tomography, finite element modeling, and mechanical testing. By combining these methods, we examined the treatment effects on the calcified matrix and trabecular architecture independently. Conventional histomorphometry and microdamage data were obtained from the second and third lumbar vertebrae of the same dogs (Mashiba et. al. 2001 *Bone* 28:524-31). Bisphosphonate treatment resulted in an increased apparent Young's modulus, decreased bone turnover, increased calcified matrix density, and increased microdamage. We could not detect any change in the effective Young's modulus of the calcified matrix in the bisphosphonate treated groups. The observed increase in apparent Young's modulus was due to increased bone mass and altered trabecular architecture rather than changes in the calcified matrix modulus. We hypothesize that the expected increase in the Young's modulus of the calcified matrix due to the increased calcified matrix density was counteracted by the accumulation of microdamage.

Day JS, Ding M, Bednarz P, van der Linden JC, Mashiba T, Hirano T, Johnston CC, Burr DB, Hvid I, Sumner DR, Weinans H. Bisphosphonate treatment affects trabecular bone apparent properties through micro-architecture rather than matrix properties. *Journal of Orthopaedic Research* 22(3):465-71 (2004).

Introduction

Bisphosphonates, specific inhibitors of bone resorption, are gaining importance in the treatment of osteoporosis (137, 138). Bisphosphonates inhibit osteoclast activity on the bone surface by causing early osteoclast death, thus reducing the remodeling space, i.e., the amount of bone undergoing active remodeling at any specific time (139, 140). Bone mineral density (BMD) as measured by dual energy X-ray absorptometry is increased by increasing either the total volume of bone (bone mass) or the mineralization of the calcified bone matrix (141-143). It has been demonstrated that the activation frequency (a histological measure of new resorption sites) is reduced during bisphosphonate therapy (144, 145), temporarily disrupting the normal equilibrium between bone resorption and formation. Although the number of new resorption sites is reduced early in the therapy program, the existing formation sites continue to produce new bone matrix. The resultant phenomenon, known as the *bone remodeling transient*, is associated with a rapid gain in bone mass early in the treatment period. This transient behaviour continues until the active remodelling sites are filled in by osteoblast activity, reducing the remodelling space until a new equilibrium is reached. The amount of bone affected by the remodelling transient is determined by the change in the number and size of active remodelling units and the duration of the resorption and formation phases (12, 146). In addition to its effect on the remodelling space, the reduction in activation frequency also results in a slower equilibrium remodeling rate. Because bone turnover is reduced, the average age of the bone packets within the calcified matrix is increased. This results in increased matrix mineralization (143, 147). The therapeutic effect of the bisphosphonate alendronate is thought to be due primarily to an increase in mineralization (143, 148). While increased mineralization should result in stiffer bone material (149), concern exists that this 'frozen bone' might become brittle and/or accumulate microdamage (150, 151). Microdamage accumulation is normally prevented by remodelling, and resorption spaces can be initiated by microdamage (29, 152, 153). Accumulated microdamage can contribute to a reduction of bone Young's modulus, strength, and toughness and could possibly increase fracture risk (28, 154).

Recently, it has become possible to quantify the effect of changes in architecture and bone mass on the apparent mechanical behavior of bone independent of the mechanical properties of the calcified matrix. Micro-computed tomography (microCT) scanning and automated finite element (FE) methods (20) can be combined to create a powerful method for the study of treatment-induced changes in bone architecture at the trabecular level (10- 20 μ m). Further, changes in the Young's modulus of the calcified matrix (hereafter referred to as the matrix modulus) can be investigated by combining these methods with conventional mechanical testing (23, 68). Thus, the contributions of both matrix properties and trabecular architecture to the overall apparent modulus can be evaluated (Figure 5.1).

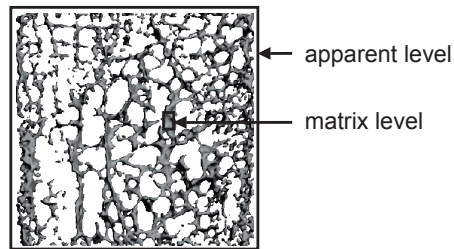


Figure 5.1: Definitions of the apparent level and the matrix level. The matrix modulus was defined as the modulus effective at the scale of tens to hundreds of microns. The apparent modulus was effective at the scale of millimeters to centimeters and includes both the influence of the matrix modulus and the influence of trabecular architecture.

In this study we examined the effect of long-term treatment with high doses of two bisphosphonates, alendronate and risedronate, in a canine model. We investigated the changes induced by bisphosphonate treatment to both bone architecture and matrix modulus as well as their contributions to the apparent Young's modulus. To interpret our findings, we examined the effect of bisphosphonates on remodeling, matrix mineralization, and microdamage accumulation. Specifically, we tested the hypothesis that high dose bisphosphonate treatment leads to increased secondary mineralization and consequently an increase in the matrix modulus.

Methods

Experimental design

The experimental design used in this study has been reported previously and will be briefly summarized (151). Thirty-six female beagle dogs aged 1 to 2 years (control: 1.2 ± 0.4 , risedronate: 1.1 ± 0.2 , alendronate: 1.2 ± 0.2 (y.o. \pm SD)) were divided into 3 weight matched groups. Dogs in the two treatment groups were treated daily with risedronate (Procter and Gamble Pharmaceuticals Inc., Cincinnati, OH) orally at a dose of 0.5 mg/kg/day or alendronate (Merck and Co., Inc., West Point, PA) orally at 1.0 mg/kg/day. Long-term treatment was simulated using doses that were 5 to 6 times higher than the clinical dose for osteoporosis. All dogs were treated for 12 months, then killed, and the first, second, and third lumbar vertebrae were removed. All procedures were in accordance with approved NIH guidelines, under a protocol approved by the Indiana University School of Medicine Animal Care and Use Committee (Study #MD 1783).

Specimen preparation: MicroCT and mechanical testing

One cubic trabecular bone specimen with dimensions 5x5x5 mm was produced from the center of each first lumbar (L1) vertebral body, aligned with the anatomical axes in the cra-

nial-caudal (CC), anteroposterior (AP), and medial-lateral (ML) planes. Low speed, water cooled diamond saws (EXAKT Apparatenbau, Norderstedt, Germany; Ernst Leitz Wetzlar GmbH, Wetzlar, Germany) were used for all sample preparation. Samples were stored in sealed plastic tubes at -20°C , and care was taken to keep specimens moist during scanning and testing.

A high-resolution microCT system ($\mu\text{-CT 20}$, Scanco Medical AG., Zürich, Switzerland) was used to scan the specimens, resulting in reconstructions with $18 \times 18 \times 18 \mu\text{m}$ cubic voxels. The microCT images were segmented using thresholds chosen such that the volume of the dataset matched that determined physically using Archimedes' principle (63). Archimedes' principle was also used to determine the bone volume fraction (BV/TV) and the density of the calcified matrix.

After scanning, each cubic specimen was tested in compression in an 858 Bionix MTS hydraulic material testing machine (MTS Systems Corporation, Minneapolis, MN). Specimens were tested non-destructively in compression to $6000 \mu\text{strain}$ (apparent strain) at a strain rate of $2000 \mu\text{strain}/\text{sec}$ in the AP and ML directions to determine the apparent Young's modulus. The apparent Young's modulus of each sample was calculated as the tangent of the linear portion of the stress strain curve at $5000 \mu\text{strain}$ for the non-destructive tests (AP and ML directions). The specimens were then tested to failure in the CC direction with the same strain rate. The apparent Young's modulus in this direction was defined as the slope of the steepest portion of the stress-strain curve. Yield stress was defined as the intercept between the stress-strain curve and the line used to define the Young's modulus offset by 0.2% strain. Ultimate stress was defined as the peak stress encountered during testing. All testing was performed on polished platens lubricated with a low viscosity mineral oil to reduce the effect of friction (17).

Finite element models

The matrix modulus was calculated for all three directions using a combination of finite element modeling and mechanical testing. This combination was used because it enables the total apparent modulus to be partitioned into contributions due to the matrix modulus and trabecular architecture (20). All voxel microCT data were coarsened to $36 \mu\text{m}$, then converted to a finite element mesh of 8 node cubic elements. Coarsening was performed using a bone volume-preserving algorithm (64). The resulting meshes typically consisted of 400,000 to 700,000 elements. All elements were assigned an arbitrary matrix modulus of 1 GPa and a Poisson ratio of 0.3. Boundary values were assigned to simulate an unconstrained compression test with no friction at the platens. Because we used a matrix modulus of unity with a linear finite element analysis, the apparent modulus obtained from the finite element model can simply be scaled to match the apparent modulus from each of the mechanical tests. The resulting scaling factor can be considered the matrix modulus of the sample (20). This modu-

lus represents the average stiffness of the voxels of the bone matrix under the assumption of homogeneous isotropic tissue properties.

Simulation of increased mineralization

Bisphosphonate treatment has been previously observed to result in both increased mineralization and a loss of the normal mineralization gradient between superficial and interstitial bone (12, 147, 148). We used 4 FE meshes from the residronate treated group to predict the effects of altered mineralization on the apparent modulus. Two conditions were simulated: homogenous mineralization representing bisphosphonate treated bone and a heterogenous mineralization that was more representative of normal bone with lower mineralization at the surface and higher mineralization of the interstitial bone (155). To accomplish the simulations, an image erosion algorithm was used to identify bone voxels within 36 μm of the surface. A 5% increase in total mineralization was assumed for the bisphosphonate treated samples (145, 147, 148). By assuming that bisphosphonate treatment mostly affected surface voxels, a lower relative mineralization was calculated for the normal surface voxels. We then used either a linear or cubic relation as the extreme boundaries for the relation between mineral content and Young's Modulus (149). After solving the FE models we compared the apparent modulus in the CC direction for the normal (inhomogenous properties) and the treated (homogeneous properties) models.

Histomorphometry and microdamage

Dynamic histomorphometry and microdamage data from the second and third lumbar vertebrae respectively were obtained from a previous study of the same animals. The following parameters were used in the current paper to aid interpretation of the results: Activation Frequency (Ac.F), Bone Formation Rate/Bone Surface (BFR/BS), Osteoid Surface/Bone Surface (OS/BS), Crack Number (Cr.N), Crack Length (Cr.Le), Crack Density (Cr.Dn), and Crack Surface Density (Cr.S.Dn) (156).

Statistical analysis

The statistical analyses included two-way analyses of variance for repeated measures for the experimental apparent modulus, apparent modulus predicted by the FE models, and matrix modulus. The group (normal, risedronate, or alendronate) was used as the between-subjects factor and testing direction (cranial-caudal, anterior-posterior, medial-lateral) as the within-subjects factor. Bone volume fraction, matrix density, histomorphometric parameters, and microdamage parameters were analyzed using standard analysis of variance. When significant main effects were found, specific comparisons were made with Dunnett two-sided t-tests. In all cases, the exact p values are given; we considered $p < 0.05$ to represent significant effects.

A stepwise multiple regression analysis was used to assess the suitability of the FE models for the prediction of the apparent modulus measured in three directions in the laboratory. In this model the dependent variable was the measured apparent modulus and the independent variables were apparent modulus predicted by FE, testing direction, and the treatment group. Correlation analysis was used to examine the relations between the matrix density, matrix modulus, and both remodelling and microdamage parameters. Statistical analyses were performed using SPSS version 8.0 (SPSS Inc., Chicago, IL, USA).

Results

One dog was excluded due to distemper at the start of treatment, and one vertebra was destroyed during preparation. This left 11 control, 11 risedronate-treated, and 12 alendronate-treated dogs.

Bisphosphonate treatment resulted in an increase in the bone volume fraction and calcified matrix density as determined using Archimedes' principle. The increase of approximately 2% in matrix density was significant for both treatments, but the change in BV/TV was only significant for the risedronate group where the increase was 18% (Table 5.1).

The experimentally measured apparent modulus was affected by bisphosphonate treatment ($p = 0.001$). A significant effect of direction ($p < 0.001$) and an interaction between direction and treatment ($p = 0.018$) were found. On average, the risedronate treated group was 37% stiffer than the control group ($p=0.001$). No significant difference was found in the alendronate group ($p=0.215$; Figure 5.2A). The apparent modulus predicted by the FE models (contribution of trabecular architecture and bone mass) was also affected by bisphosphonate treatment ($p = 0.001$) with effects similar to the mechanical tests (Figure 5.2B). As in the mechanical testing, there was a significant effect of direction ($p < 0.001$), but no interaction between direction and treatment ($p = 0.246$). The predicted apparent modulus in the risedronate group was approximately 40% higher than the control group ($p < 0.001$). No significant effect of alendronate treatment was found ($p = 0.283$; Figure 5.2B). The matrix modulus was not significantly affected by treatment ($p = 0.517$), nor was there significant interaction between direction and treatment group ($p = 0.893$). Direction significantly affected the matrix modulus, which was 20 to 30% larger in the CC than in the AP or ML directions ($p < 0.001$; Figure 5.2C). Bisphosphonate treatment resulted in an increase in both the ultimate stress and the yield stress. However, after correcting for architecture, this difference was not significant (Table 5.1).

	Control	Risedronate	Alendronate	ANOVA	Control vs. Risedronate	Control vs. Alendronate
BV/TV	0.22 (0.20, 0.24)	0.26 (0.23, 0.28)	0.23 (0.22, 0.24)	0.009	0.007	0.657
ρ_{matrix} (g/cc)	2.09 (2.08, 2.11)	2.14 (2.11, 2.16)	2.13 (2.12, 2.14)	0.005	0.005	0.013
σ_{ultimate} (Mpa)	8.3 (6.9, 9.6)	11.4 (10.4, 12.3)	9.8 (8.6, 10.9)	0.008	0.004	0.120
σ_{yield} (Mpa)	7.4 (6.1, 8.7)	10.2 (9.4, 11.0)	8.9 (8.0, 9.8)	0.004	0.002	0.070
Ac.F (year ⁻¹)	1.65 (0.33, 4.18)	0.18 (0.03, 0.60)	0.09 (0.024, 0.16)	0.000	0.000	0.000
BFR/BS ($\mu\text{m}^3/\mu\text{m}^2/\text{year}$)	80.0 (18.6, 152.2)	10.5 (1.1, 36.9)	5.5 (1.4, 11.7)	0.000	0.000	0.000
OS/BS (%)	8.5 (5.8, 11.2)	1.5 (0.7, 2.2)	1.0 (0.6, 1.3)	0.000	0.000	0.000
Cr.N (#)	0.7 (0.3, 1.2)	3.3 (1.5, 5.0)	3.7 (2.8, 4.5)	0.001	0.003	0.001
Cr.Le (μm)	39.2 (22.3, 56.2)	49.4 (31.4, 67.4)	45.7 (40.6, 50.9)	0.557	-	-
Cr.Dn (#/mm ²)	0.33 (0.11, 0.54)	0.80 (0.41, 1.19)	1.19 (0.88, 1.51)	0.001	0.052	0.000
Cr.S.Dn ($\mu\text{m}/\text{mm}^2$)	11.6 (3.8, 19.5)	39.8 (19.5, 60.0)	53.1 (39.8, 66.3)	0.000	0.011	0.000

Table 5.1: Results for one-way ANOVA. Mean values and 95% confidence intervals are presented on the left for histomorphometry (top), mechanical properties (middle), matrix density (middle: pmatrix), and microdamage (bottom). On the right p values are presented for both the ANOVA and the post hoc tests.

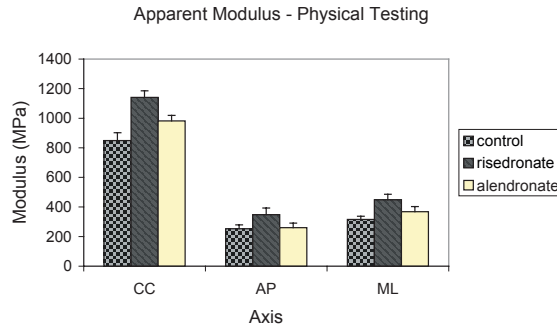


Figure 5.2A: Apparent Young's modulus from physical testing. Two-way ANOVA indicated an effect of treatment ($p = 0.015$) and direction ($p < 0.001$). Risedronate treated samples were significantly stiffer than the control group ($p = 0.012$).

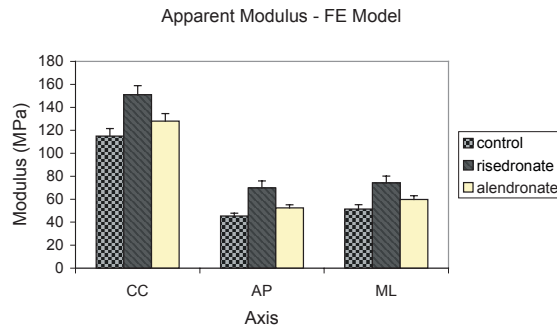


Figure 5.2B: Relative modulus calculated using FE models. Two-way ANOVA indicated an effect of treatment ($p = 0.001$) and direction ($p < 0.001$). The simulated apparent modulus of risedronate treated samples was significantly stiffer than the control group ($p < 0.001$).

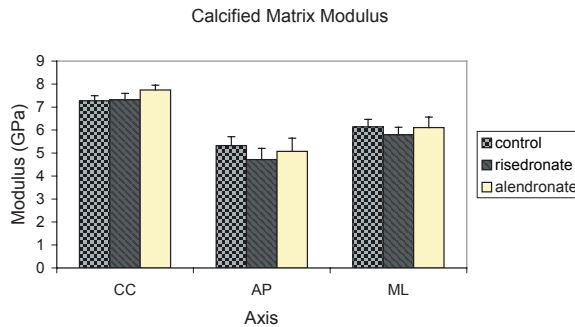


Figure 5.2C: Matrix modulus. Bisphosphonate treatment had no effect on the matrix modulus ($p = 0.699$). There was an effect of direction ($p < 0.001$).

Figure 5.2: Mechanical testing and FE simulation results. Cubes of trabecular bone from the first lumbar vertebra were tested in three directions in compression (Fig. 2A). FE models with a matrix modulus of 1 GPa were used to quantify the contribution of trabecular architecture (Fig. 2B). The mineralized matrix modulus was the scaling factor between the physical tests and the FE simulated results (Fig. 2C). Testing directions were cranial-caudal (CC), anteroposterior (AP) and medial-lateral (ML). Results (mean + SEM) are grouped by test direction on the x-axis of each graph. Treatment group is indicated by the shading of the bars.

In the multiple regression analysis, the FE models (i.e., effect of architecture and bone mass) accounted for 89.3% ($p < 0.0001$) of the variance in the experimentally measured modulus. A small architecture independent effect of direction was found, which contributed to 0.5% of the variance ($p = 0.04$). Treatment group and direction-group interaction were not significant. The residual variance was 10.2%.

To estimate the statistical power of our results, we simulated the predicted effect of increased mineralization on the matrix modulus. We assumed an increase of 5% in the mineralization of the bisphosphonate treated group. For bone with a mineral fraction of approximately 40%, this agreed well with our observed matrix density measurements. Based on the simulations we predicted that the matrix modulus should increase by between 5% (conservative linear model) and 14% (cubic model) in the treated animals. From these simulations we could estimate that, for the sample size used, the power (β) to detect a difference in the group mean matrix modulus with a two-sided t -test ($\alpha=0.05$) was between 0.12 (for the conservative linear model) and 0.65 (for the cubic model). Because of the limited power of our results, care must be taken when comparing the group means for matrix modulus.

Because one sample from the control group was destroyed during preparation, we reworked our previous data (156), which are included in Table 5.1. From these data a large significant decrease in bone remodeling activity is apparent in the bisphosphonate treated groups, as well as an increased microdamage burden in the treated animals as indicated by significant increases in Cr.N, Cr.Dn and Cr.S.Dn.

Linear regression analysis revealed that the matrix density was significantly correlated to both the remodeling (ES/BS $r=-0.555$, $p=0.001$; OS/BS $r=-0.594$, $p < 0.001$; BFR/BV $r=0.487$, $p=0.004$; Ac.F $r=-0.353$, $p=0.044$) and microdamage parameters (Cr.N $r=0.456$, $p=0.007$; Cr.Dn $r=0.412$, $p=0.015$; Cr.S.Dn $r=0.511$, $p=0.002$). The matrix modulus, however, was not significantly correlated to the matrix density, remodelling, or microdamage parameters.

Discussion

The major purpose of this study was to determine whether the increased levels of matrix mineralization seen after long-term bisphosphonate therapy affected the matrix mechanical properties. We used a high dose to simulate long-term effects in the bone. Bone remodeling was greatly reduced, resulting in both a 2% increase in the matrix density (indicative of increased mineralization) and increased microdamage accumulation. By using a combination of FE modelling, microCT scanning, and mechanical testing, we investigated the effects of treatment on the apparent Young's modulus, bone architecture, and calcified matrix proper-

ties. A significant increase of the apparent modulus was observed in the risedronate treated group. This increase was predicted by the FE models, indicating a strong effect of trabecular architecture and bone mass. The importance of architecture was further indicated by the results of the multiple regression analysis where 89.3% of the variance in the mechanical testing was accounted for by the FE models with no independent effect of treatment group (an effect of treatment group would indicate a group specific difference independent of the FE results, i.e., matrix modulus). Although the matrix density was increased, there were no significant differences in the group mean matrix moduli.

A limitation of our study design is that we used intact, 'normal' dogs. In an osteoporotic population bone turnover is likely increased, resulting in lower mean mineralization of the calcified matrix. Hypomineralization in an osteoporotic population could lead to a decrease of the matrix modulus compared to the 'normal' population used in this study.

Using microCT scans to create trabecular level FE models requires that the scan be of sufficient resolution and quality to resolve individual trabeculae accurately. Our use of 36 μ m voxels and individual thresholds was sufficient to create accurate meshes (156). We found an average matrix modulus of 5.9 GPa, well within the range previously reported using this method (20, 23, 25, 157). Initially, we were concerned that the reduction in the amount of osteoid in the bisphosphonate treated groups could bias our segmentation of the CT data. Calculations indicated that the quantity of unmineralized osteoid tissue was not large enough to influence the choice of thresholds (data not shown). Further, we found no significant relation between OS/BS and matrix modulus ($0.41 \leq p \leq 0.72$ for Pearson correlation depending on direction) and concluded that this factor had little or no effect on the model results.

We found that the matrix modulus was influenced by the testing direction (Figure 5.2C). This could be due to preferential loss of material due to thresholding in the presence of strong anisotropy at the trabecular level (158), nonideal behaviour (i.e. buckling of trabeculae) that is not represented in the FE model's boundary conditions (15, 70), nonideal behavior of the model's linear brick-shaped elements (16), or true material anisotropy at the sub-trabecular level (159).

Clinically a large increase in BMD has been observed in the first year of antiresorptive therapy. Following this, BMD either slowly increases or reaches a plateau (160, 161). It was believed that the initial gain in BMD was indicative of an increase in bone mass due to the transient change in remodeling space and that the later gain in BMD was the result of increased mineralization. It has recently been suggested that increased secondary mineralization, rather than bone mass, is responsible for the reduced fracture risk after alendronate therapy (148). In a two-year clinical study of alendronate therapy, the authors observed an increase in spinal

BMD, but no significant increase in bone mass in transiliac biopsies. Analysis of the biopsies by contact microradiography revealed 9.3% and 7.3% increases in the mean degree of mineralization of cortical and trabecular bone, respectively. Based on these findings, the authors concluded that the reduction of fracture incidence was due to secondary mineralization rather than increased bone mass. This contradicts a previous study of ovariectomized primates where an increase in the bone volume fraction was measured after two years of treatment with alendronate as compared to saline vehicle treated animals (162). The extrapolation of results obtained from iliac biopsies to spine BMD as measured by DEXA is tenuous as this study was underpowered to detect differences in the iliac crest. Also, large differences in remodelling can exist between the spine and iliac crest (163).

While it is logical that normalizing the mineralization of hypomineralized bone in osteoporotics to normal levels should be beneficial to the patient, the exclusion of the contribution of increased bone mass is not supported by our data. Although we predicted an increase of at least 5% for the matrix modulus based on our measurements of increased matrix density, we observed only small insignificant changes in the moduli of the calcified matrix in the bisphosphonate treated groups (5% decrease in risedronate treated group and a 1% increase in the alendronate treated group; Figure 5.2C).

Based on our data, we conclude that the increased apparent modulus seen in bisphosphonate therapy results from increased bone mass and altered trabecular architecture. This is supported by a concurrent study of the three-dimensional morphology of specimens from the same animals (164). Our results are in agreement with the clinical data, where the greatest reduction in fracture risk occurs during the first year of treatment, but fewer fractures are also found in subsequent years compared to placebo treated controls (27, 142, 165). It would seem likely that reduction of fracture risk seen clinically in bisphosphonate therapy is the result of the increase in bone mass early in the treatment as the remodeling space is 'filled in'. Further increase in BMD through secondary mineralization could provide some benefit in the short term at clinical doses but may be harmful to the patient in the long term as microdamage accumulates. In the present study there was a significant positive correlation between tissue density and microdamage accumulation. We speculate that increased matrix mechanical properties due to mineralization may have been obscured by increased microdamage. Therefore, clinical dosing regimens should be chosen carefully to ensure adequate bone turnover.

Acknowledgements

Support for this work was received from NIH grants 2 PO1 AG05793-12, AR46225, and AR39239 and the Danish Health Research Council grant 9601833_lpa. Computing time was

provided by The Netherlands Computing Facility. Jacqueline van der Linden was supported by the Dutch Foundation for Research (NWO/MW). The authors wish to thank Mary Hooser, Diana Jacob, and Thurman Alvey for histological preparation, Jian-Hua Hu for preparation of the samples for mechanical testing, and Paul Mulder of NIHES for statistical assistance. Merck and Co., Inc. and Procter and Gamble Pharmaceuticals Inc. kindly supplied the bisphosphonates.

Chapter 6

The parallel plate model for trabecular bone exhibits volume fraction dependant bias

J.S. Day, M. Ding, A. Odgaard, D.R. Sumner, I. Hvid and H. Weinans

Abstract

Unbiased stereological methods were used in conjunction with micro computed tomographic (microCT) scans of human and animal bone to investigate errors created when the parallel plate model was used to calculate morphometric parameters. Bone samples were obtained from the human proximal tibia, canine distal femur, rat tail and pig spine and scanned in a microCT scanner. Trabecular thickness, trabecular spacing and trabecular number were calculated using the parallel plate model. Direct thickness, and spacing and connectivity density were calculated using unbiased three-dimensional methods. Both thickness and spacing calculated using the plate model were well correlated to the direct three-dimensional measures ($r^2 = 0.77-0.92$). The correlation between trabecular number and connectivity density varied greatly ($r^2 = 0.41-0.94$). While trabecular thickness was consistently underestimated using the plate model, trabecular spacing was underestimated at low volume fractions and overestimated at high volume fractions. Use of the plate model resulted in a volume dependant bias in measures of thickness and spacing ($p < 0.001$). This was a result of the fact that samples of low volume fraction were much more “rod-like” than those of higher volume fraction. In conclusion, our findings indicate that the plate model provides biased results, especially when populations with different volume fractions are compared. Therefore we recommend direct thickness measures when three-dimensional data sets are available.

Day JS, Ding M, Odgaard A, Sumner DR, Hvid I, Weinans H. Parallel plate model for trabecular bone exhibits a volume fraction-dependant bias. *Bone* 27(5):715-20(2000).

Introduction

Morphological properties of trabecular bone are often calculated by assuming that the structure consists of a series of parallel plates (166). Area fraction and bone perimeter are measured from histological sections. These values are then extrapolated into three dimensions using stereological principles to estimate volume fraction and surface area which are in turn used to calculate trabecular thickness (TbTh), trabecular spacing (TbSp) and trabecular number (TbN). A summary of the calculations involved is included in the appendix. Because the area fraction and bone perimeter can be obtained from standard histological sections this method is used widely. However, trabecular bone does not consist of plates, but is in fact a mixture of complex irregular geometries which can at best be approximated as plates and rods. As a result, trabecular thickness and trabecular spacing derived using the plate model are often smaller than when measured directly in three dimensions and may include other model-dependant biases (43, 45, 167).

During the past decade new methods have been introduced to obtain three-dimensional datasets of trabecular bone using serial sectioning (168), microCT (169) or MRI (170). New measures of three-dimensional architecture have accompanied these advances. The direct thickness method provides a model free measure of trabecular thickness (TbTh*) and trabecular spacing (TbSp*) (45). Using a three-dimensional representation of the trabecular architecture, a series of spheres is fit inside of either the bone or marrow phase. The largest sphere associated with each bone or marrow voxel is found and used to calculate a volume weighted average thickness or spacing. Histograms can also be created to show the distribution of these parameters providing further details about the 3D architecture (45).

Connectivity density can also be calculated directly from three-dimensional datasets using topological principles. The connectivity represents the number of connections which can be severed without separating the network. This is considered to be the number of trabeculae minus one in a topological sense (49). Connectivity density is simply the connectivity per unit of volume. The trabecular number, as calculated using the plate model, is simply the inverse of the centre to centre distance between parallel plates and is calculated as the ratio between volume fraction and trabecular thickness. This measure is not necessarily an alternative to connectivity density, but has been used as such.

In addition to the direct thickness method Hildebrand and Rueggsegger introduced another three-dimensional measure called the structure model index (SMI) which allows objective quantification of how “rod-like” or “plate-like” an object is (46). A three-dimensional data set is used to create a smooth model of the bone surface. Using this model the surface area, first derivative of surface area and volume are used to calculate the structure model index.

An object consisting purely of plates would have a structure model index of 0 and an object consisting purely of rods would have a structure model index of 3. Objects containing a mixture of elements would have intermediate values. In our previous research, we have noted that the structure model index has a strong negative correlation to the volume fraction (171). This relation was also noted in a study of 4 sites in the human body (172). We were concerned that this change of structure type within bone samples of varied volume fraction could influence the histomorphometric parameters obtained using the plate model. The purpose of this work was to use unbiased three-dimensional methods to investigate the errors produced using the plate model with various types of bone samples.

Methods

Data were collected from four studies of trabecular architecture in the i) human proximal tibia, ii) canine distal femur, iii) rat vertebra and iv) porcine lumbar spine. Human samples were acquired during a research project investigating the effects of aging in the proximal tibia (173). Forty samples were acquired from donors aged from 16 to 85 years. Samples were drilled out from the tibial condyles using a trephine with an inner diameter of 7.5 mm. They were cut 1 mm beneath the subchondral bone plate and again at the distal end to create a 7.5 mm long sample. Canine distal femur samples were collected from 38 dogs aged from 14 to 167 months. All canine samples were harvested from the femoral intercondylar fossa using a 9.5 mm trephine then cut to a length of 10mm. The first three tail vertebrae were collected from 8 rats of age 6 months. These vertebrae were scanned intact. Eleven L3 lumbar vertebrae were harvested from 6 month old pigs. The vertebrae end plates and facets were removed and a brick shaped sample was cut from the trabecular core.

Specimens were scanned using a CT scanner with a maximum resolution of 20 μm (μCT 20 Scanco Medical AG., Zürich Switzerland). Scanning resulted in cubic voxels with 22, 26, 11 and 30 μm edge lengths for the human, canine, rat and pig samples respectively. After scanning, the data sets were segmented using thresholds which were determined experimentally (63). Because the rat vertebrae were scanned intact, the trabecular core was digitally separated from the cortical shell by manually outlining the contour of the boundary in each specimen. A triangularized three-dimensional virtual object was created from the resulting voxel data. This object was used to determine the surface area of the trabecular bone. Trabecular thickness (Tb.Th), trabecular spacing (Tb.Sp) and trabecular number (Tb.N) were determined for all samples using the plate model. Bone volume fraction (Vv), direct trabecular thickness (Tb.Th*) and spacing (Tb.Sp*), connectivity density (CD) and structure model index (SMI) were calculated directly from the three-dimensional data set.

Unbiased quantification of the connectivity required splitting the data set in order to avoid edge artifacts (49). This method has been described previously (173). In short, the dimensions of the data set are reduced by approximately 0.4 mm to create a smaller inner cylinder and an outer shell. The Euler number of the original set, the smaller cylinder and the outer shell are calculated and the Euler number of the interface is defined as the difference between the Euler number of the original object and the sum of the two smaller objects. Half of the connectivity of the interface is added to that of the inner cylinder before calculating the connectivity density of the cylinder. The entire data set was used to calculate all other parameters.

Statistical analyses were performed using a statistical software package (SPSS, SPSS Inc. Chicago, Illinois). Linear regression models were used to determine how well the model-based parameters were correlated with the direct three-dimensional measurements. In order to determine whether volume fraction related changes in the structure type caused a bias in the plate model results, regression models were made for each of the parameters vs. the volume fraction and the ratio of the model-based/directly measured parameters vs. volume fraction. Differences in the slopes and intercepts in the two methods were evaluated using the 95% confidence intervals. Stepwise linear regression was used to determine whether trabecular number was correlated to connectivity density after controlling for volume fraction.

Results

The model-based thickness (Tb.Th) and directly measured thickness (Tb.Th*) were well correlated as were the two measures of trabecular spacing (Tb.Sp, Tb.Sp*). However, the correlation between trabecular number (Tb.N) and connectivity density (CD), while reasonable in the dog and pig, was low in humans. A summary of the regression analyses is displayed in Table 6.1.

The model-based trabecular thickness was consistently smaller than the directly measured thickness. The slopes of the two were not different when plotted against the volume fraction and the intercepts were different in the human and dog only. For trabecular spacing, the slopes and intercepts were different for the human and dog when plotted against the volume fraction. For the pig only the intercept was significantly different and for the rat there were no significant differences (Figure 6.1).

In order to further investigate the difference between the results from the plate model and the direct thickness method, the ratio of the two thickness measures and the ratios of the two spacing measures were plotted against the volume fraction (Figure 6.2A, B). There was a

		dog	human	pig	rat
Tb.Th vs. Tb.Th*	slope	0.87	0.92	1.14	1.16
	intercept	-0.02	-0.04	-0.04	-0.02
	r^2	0.84	0.88	0.92	0.83
	$p <$	0.001	0.001	0.001	0.001
Tb.Sp vs. Tb.Sp*	slope	1.39	1.47	1.69	0.79
	intercept	-0.22	-0.22	-0.36	0.02
	r^2	0.77	0.80	0.78	0.75
	$p <$	0.001	0.001	0.001	0.001
Tb.N vs CD	slope	0.05	0.09	0.07	N.A.
	intercept	1.20	1.29	1.18	N.A.
	r^2	0.75	0.41	0.94	N.A.
	$p <$	0.001	0.001	0.001	N.A.

Table 6.1: Regression of the correlation between the 2D and 3D parameters. The p value indicates the two-tailed probability that the slope of the regression line is not equal to zero.

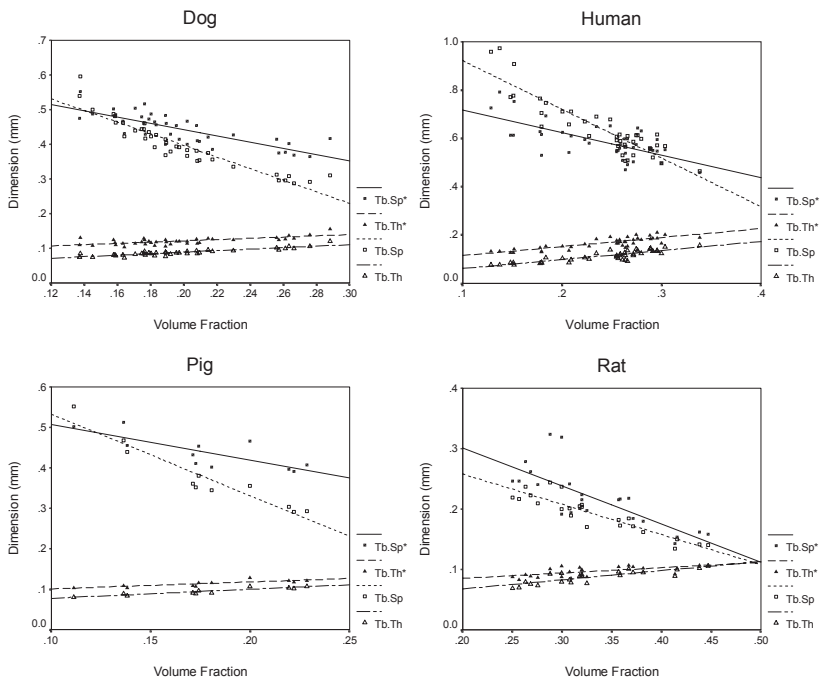


Figure 6.1: 2D and 3D parameters plotted against varying volume fraction. Trabecular thickness was consistently underestimated by the plate model. For trabecular spacing the plate model overestimated spacing at low volume fractions but underestimated as the volume fraction increased.

		dog	human	pig	rat
Tb.Th/Tb.Th* vs. Vv	slope	0.67	0.75	0.76	0.70
	intercept	0.60	0.49	0.70	0.67
	r ²	0.68	0.48	0.79	0.75
	p <	0.001	0.001	0.001	0.001
Tb.Sp/Tb.Sp* vs. Vv	slope	-1.98	-1.59	-0.28	-0.11
	intercept	1.29	1.46	1.34	0.93
	r ²	0.76	0.78	0.91	0.03
	p <	0.001	0.001	0.001	N.S.
Tb.N/CD vs. Vv	slope	-0.24	-0.06	-0.81	N.A.
	intercept	0.18	0.28	0.30	N.A.
	r ²	0.15	0.00	0.89	N.A.
	p <	0.05	N.S.	0.001	N.A.

Table 6.2: Regression of the volume fraction dependant bias. The *p* value indicates the two tailed probability that the slope of the regression line is not equal to zero.

significant relation in all cases (Table 6.2). This trend did not always exist for the trabecular number/connectivity density ratio (Figure 6.2C).

Although the one-dimensional trabecular number is not directly comparable to the three-dimensional connectivity density there was a moderate correlation between these parameters (Table 6.1). Stepwise linear regression indicated that prediction of the connectivity density was significantly increased when the trabecular number was added to a model of volume fraction alone ($p < 0.05$).

As was the case in our previous studies, there was a strong inverse relation between structure model index and volume fraction (Figure 6.3).

Discussion

In this work we have shown that there is a volume fraction dependant bias in the morphometric parameters determined using the plate model. A similar bias has previously been noted in a two-dimensional comparison of directly measured and model-based thickness (167). As illustrated by the nearly parallel regression lines in Figure 6.1, there was a consistent difference up to 40 microns between the model-based and directly measured trabecular thickness, independent of volume fraction. Hildebrand et.al (172) have previously reported that the plate model underestimates trabecular thickness. This finding has been repeated in our study.

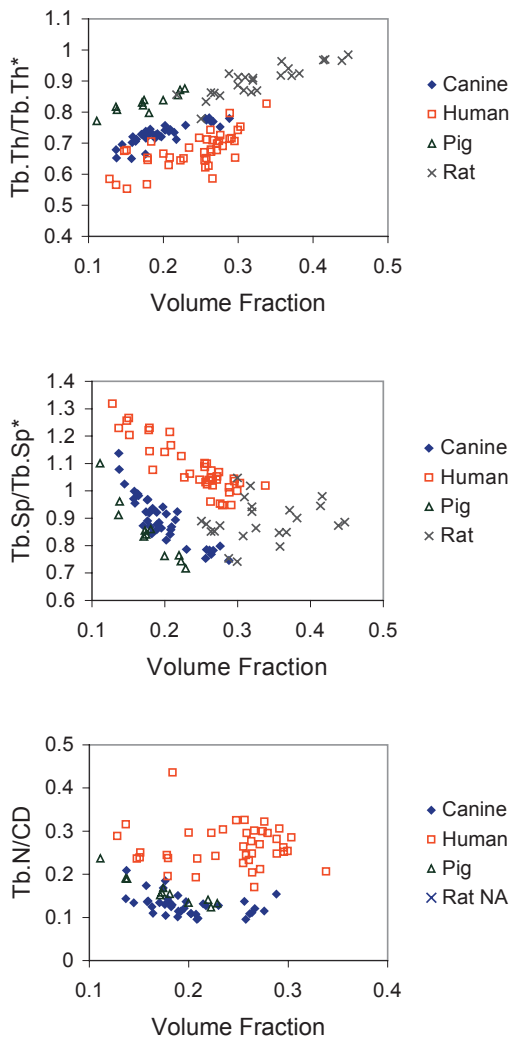


Figure 6.2: Illustration of volume fraction dependant bias in trabecular thickness, spacing and trabecular number. The ratio between the model-based and directly measured parameters were plotted against the volume fraction.

However, the magnitude of the increase in thickness relative to increased volume fraction was similar for both the two-dimensional and three-dimensional methods. This could be problematic if changes in thickness measured using the plate model are interpreted as percentages of the original thickness. In this case, use of the plate model would result in exaggerated relative changes in thickness. This is clearly illustrated in Figure 6.2. The relation between model-based and directly measured trabecular spacing was not as simple as for thickness. Plate model spacing was neither consistently underestimated nor overestimated (Figure 6.1).

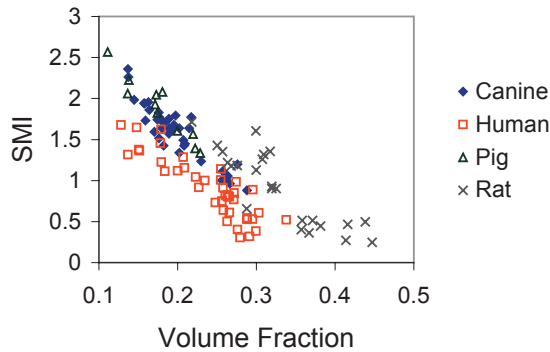


Figure 6.3: Structure model index was plotted against the volume fraction. A material composed of ideal rods would have a structure model index of 3 whereas a structure composed only of plates would have a structure model index of 0. There was a strong negative correlation between structure model index and volume fraction.

The difference in the slopes of the regression lines resulted in the volume fraction dependant bias, which is illustrated in Figure 6.2.

In order to use model-based methods to determine morphological parameters, assumptions must be made about the structure of the material. Although the plate model can be modified for use with rod-like or plate-like materials, the model type cannot be used effectively when materials are composed of an unknown proportion of plates and rods. It is the requirement for a fixed model type that leads to bias in the model. By using the structure model index to measure how “rod-like” or “plate-like” the samples used in this study were, the mechanism responsible for bias in the plate model could be demonstrated (Figure 6.3). Structure model index had strong inverse relation to volume fraction i.e. as the volume fraction increased the structure model index decreased indicating that the material was more plate-like. The inverse relation between structure model index and volume fraction may be due to the perforation of trabecular plates during resorption. As plate-like trabeculae are perforated, they become more rod-like and present a higher surface area. Thus, their trabecular thickness is systematically underestimated using the plate model. The converse is true when using a rod based model. As volume fraction increases there are more plate-like structures whose thickness is systematically overestimated. The strong relation between structure model index and volume fraction has been noted in previous three-dimensional studies of trabecular architecture (171, 172).

Connectivity is a measure of number of branches in the trabecular network that may be cut without separating the structure. As a topological property, connectivity density can not be measured using 2D data. However, the trabecular number and connectivity density, or connectivity per unit volume, were significantly correlated. This has been demonstrated

previously (49). There was no significant volume fraction related bias in the ratio of the two connectivity measures. Stepwise regression analysis indicated that the trabecular number was a better predictor of connectivity density than volume fraction alone, in particular for the canine bone. This would indicate that the trabecular number does have some utility in estimating the connectivity density. However, the use of connectivity as a measure of bone quality is a hotly debated subject (174-176).

Although unbiased 3D methods have been presented in the literature, model-based methods are still commonly used to examine 3D data sets (177-180). Where three-dimensional data are available only direct unbiased methods should be used to measure histomorphometric parameters.

In this work, we have chosen to use the direct thickness measure (45) as a “gold standard.” This method calculates a volume weighted average thickness from a three-dimensional data set and assigns heavier weighting to larger trabeculae. It is possible that thin trabeculae form the “weak link” in terms of the mechanical properties of the structure. Another possibility for weighting includes skeletonizing the trabecular structure and calculating the thickness at regular intervals along the branches. This produces a length-weighted measure of trabecular thickness and has been used in a two-dimensional study of trabecular bone (181).

The results presented in this work are from a small number of selected locations and do not represent the full range of volume fractions seen in the body. In the samples investigated there was a strong negative correlation between volume fraction and the structure model index. This indicates that bone becomes more “rod-like” at lower volume fractions and that this trend is quite predictable. If true, one may be tempted to make a generalized correction to the plate model such that it can be adjusted to more accurately represent the direct thickness. One may try to justify this correction by the high correlation between the direct and model-based methods. However, our results varied with the species investigated and may be further affected by the scanning resolution. Additionally, it must be stressed that this relation may not be valid for diseased bone. Thus, a generalized correction to the plate model is not appropriate for the study of pathologic states or drug treatments.

The plate model is commonly used in studies where changes in trabecular morphology are examined in the presence of changes in volume fraction. This is true for studies of aging (54, 182-184), osteoporosis (185, 186), osteoarthritis (100), the effect of electromagnetic fields (187) and many others. Because of the convenience and relatively low expense of two-dimensional histomorphometry its use will probably continue in the future. When conventional two-dimensional histomorphometry is used to measure the trabecular morphology care must be taken when interpreting the results. It must be remembered at all times that

the only parameters that are truly measured using this method are the bone perimeter and bone area. A reported change in trabecular thickness may be simply the result of a change in volume fraction. Conversely it may be the result of a change in structure type of the specimen. The only way to determine whether there are pathological changes in bone structure which are different than the normal change associated with a change in volume fraction would be to plot the surface/volume ratio against the volume fraction and determine whether there was a difference in the regression lines.

The use of model-based methods requires that adjustments must be made for both the structure type and anisotropy of the material (see appendix). In anisotropic structures the orientation of the cutting-plane can seriously influence the measured parameters. Object dimensions vary greatly depending on whether they are viewed from a direction perpendicular or parallel to the principal axis of anisotropy (188). Thickness, as calculated using the plate (or rod) model is the ratio of perimeter to area and nothing more. Correcting for anisotropy as well as the choice of a plate model, rod model or a combination of the two requires *a priori* knowledge of the structure of the sample. Thus, the conversion to trabecular thickness simply provides a conceptual tool that is useful for the interpretation of the data. The calculations of trabecular number and trabecular spacing are extensions of this conceptual tool, fraught with the same limitations. Thickness will be underestimated using the plate model and there will be volume fraction dependant biases, especially in the estimation of trabecular spacing. The trabecular number provides only a rough estimate of the true connectivity but is free of volume fraction dependant bias. It is not possible to predict the effects of disease or new drug treatments upon the model assumptions and therefore we do not see a possibility for a generalized correction for these model-based parameters.

Acknowledgements

Funding for this work was received from NIH grants AR14685 and AR42862 and the Danish Health Research Council grant 9601833_lpa. The author's would like to thank Aivars Berzins for preparing canine femoral samples, Hans Gregersen and Jingbo Zhao for contributing rat vertebrae and Wolf Drescher for the pig vertebrae. The research of Harrie Weinans has been made possible by the Netherlands Royal Academy of Arts and Sciences.

Appendix: Formulas for morphometric parameters

$$BV/TV = B.Ar/TA$$

$$BS/BV = B.Pm/B.Ar * 4/\pi^*$$

Plate Model (166)

$$Tb.Th = 2/(BS/BV)$$

$$Tb.N = (BV/TV)/Tb.Th$$

$$Tb.Sp = (1/Tb.N) - Tb.Th$$

Rod Model

$$Tb.Dm = 4/(BS/BV)$$

$$Tb.N = (4/\pi * BV/TV)^{0.5} / Tb.Dm$$

$$Tb.Sp = Tb.Dm * ((\pi/4 * TV)/BV)^{0.5} - 1$$

* The value $4/\pi$ (1.27) can be modified to correct for anisotropy in specimens. A value of 1.2 has been experimentally determined for use in the human ilium.

Chapter 7

Inter-individual and inter-site variation in human trabecular bone morphometry

J.S. Day, J.H. Waarsing, G.H. van Lenthe, M. Stauber, P.G. Mulder, J.A.N. Verhaar, D.R. Sumner, and H. Weinans

Abstract

While bone mass is a major predictor of the mechanical properties of trabecular bone it is believed that trabecular micro-architecture is also important. The effect of anatomic site and individual donor on trabecular micro-architecture was examined, independent of bone mass, using micro-CT and unbiased three-dimensional morphometric parameters. This study was comprised of two donor populations. In the first group samples were harvested from 70 donors from the following sites: L2, L4, femoral head, iliac crest and calcaneus. In the second group approximately 15 samples were harvested from the proximal tibia and 2 from the talus of 35 donors. All samples were micro-CT scanned and the BV/TV, BS/BV, Tb.Th, Tb.Sp, Tb.N, connectivity density and degree of anisotropy were measured. A random coefficients model was used to evaluate the relations of the measured parameters with BV/TV allowing for inter-individual variability and inter-site differences while adjusting for age, gender and the presence of fractures. All of the measured parameters showed strong relations with BV/TV with the exception of the degree of anisotropy. Different individuals displayed remarkably different trabecular micro-architecture even at the same BV/TV. Anatomic site also had a strong effect on the relation between micro-architecture and BV/TV. Gender, age and previous fracture were significant confounders. Inter-site differences were present in all parameters except the degree of anisotropy. The control of trabecular bone micro-architecture is not simply a function of BV/TV but is also strongly influenced by inter-subject variation and the anatomic site.

Introduction

Osteoporosis, and its association with an increased risk of bone fracture is a growing source of concern within most industrialized countries. Anatomic sites with the highest risk of osteoporotic fracture include the distal radius, spine and proximal femur. Osteopenia and osteoporosis, as defined by the World Health Organization, are the presence of a bone mineral density (BMD) of respectively 1.0 and 2.5 standard deviations below the population average for healthy young persons of the same gender. While fracture risk is increased by two to three times for each standard deviation below peak young adult mean bone mass, there is a large overlap in bone mass between patients who experience fractures and those who don't (26). This observation has led to the concept that fracture risk is not only a function of bone mass alone but also bone quality. Bone quality is, in essence, a term that encompasses all of the properties of the bone that contribute to the mechanical properties with the exception of bone mass (i.e. micro-architecture, matrix quality, presence of micro-damage etc). The concept that fracture risk is related not only to bone mass (quantity) but also to micro-architecture is supported by in vitro mechanical testing where it has been demonstrated that the mechanical properties of bone are not only a function of bone mass but also trabecular micro-architecture (55, 171, 189-191). Currently, the most common and practical method of estimating fracture risk in the spine and hip is through the use of dual energy x-ray absorptiometry (DXA). Unfortunately, this method gives only BMD without any measurement of bone micro-architecture or quality. For this reason, other methods such as pQCT or ultrasound have been developed in order to produce a combined measure of bone mass and quality. These methods are, however, most practical when used to measure peripheral sites such as the wrist (humerus) or ankle (calcaneous). Thus the consistency of bone mass and quality between anatomic sites becomes a clinically relevant issue.

Recent advances in desktop micro computed tomography (micro-CT) have made it possible to quickly quantify the three-dimensional (3D) micro-architecture of bone biopsies. Morphometric parameters can be calculated directly from 3D datasets, which do not require model related assumptions and are not biased by specimen anisotropy. Parameters that are often reported include the direct trabecular thickness, spacing and number (Tb.Th^{3D}, Tb.Sp^{3D}, Tb.N^{3D}) (45), connectivity density (CD) (49), structure model index (SMI) (46), and various measures of trabecular anisotropy (43, 44, 192). The direct thickness method is conceptually similar to the plate model originally proposed by Parfitt et al (54). However, because the plate model was originally used on histological sections an assumption had to be made *a priori* as to whether the structure of the bone consisted of rods or plates. This assumption leads to a bias in the resulting measurements and constrains the possible solution space (172, 193). The direct thickness method has the advantage that it is not necessary to make any assumptions regarding the structure of the material. Connectivity density and structure model index are

topological measures of the curvature of the bone surface and give information regarding how interconnected the trabecular micro-architecture is (47). The structure model index, which is similar to the two-dimensional trabecular bone pattern factor (TBPf) (194), is defined in such a way that it describes how ‘plate-like’ or ‘rod-like’ a structure is. Structural anisotropy can be measured in a variety of ways that quantify the preferential orientation of either surfaces or volumes. The resulting data can be fit to an ellipsoid that is reported as the fabric tensor. The ratio of the largest to smallest radii of the resulting ellipsoid is used to quantify the degree of anisotropy (DA) of the specimen.

It is known that many morphometric parameters such as trabecular thickness, structure model index and connectivity density are highly correlated with the bone volume fraction (193, 195, 196). Therefore, much of the correlation of the micro-architectural parameters between sites can be explained by the correlation of bone mass between sites. However, little is known about how the relation between bone volume fraction and bone micro-architecture varies between anatomic sites or whether different individuals use different architectural ‘strategies’ for similar BMD *i.e.* do some individuals have thicker, thinner, or more trabecula yet the same BMD or BV/TV. For that reason, the purpose of the present study was to investigate how bone morphometry varies both between people and between anatomic sites. A particular focus was placed on investigating the variation in bone morphometry over a range of BV/TV. The following specific questions were investigated: 1) Is there a difference between individuals in the utilization of available bone? 2) Is there a difference between anatomical sites? 3) Are inter-individual differences consistent between anatomic sites?

Materials and Methods

Donor populations

Approximately 15 trabecular bone specimens were cut from one proximal tibia and 2 from one talus of each of 35 donors supplied by the Gift of Hope (GOH) Organ and Tissue Donor Network (male: $n = 18$, $\text{age}_{\text{mean}} = 65$ $\text{age}_{\text{sd}} = 12$; female: $n = 17$, $\text{age}_{\text{mean}} = 67$ $\text{age}_{\text{sd}} = 12$). This population included both intact and osteoarthritic donors. Osteoarthritic grade was scored using a modified Collins Grading system (197). Tibial samples were prepared by cutting a transverse bone slab from the proximal end of the tibia. The first cut was taken immediately distal and parallel to the subchondral bone plate at the proximal aspect of the tibial tuberosity. The thickness of the slab was scaled to 16% of the medial-lateral width of the tibia resulting in thicknesses that varied between 10-14mm. A rectangular grid of 7.5mm cylindrical specimens was then drilled from this slab using a diamond core drill. This grid contained rows of 3 samples in the anterior-posterior direction and rows of 5 samples in the medial lateral direction, yielding ~15 samples per donor. Talar samples were drilled through the

entire thickness of the talus ventral and dorsal to the talar dome. The central portion of the core was trimmed to the same length as the tibial samples.

A second set of human trabecular bone specimens was obtained from the European Union BIOMED I Concerted Action "Assessment of Bone Quality in Osteoporosis" sample. This population has been previously described in detail (198). Briefly, trabecular bone samples originated from 70 human cadavers with ages ranging from 23-92 years (male: $n = 38$, $age_{mean} = 67$ $age_{sd} = 15$; female: $n = 32$, $age_{mean} = 73$ $age_{sd} = 15$). For the present study, 242 specimens from the right femoral head (FRA), center of the second lumbar vertebral body (L2B) and fourth lumbar vertebral body (L4B), calcaneus (CAB), and anterior-superior part of the iliac crest were used (ICF). Samples were excluded if they contained compact bone, could not be harvested in one piece or contained large voids.

Micro-CT analysis

Specimens were scanned in one of two high-resolution micro-tomographic systems. GOH specimens were scanned at a nominal resolution of $20\mu\text{m}$ ($\mu\text{CT 40}$, Scanco Medical AG.) and the entire biopsy core was used for the subsequent analysis. A low-pass gaussian filter was used to remove noise before segmenting the gray scale images using individual thresholds as determined using Archimede's principle (63). BIOMED specimens were scanned at a nominal resolution of $14\mu\text{m}$ ($\mu\text{CT 20}$, Scanco Medical AG.) and a 4mm cubic volume of interest was chosen for further analysis. A low-pass gaussian filter was used to remove noise before segmenting the gray scale images using a fixed threshold.

Segmented data were then analyzed using 3D morphometry software (IPL © Scanco Medical AG). The following parameters were included in the present analysis: bone volume fraction (BV/TV), bone surface over bone volume (BS/BV), structure model index (SMI), connectivity density (CD), direct trabecular thickness (Tb.Th^{3D}), direct trabecular spacing (Tb.Sp^{3D}) and direct trabecular number (Tb.N^{3D}). The geometrical degree of anisotropy (DA) was also determined from the ratio between the maximal and minimal eigenvalues of the fabric tensor.

Statistical analysis

Analyses were performed on each dataset separately using PROC MIXED (random coefficients model) in SAS (version 8.2). The use of this type of model was appropriate because of the presence of both fixed and random effects. Generally, fixed effects are defined when all levels of interest of a variable are included in the study. For example, in the current study, gender was considered a fixed effect with two levels, male and female. Random effects occur where a limited number of possible levels of a variable are observed in a study but the results are generalized to a level that is not observed. In the current study, it was presumed that the

general population of all possible donors was represented by those that were included in the current sample. Therefore, donor was included as a random effect and the results were generalized in a probabilistic manner to the population of all possible donors. In order to aid in the interpretation of the model we used adjusted means for the explanatory variables BV/TV and age. To estimate adjusted means, BV/TV and age were transformed into deviations from their overall means and the intercept was removed from the random coefficients model (i.e. $\text{age}_{\text{reparameterized}} = \text{age} - \text{age}_{\text{mean}}$). At this point, the outcome (dependant) variable after log transformation where appropriate, was assumed to have a linear relationship with BV/TV within each subject. The intercepts and slopes were assumed to have a bivariate normal distribution between donors (random variable). The within-subjects residual term was assumed to have the same variance across all subjects. The other explanatory variables (gender, anatomic location, age, and presence of osteoarthritis or a fracture) as well as their interaction with BV/TV were assumed to have a fixed effect on the outcome variable. Non-significant terms were removed from the model in a hierarchical way, one variable at a time starting with the highest p -value above 0.05 using a t-test for the estimated fixed effect. The suitability of the random coefficients was assessed by performing a likelihood ratio Chi-Squared test comparing a model in which the coefficients were fixed to a model in which the two coefficients (intercept and slope) were normally distributed between subjects. Using this Chi square test the null hypothesis was tested that the between-subject variance of intercepts and slopes and their covariance were simultaneously equal to zero.

Results

Generally, the two data sets produced similar results. Most of the morphometric parameters were strongly correlated with BV/TV (Figures 7.1 and 7.2). This relation was linear for all of the morphometric parameters except for BS/BV and Tb.Sp which exhibited negative power relations (convex shape) and were therefore log transformed (Table 7.1). Because the relation between CD and BV/TV was linear but heteroscedastic (variance increased with BV/TV), both variables were log transformed before any further statistical investigation. Pearson correlation coefficients of the resulting linearized data are displayed in Table 7.1. The overall relation between DA and BV/TV was weak ($r_{\text{BIOMED}} = 0.05$; $r_{\text{GOH}} = 0.35$). When examined on a site-by-site basis the Pearson correlation coefficient between DA and BV/TV had somewhat larger and negative values ($r_{\text{fra}} = -0.45$, $r_{\text{icf}} = -0.36$, $r_{\text{L2B}} = -0.43$, $r_{\text{L4A}} = -0.45$, $r_{\text{cab}} = \text{n.s.}$) except in the GOH tibia data where it was positive ($r_{\text{tibia}} = 0.45$, $r_{\text{tal}} = \text{n.s.}$).

The results of the regression analysis are summarized in Table 7.2 and Table 7.3. The significance of the coefficients from each model are displayed in Table 7.2 (i.e., which effects were significant) and select coefficients from the model are displayed in Table 7.3. These

	BV/TV	Parameter	r_{BIOMED}	r_{GOH}
BS/BV	Log	Linear	-0.84	-0.91
SMI	Linear	Linear	-0.93	-0.89
CD	Log	Log	0.43	0.77
Tb.N	Linear	Linear	-0.82	0.72
Tb.Th	Linear	Linear	0.81	0.86
Tb.SP	Log	Log	-0.70	-0.74
DA	Linear	Linear	0.05	0.35

Table 7.1: Pearson correlation between each morphometric parameter and bone volume fraction treating each sample as an independent measure. Where relations were not linear, the BV/TV and/or the variable in question was log transformed as indicated.

coefficients, divided into fixed effects, inter-individual effects and the intra-individual residual should be interpreted as follows; the fixed effect of ‘BV/TV’ is the mean slope of each parameter plotted against the BV/TV. Because we reparameterized the data, the fixed effect ‘intercept by site’ can be interpreted as the expected value of the parameter at each site for a sample with the mean BV/TV from a donor with mean age (mean values: $\text{BV/TV}_{\text{BIOMED}} = 0.138$, $\text{age}_{\text{BIOMED}} = 69.1$, $\text{BV/TV}_{\text{GOH}} = 0.124$, $\text{age}_{\text{GOH}} = 65.9$). In a similar manner the ‘interaction by site’ can be interpreted as the modification of the mean slope due to anatomic site. Because the inter-individual donor effect was modeled using random coefficients there is not a simple fixed modification of the intercept or slope due to the donor. Instead, the expected standard deviation of the mean slope and intercept due to the variation in the donor population was calculated. Because the data had been reparameterized, the magnitude of the donor effect could be quickly evaluated by comparing the standard deviation of the intercept due to inter-individual effects to the residual intra-individual variance. This comparison, in essence, gives the variability of the parameter of interest for a sample with mean BV/TV from a donor with mean age compared to the residual variation after adjusting for gender and disease status. To further aid in the interpretation of the data we will present an example using the relation between SMI and BV/TV from the BIOMED donor population. This relation was linear (Table 7.1) and varied significantly between individual donors. This relation varied between anatomic sites and there was interaction between site and BV/TV. There was no effect of gender, age, the presence of previous fractures or OA (Table 7.2B). The adjusted mean slope for the relation between SMI and BV/TV was -6.96 but this would vary from -4.96 to -8.96 if we considered 95% of the donor population (Table 7.3B: 2 standard deviations from the inter-individual effect). The mean value of the slope varied from -6.96 at L4 to -11.01 in the iliac crest (Table 7.3B: interaction by site). If we considered a sample with a BV/TV of 0.138 we would expect the SMI to vary from 0.9 ± 0.147 at the femur and iliac crest to 1.37 ± 0.147 at L4 (Table 7.3B: intercept by site \pm inter-individual effect). The magnitude of the variance

	Inter-Individual	BV/TV	Site	Site* BV/TV	Gender	Gender* BV/TV	OA	OA* BV/TV	Age	Age* BV/TV
BS/BV	<0.0001	<0.0001	n.s.	n.s.	0.001	n.s.	n.s.	n.s.	n.s.	n.s.
SMI	<0.0001	--	<0.0001	n.s.	--	0.0139	n.s.	n.s.	0.029	n.s.
CD	<0.0001	--	<0.0001	n.s.	0.0083	n.s.	n.s.	n.s.	--	0.0021
Tb.Th ^{3D}	<0.0001	<0.0001	<0.0001	n.s.	n.s.	n.s.	n.s.	n.s.	n.s.	n.s.
Tb.Sp ^{3D}	<0.0001	<0.0001	<0.0001	n.s.	0.0003	n.s.	n.s.	n.s.	n.s.	n.s.
Tb.N ^{3D}	<0.0001	--	--	<0.0001	0.0007	n.s.	n.s.	n.s.	--	0.0154
DA	<0.0001	--	--	<0.0001	0.0037	n.s.	n.s.	n.s.	n.s.	n.s.

Table 72A: GOH donor population.

	Inter-Individual	BV/TV	Site	Site* BV/TV	Gender	Gender* BV/TV	OA	OA* BV/TV	Fracture	Fracture* BV/TV	Age	Age* BV/TV
BS/BV	<0.0001	--	<0.0001	n.s.	n.s.	n.s.	n.s.	n.s.	0.041	n.s.	--	0.0001
SMI	<0.0001	--	--	<0.0001	n.s.	n.s.	n.s.	n.s.	n.s.	n.s.	n.s.	n.s.
CD	<0.0001	--	--	0.010	n.s.	n.s.	n.s.	n.s.	n.s.	n.s.	--	0.0008
Tb.Th ^{3D}	<0.0001	--	--	0.0009	n.s.	n.s.	n.s.	n.s.	0.052	n.s.	n.s.	n.s.
Tb.Sp ^{3D}	<0.0001	<0.0001	<0.0001	n.s.	n.s.	n.s.	n.s.	n.s.	0.017	n.s.	n.s.	n.s.
Tb.N ^{3D}	<0.0001	--	--	0.0085	n.s.	n.s.	n.s.	n.s.	0.030	n.s.	n.s.	n.s.
DA	0.0002	--	--	0.0013	n.s.	n.s.	n.s.	n.s.	n.s.	n.s.	--	0.011

Table 72B: BIOMED donor population.

Table 72: Significance of coefficients in the mixed random coefficients model. All predictors and their interaction with BV/TV were entered into the statistical model and removed in a backward hierarchical fashion beginning with the interaction terms. The final significance values of the t-test for each predictor are indicated in the table above. The suitability of the random coefficients model for the inter-individual effect was evaluated by performing a likelihood ratio Chi-squared test of the null hypothesis that between-subject variance of the intercepts and slopes and their covariance were simultaneously zero (n.s. indicates non-significant results, -- indicates results that were not reported because significant differences depend on the location of the zero point when in the presence of a significant interaction term).

	Fixed Effects				Inter-Individual			
	Main Effect	Intercept by Site		Interaction by Site		Covariance (Correlation)	Slope (St. Dev)	Residual (St.Dev)
		talus	tibia	talus	tibia			
BS/BV	-19.47	n.s.	n.s.	n.s.	n.s.	-0.201	2.259	1.334
SMI	-9.69	1.74	1.32	n.s.	n.s.	0.035	1.327	0.141
CD	0.60	0.75	0.68	n.s.	n.s.	0.143	0.110	0.072
Tb.Th	0.40	0.121	0.128	n.s.	n.s.	0.050	0.066	0.010
Tb.Sp	-0.29	-0.143	-0.111	n.s.	n.s.	0.162	0.050	0.029
Tb.N	3.06	1.39	1.24	-1.23	0	0.115	0.495	0.086
DA	4.78	1.68	1.77	-3.69	0	4.638	0	0.272

Table 7.3A: GOH Donor Population.

	Fixed Effects														
	Main Effect	Intercept by Site				Interaction by site (site*BV/TV)				Inter-Individual					
		calc	femur	iliac	L2b	L4a	calc	femur	iliac	L2b	L4a	Intercept (St.Dev)	Covariance (correlation)	Slope (St.Dev)	Residual (St.Dev)
BS/BV	-28.57	21.17	18.94	20.25	21.31	18.66	n.s.	n.s.	n.s.	n.s.	1.204	-0.649	1.977	1.865	
SMI	-6.96	1.23	0.90	0.90	1.25	1.37	-1.03	-0.03	-4.05	-1.13	0	0.147	0.036	1.000	0.186
CD	-0.050	0.75	0.56	0.67	0.89	0.66	0.01	-0.20	0.25	0.37	0	0.099	0.166	0.194	0.104
Tb.Th	0.63	0.13	0.16	0.14	0.15	0.17	-0.29	-0.30	-0.27	-0.11	0	0.012	-0.003	0.086	0.018
Tb.Sp	-0.33	-0.19	-0.10	-0.11	-0.16	-0.12	n.s.	n.s.	n.s.	n.s.	n.s.	0.033	0.168	0.053	0.013
Tb.N	3.11	1.47	1.10	1.30	1.48	1.22	0.26	1.18	1.63	2.04	0	0.086	0.062	0.620	0.107
DA	-0.73	1.56	1.56	1.36	1.18	1.30	1.87	0.81	0.58	-0.52	0	0.043	0	0	0.095

Table 7.3B: BIOMED Donor Population.

Table 7.3: Select coefficients from the mixed random coefficients model. The data in the table above should be interpreted as follows; the coefficient Main Effect indicates the adjusted slope of the relation between each parameter and BV/TV. Because the data were reparameterized, the Intercept by Site simply indicates the expected value of each parameter at the anatomic site of interest for a sample with mean age and BV/TV. The interaction by site indicates the modulation of the main effect for each anatomic site. The Inter-Individual Intercept indicates the expected deviation due to inter-donor differences for a sample with mean age and BV/TV. The Inter-Individual Slope indicates the modulation of the main effect due to inter-donor differences. The Covariance term indicates the correlation between the Inter-Individual Slopes and Intercepts. Note that the BS/BV, Tb.Sp and connectivity density relations have been log transformed

explained by the individual donor was about 62% compared to the magnitude of the residual variation ($0.147^2/0.186^2$).

The relation between the morphometric parameters and bone volume fraction was similar for all donors with respect to sign. However, there were strong inter-individual effects for all of the parameters (Table 7.2, donor effect). These inter-individual effects can be visualized most easily in the GOH tibia data where there are multiple specimens for each donor from a single anatomic site. In order to illustrate the inter-individual effect we have plotted the results of four donors from the present data on top of the population (Figure 7.2). It is obvious that Donors 1 and 2 had a much more rod-like, highly connected structure than Donors 3 and 4, even at equal bone volume fractions. This can be confirmed visually by examining three-dimensional renderings of a selection of core biopsies from the same donors (Figure 7.3). In order to evaluate the magnitude of the inter-individual differences we compared the inter-individual variance of the intercept to the residual variance (using the squares of the standard deviations from Table 7.3). In the GOH data the individual effect varied from a low of 0.16 times the residual variance for the degree of anisotropy to a high of 1.7 times the residual variance for the trabecular spacing with all other parameters falling between 0.64 and 1.7 times the residual. Similar results were seen in the BIOMED data where the ratio varied between 0.20 for the degree of anisotropy to 6.44 for the trabecular spacing with all of the other parameters falling between 0.42 and 0.91.

Like the inter-individual data, the site-specific relations between bone volume fraction and the other parameters were similar between sites with respect to sign. However, there were site-specific differences, especially for the connectivity density, Tb.Sp and Tb.N (Figure 7.1). These site-specific differences were significant for either the fixed effect or its interaction with BV/TV for all parameters with the exception of the BS/BV in the GOH data (Table 7.2) and Tb.Th in the BIOMED data. The most obvious example of this site dependant effect was seen in the femoral head where the structure had a wider spacing, was more rod-like as expressed by a higher structure model index and had a lower connectivity than would be expected for bone with this volume fraction compared to the other sites (Figure 7.1).

As stated previously, the relation between each parameter and the bone volume fraction was adjusted for possible confounding due not only to the anatomical site, but also to gender, age, and disease status. Gender had significant effects in the GOH data on all parameters with the exception of Tb.Th. To illustrate this effect an example plot has been presented for Tb.Sp in Figure 7.4. This effect was not seen in the BIOMED data (Table 7.2). The presence of osteoarthritis had no effect on either dataset (Table 7.2), but the presence of fracture was a significant confounder for multiple parameters in the BIOMED data. An example of this

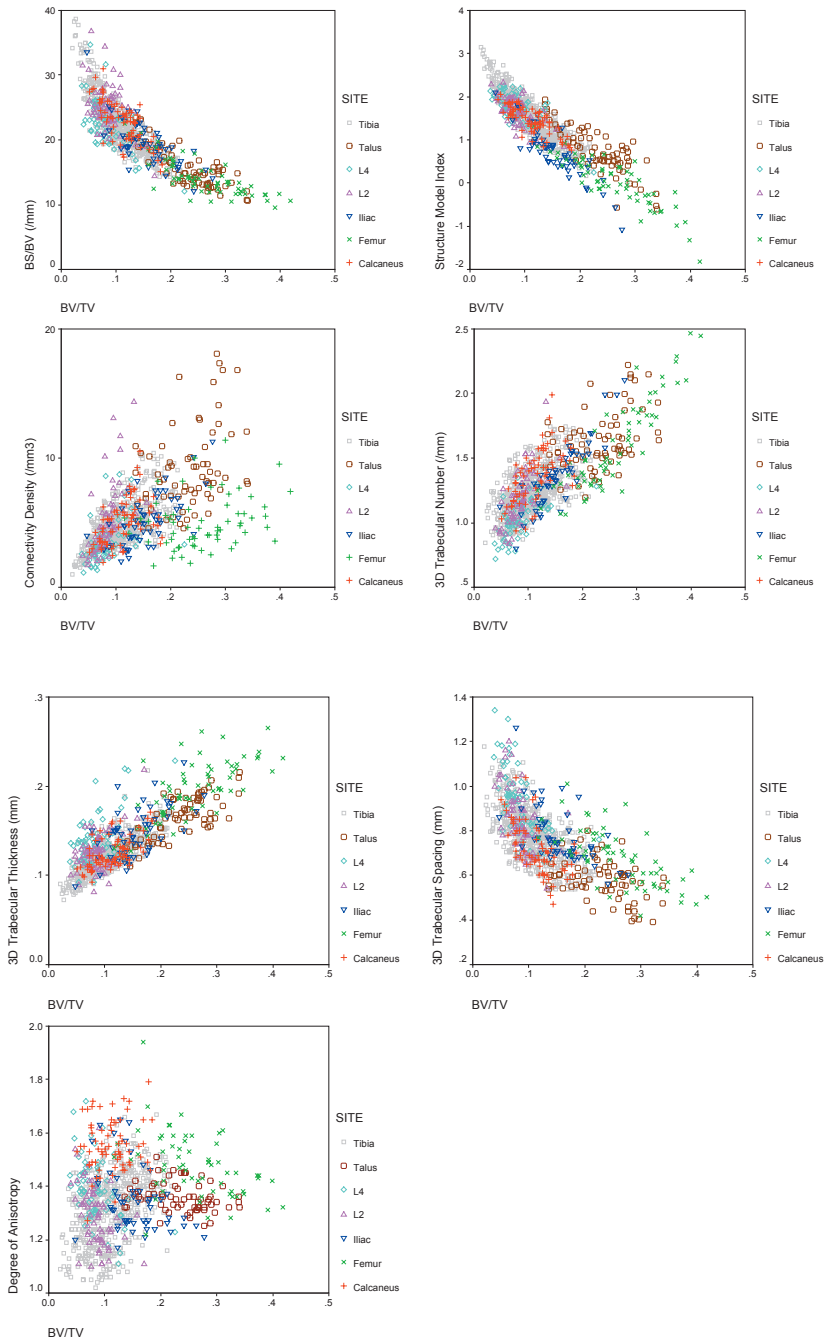


Figure 7.1: An illustration of site-dependent effects. Morphometric parameters were plotted against BV/TV for all of the biopsies.

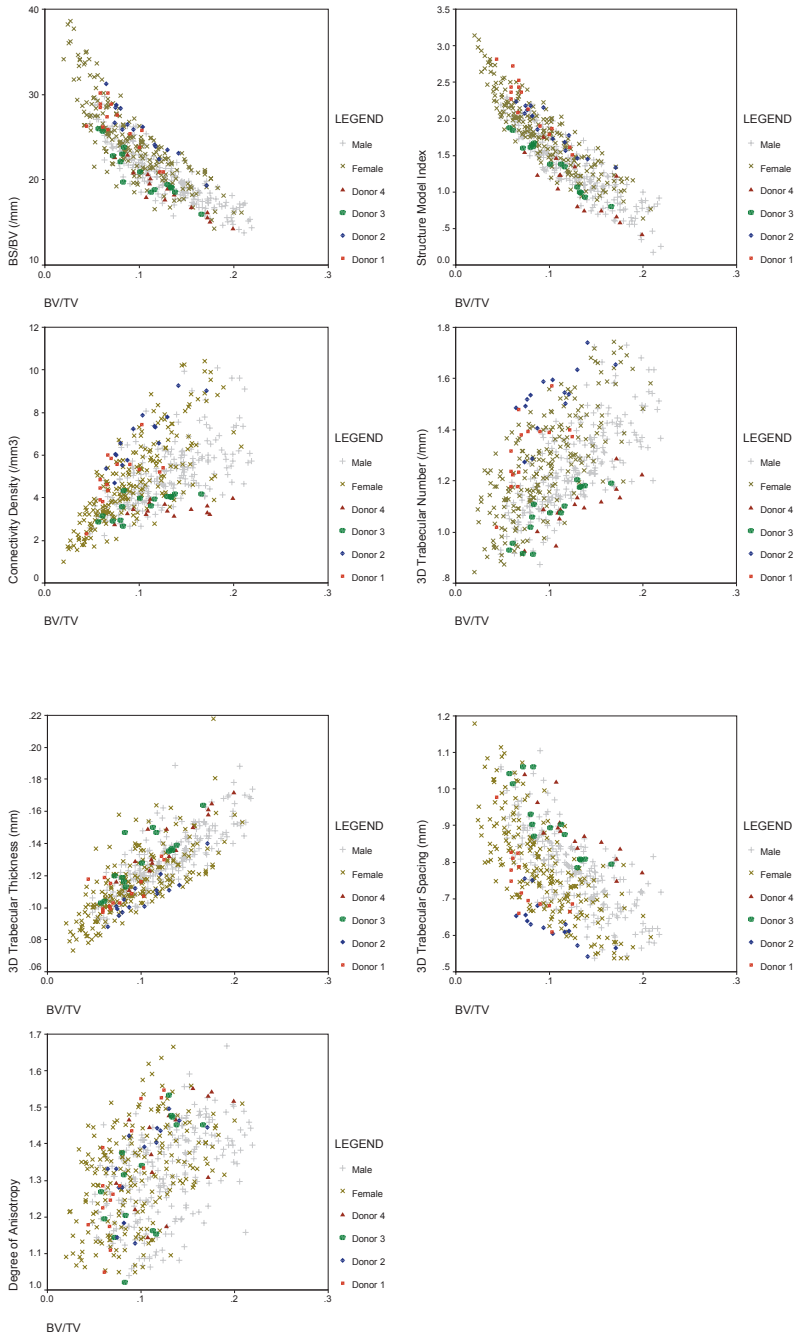


Figure 7.2: An illustration of inter-individual effects. Morphometric parameters were plotted against BV/TV for multiple biopsies from the proximal tibia. Four extreme donors were selected and plotted on top of the population.

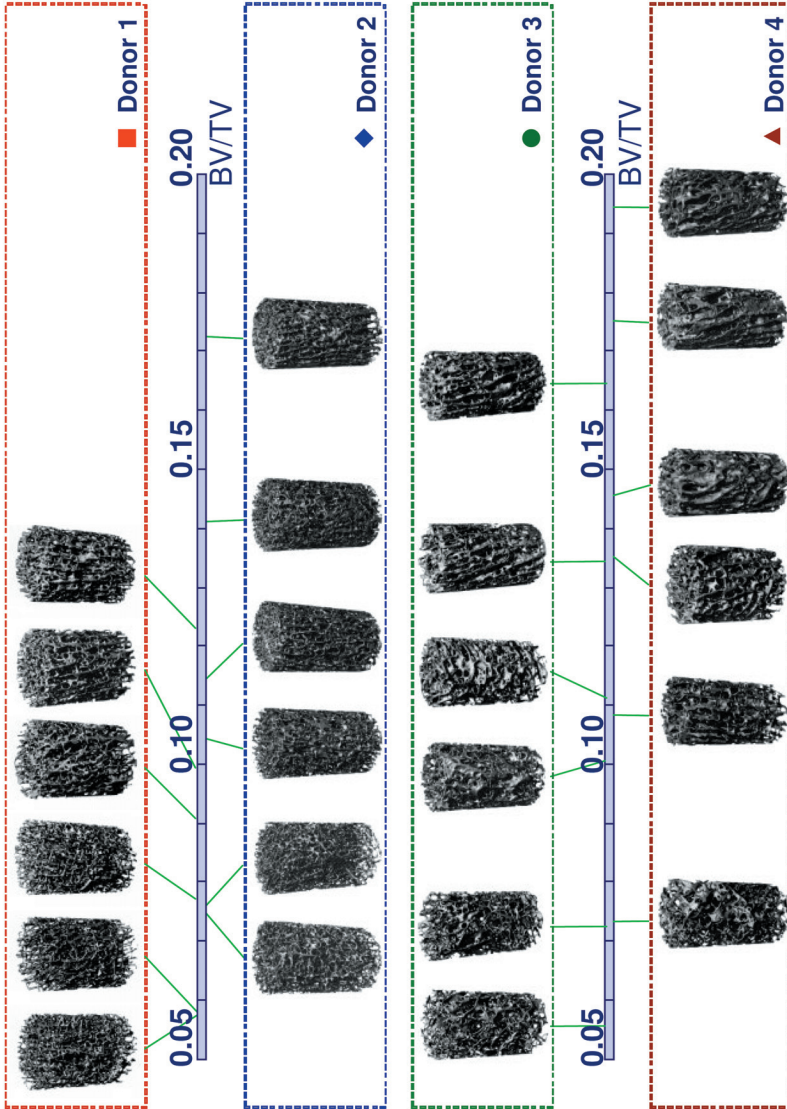


Figure 7.3: Renderings of biopsies from 4 donors. A random selection of biopsies was chosen from the extreme donors in Figure 7.2. Samples are displayed along the BV/TV axis so that samples with equal bone mass are aligned vertically. Note the fine highly connected structure for Donors 1 and 2 compared to the more coarse structure of the Donors 3 and 4.

effect can be seen in Figure 7.5. Age and interaction between age and BV/TV were significant for several of the parameters in each data set (Table 7.2).

The Pearson correlation coefficients between the proximal tibia and talus, in the GOH data using the average value for each anatomic site were: $r_{\text{BV/TV}} = 0.81$, $r_{\text{CD}} = 0.73$, $r_{\text{SMI}} = 0.79$, $r_{\text{Tb.N}} = 0.77$, $r_{\text{Tb.Th}} = 0.72$, $r_{\text{Tb.Sp}} = 0.81$, $r_{\text{BS/BV}} = 0.76$, $r_{\text{DA}} = 0.13$. This analysis was not repeated on the BIOMED data because there was a high sensitivity to regional heterogeneity of the bone volume fraction due to the small size of the biopsy samples.

Discussion

In this study we have investigated inter-individual differences and the effect of anatomic site on bone trabecular micro-architecture. We have used micro-computed tomography to measure bone morphometry from two large donor populations. The morphometric parameters used in this work were derived from three-dimensional micro-CT data to produce results that required no *a priori* assumptions regarding bone structure. By investigating the relation between morphometry and bone volume fraction we could quantify the effects of individuals and anatomic site on the architectural aspects of ‘bone quality’.

Generally all of the morphometric parameters measured in this study were highly correlated with the bone volume fraction, both between and within sites and individuals, with the exception of the degree of anisotropy. The strong correlation of BS/BV, Tb.Th, Tb.Sp, Tb.N (54, 184, 193, 195, 199), SMI (193, 196), and connectivity (38, 179, 200) with bone volume fraction has been noted previously. The lower degree of correlation between the degree of anisotropy and bone volume fraction has also been previously noted (38, 199).

In the analysis of the present data, strong inter-individual effects were seen on the trabecular micro-architecture. These inter-individual differences were statistically significant and could be visualized both in the scatter plots (Figure 7.2) and in renderings of individual biopsies (Figure 7.3). From the figures it is clear that donors could have very different trabecular bone micro-architecture even for samples with equivalent bone mass. While it has been debated whether having a highly connected trabecular network is advantageous in terms of the resulting mechanical properties (174, 175, 201), in the present data high connectivity comes at the expense of thinner trabeculae. This highlights one of the shortcomings of using connectivity as a surrogate measure of bone strength as connectivity can be increased both by increasing the number of trabeculae within a structure or by fenestrating existing plates. The mechanical consequence of choosing a highly connected structure consisting of thin trabeculae compared to a more coarse structure with thicker trabeculae is currently unknown. Because of the cross-

sectional nature of our study, it was not possible to determine how these individuals developed such different bone micro-architectures. As indicated by the significant effects in the statistical model, gender, aging and the presence of fractures were associated with differences in micro-architecture. Other factors that could possibly affect bone micro-architecture include genetic differences, the donor's medical history, mechanical loading history or differences in bone remodeling dynamics.

There were strong statistical effects due to anatomic site in this study. It has been previously noted that there can be large differences in bone volume fraction, mean values of morphological parameters, and the degree of mechanical anisotropy between anatomic sites (53, 172, 195, 199, 202). Few studies have examined the volume fraction-independent effect of site on morphometry. A previous 3D micro-CT study of seven sites from four cadavers noted site-dependant effects (38). This observation was not seen in a large histological study of eight sites from 113 cadavers (195), possibly because of limitations in the use of 2D model-based measurements. The reason for site-dependant differences in bone micro-architecture is unclear at this time. One possibility is that the micro-architecture is dictated by the regional mechanics. It is well known that trabecular bone is adapted to its mechanical environment, resulting in a structure that is aligned with the trajectories of the principal stresses that it experiences. It is also known that bone density is highest in areas of highest loading (4, 203). The implication of this adaptation with regards to other morphometric parameters is presently unknown. Other possible reasons for differences in the structure-volume relations between sites include developmental differences, or differences in bone remodeling rates at different anatomical sites (198, 204).

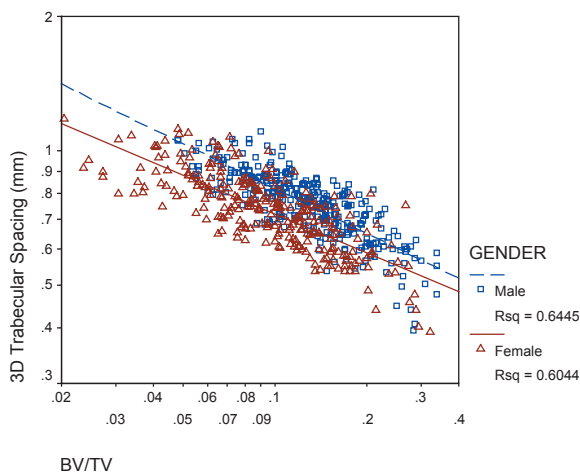


Figure 7.4: An example of gender effects in the GOH data.

In the present study, we were most interested in the inter-individual and site-specific effects on the relation between morphometric parameters and BV/TV. In our statistical models we have controlled for gender, age and disease status (presence of OA or existing fractures) as possible confounding effects. In the GOH data there was a strong effect of gender for all parameters with the exception of Tb.Th. This gender-specific effect was completely absent in the BIOMED data (Table 7.2, Figure 7.4). Generally, it is believed that differences exist between the mechanisms of age-related bone loss between genders. It has been reported that bone loss in males is due primarily to the thinning of individual trabecula while bone loss in females is due to a combination of trabecular thinning and a reduction of trabecular connectivity due to the loss of entire trabecula (182, 205-208). While previous studies have reported architectural differences between male and female trabecular bone, few have corrected for the effect of BV/TV; either by choosing samples with equivalent BMD (209, 210) or by reporting the relation between parameters and BV/TV (54, 195, 211). It should also be noted that many of the previous studies were limited by their use of 2D histological sections or reliance on model-dependant morphometric parameters, mainly Parfitt's plate model (54, 193). In the present study we found a lack of gender specific effects when using a pool of small biopsies from multiple anatomic locations (BIOMED data). This finding is in agreement with the results from a similar 2D histological study (195). In the GOH data set we used a much larger number of biopsies, albeit from a smaller pool of donors. These data indicate that the trabecular thickness of male and female bone is similar but that female bone has a much more highly connected rod-like structure with closer trabecular spacing. The 3D interpretation of these data is that females experience more perforation of trabecular plates than loss of entire trabeculae. This interpretation should be regarded very carefully however because the GOH study population was not optimized for a gender study and the gender groups were not balanced with respect to age. A close inspection of the GOH data also reveals that several males and females that were highly leveraged in the regression analysis and may have had a strong influence on the resulting conclusions. Like gender, aging was a statistically significant confounding effect. This effect was apparent for multiple morphometric parameters in both datasets although the particular parameters affected varied between the two donor populations. Generally however, the overall effect was consistent where aging was associated with a finer more highly connected rod-like structure. Previous histological studies of aging have concluded that age-related bone loss is due to the loss of entire trabecula in women and due to trabecular thinning in men (207, 208). This view is likely to be overly simplified as it has been demonstrated that there are changes in the connectivity and thickness of trabeculae in both genders during aging (182, 206). In the current study, we have demonstrated that it is likely that some of these alterations of bone micro-architecture are independent of the general loss of bone mass. Again, this interpretation should be regarded carefully because of possible interaction between gender and aging effects.

The presence of a previous fracture was the final confounding effect. Trabecular bone in donors who had suffered a previous fracture at any location had a reduced surface with thicker more widely spaced trabeculae. Bone fragility is associated both with increasing age and with female gender and it is, therefore, surprising that the effect of the presence of a previous fracture remained even after correcting for age and gender. A previous study has noted increased trabecular anisotropy in bone biopsies from the femoral head of fracture patients compared to cadaveric donors with an equal bone volume fraction (177, 212). There has also been a previous association between loss of connectivity in iliac crest biopsies of subjects with vertebral compression fractures as compared to controls with similar bone mass (210). This was in agreement with a previous study of a large pool of iliac crest biopsies (54). Because of the cross-sectional nature of the present study it is not possible to determine whether differences in bone micro-architecture were a cause or effect of the previous fracture. However, the association between fracture and micro-architecture is interesting and warrants further study.

It has been proposed that the measurement of bone density or a combination of bone density and quality at remote sites may be useful in assessing fracture risk in individuals. Typically methods such as pQCT of the radius or ultrasonic measurement of calcaneal properties are used. For this reason we investigated the relation between bone mass, micro-architecture and anatomic site. Previously, it has been demonstrated that BMD and micro-architecture are heterogeneous between anatomic sites in the human body. In a study of trabecular bone necropsies from 12 donors the correlations between spinal BV/TV and that measured at the iliac crest, proximal femur and calcaneus varied from $r = 0.67$ to $r = 0.80$. Connectivity density, as

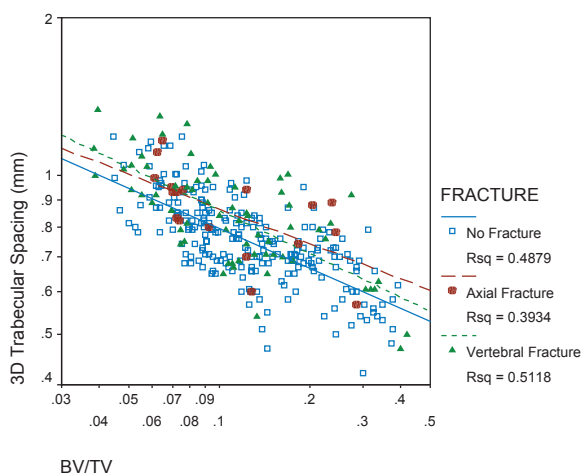


Figure 7.5: An example plot illustrating confounding due to previous fractures in the BIOMED data.

estimated using the trabecular bone pattern factor (TBPf), was poorly correlated between the sites with a maximum correlation ($r = 0.60$) between the lumbar spine and femoral neck (198, 202). A similar study of bone mass as measured by DXA and ultrasound at the lumbar spine, radius and calcaneus reported correlations which ranged from $r = 0.52$ to $r = 0.76$ (213). In a study of necropsies of the femur, lumbar spine and iliac crest, Pødenphant (185) reported a maximum correlation of $r = 0.86$ between BV/TV of the spine and iliac crest. Architectural measures (Tb.Th, Tb.Sp, Tb.N) had lower correlations varying from $r = 0.46$ to $r = 0.58$. These results are similar to those reported by Thomsen et al. where the correlation between BV/TV of the iliac crest and lumbar vertebra was $r = 0.59$. The correlation of architectural parameters between sites varied from $r = 0.63$ for Tb.Sp to non-significant for measures of anisotropy (199). In the current results, the correlation of the bone volume fraction between the tibia and talus in the GOH data was $r = 0.81$. The other morphometric parameters ranged between $r = 0.73$ and 0.81 with the exception of the degree of anisotropy. All of these data agree strongly with previous studies (199, 202).

Compared to the other morphometric parameters examined in the present study anisotropy stood out as being unusual. The correlation between the degree of anisotropy and BV/TV was low and differed in sign between the populations. The difference in sign between the two populations could be explained by the method of sampling. In the GOH set, multiple specimens were taken from a single site, the tibia. In the BIOMED populations, a single sample was taken from multiple sites. Thus the positive correlation between BV/TV and the degree of anisotropy in the GOH data implies that highly loaded areas within a single bone have not only increased bone mass, but also a higher degree of anisotropy. The negative correlations observed in the BIOMED data imply that individuals with lower bone mass exhibit a higher degree of morphometric anisotropy. This observation is in agreement with previous observations that horizontal trabeculae are preferentially resorbed during age-related bone loss in the lumbar spine (214). Also interesting in the present data was the observation that anisotropy was the only parameter that was not correlated between the tibia and the talus. This implies the regulation of bone anisotropy between anatomic sites was not only independent of bone volume fraction but also largely independent of individual effects. Previous studies have demonstrated that incorporating anisotropic fabric along with bone volume fraction into a statistical model for the estimation of bone mechanical properties increases model fit from an R^2 of 60-80% to over 90% (38, 55, 191, 215). Since the anisotropy was not highly correlated with the bone volume fraction and is, therefore, somewhat independent, it is not surprising that the prediction of mechanical properties is greatly enhanced by using bone volume fraction in conjunction with the fabric tensor (a mathematical expression of the anisotropy) as opposed to using bone volume fraction alone. However, while it is known that the direction of the trabecular structure is aligned with the principal stresses in the bone, little is known about factors that regulate the degree of anisotropy.

In conclusion, we observed significant variation in the types of trabecular micro-architecture found in different donors. Interestingly these effects were independent of bone mass. There were also significant differences between anatomic locations. The type of architecture present seemed to be influenced by age, the presence of previous fractures and possibly gender but not the presence of osteoarthritis. It is not presently clear if the observed inter-individual differences were genetic, related to development or due to differences in the life history of the donors. It is likely that the development of trabecular micro-architecture at various anatomic locations was heavily influenced by regional mechanics. From the present data it is clear that the control of trabecular bone micro-architecture is not simply a function of BV/TV but is also strongly influenced by both inter-subject variation and the anatomic site.

Acknowledgements

The authors of this study would like to thank the Gift of Hope Organ and Tissue Donor Network and the BIOMED I project for the material used in this study. We would also like to thank Dr. Ada Cole, Dr. Arkady Margulis and Eileen Broderick for help in obtaining and preparing specimens. This work was funded by EU Grant QLRT-1999-02024 and NIH grants AR39239 and RR16631.

Chapter 8

The effect of donor and skeletal site on morphology-elasticity constitutive models for trabecular bone

J.S. Day, J.H. Waarsing, G.H. van Lenthe, M. Stauber, B. van Rietbergen, D.R. Sumner, and H. Weinans

Abstract

Multiple constitutive relations have been proposed to relate the orthotropic elastic constants of trabecular bone to measures such as density and the fabric tensor (a morphometric description of anisotropy). In the current study, two data sets were used to evaluate the performance of three constitutive relations. In the first set, 496 trabecular bone specimens from the proximal tibia of 35 donors were used to evaluate sensitivity of the resulting models to subject-specific effects. In the second set, 235 specimens from the calcaneus, femoral neck, iliac crest, and second lumbar vertebra of 70 donors were used to evaluate the influence of skeletal site. Morphometry was quantified using microCT. Finite element models, created from the microCT images, were used to fully characterize the mechanical properties of each specimen. The analysis revealed significant subject and site-specific effects. Use of site-specific fits reduced the range and standard deviation of the residuals 20-50% and 16-42% respectively. Use of donor-specific fits reduced the average residual error by 15-22%. For donors with a very low bone volume fraction, donor-specific fits could halve the residual error. A cross-validation analysis indicated that excellent model stability could be reached with 35 donors. In conclusion, although there were both site-specific and donor-specific effects, all three constitutive relations performed reasonably well when a general fit was used. However, in applications where a high degree of accuracy is required, site-specific fits should be used and results should be interpreted carefully for samples with a low bone volume fraction.

Introduction

Trabecular bone is a highly complex porous anisotropic material that shares many similarities with a class of materials called cellular solids. The mechanical properties of a specimen of trabecular bone at the continuum or apparent level are determined by the apparent density, trabecular microarchitecture and tissue material properties. The relation between the apparent density and uniaxial mechanical properties of trabecular bone have been studied extensively, especially in compression and the results of this work have been thoroughly reviewed (52, 53). While a number of empirical studies have attempted to improve the prediction of bone mechanical properties by including morphometric parameters (i.e. connectivity, thickness, spacing etc.), consistently successful results have been achieved using models that account for bone anisotropy (38, 171, 189, 192, 215-217).

It has long been noted that the structure of trabecular bone is highly anisotropic and well aligned to the directions of the principal mechanical stresses (3). The degree of anisotropy varies widely between individuals and locations, even within a single skeletal site (37-42). It has been observed that the anisotropic spatial distribution of the trabecular structure could be measured using the method of directed secants, also referred to as the Mean Intercept Length (MIL), and approximated as an ellipse in two dimensions or using the positive definite second order tensor definition of an ellipsoid in three dimensions. This led to the development of a general theory relating the fabric tensor to the orthotropic elastic properties (43, 44, 56, 218). This was followed a number of alternative formulations and refinements of the original model (217, 219-221).

While the development and performance of morphology-elasticity constitutive relations has recently been reviewed (55), there have been few previous attempts to rigorously validate them, especially with respect to the possible effects of inter-individual or inter-site variation. It is the purpose of the current study to evaluate three relations, those presented by Cowin & Yang (217, 222), Zysset & Curnier (221) and Turner & Cowin (219). In particular, the sensitivity and robustness of the resulting models will be evaluated with respect to inter-site and inter-individual influences. Cross-validation and donor/site-specific fitting procedures will be used to evaluate the performance of the three relations for the prediction of the mechanical properties for a large group of human bone biopsies.

Materials and Methods

Donor populations

Trabecular bone specimens were cut from the proximal tibia of 35 donors supplied by the Gift of Hope (GOH) Organ and Tissue Donor Network (male: $n = 18$, $\text{age}_{\text{mean}} = 65$ $\text{age}_{\text{sd}} = 12$; female: $n = 17$, $\text{age}_{\text{mean}} = 67$ $\text{age}_{\text{sd}} = 12$). Samples were prepared by cutting a transverse bone slab from the proximal tibia. The first cut was taken immediately distal and parallel to the subchondral bone plate at the proximal aspect of the tibial tuberosity. The thickness of the slab was scaled to 16% of the medial-lateral width of the tibia resulting in thicknesses that varied between 10-14mm. A rectangular grid of 7.5 mm cylindrical specimens was drilled from this slab using a diamond core drill. This grid contained 3 samples in the anterior-posterior direction and 5 samples in the medial lateral direction, yielding ~15 samples per donor.

A second set of human trabecular bone specimens was obtained from European Union BIOMED I Concerted Action “Assessment of Bone Quality in Osteoporosis”. This population, including cause of death, has been previously described in detail(198, 223). Briefly, trabecular bone samples originated from 70 human cadavers with ages ranging from 23-92 years (male: $n = 38$, $\text{age}_{\text{mean}} = 67$ $\text{age}_{\text{sd}} = 15$; female: $n = 32$, $\text{age}_{\text{mean}} = 73$ $\text{age}_{\text{sd}} = 15$). For the present study, 235 specimens from the right femoral neck, center of the second lumbar vertebral body, calcaneus, and anterior-superior part of the iliac crest were used. Samples were excluded if they contained compact bone, could not be harvested in one piece or contained large voids. A portion of the analysis of this data has been previously reported (189).

Micro-CT analysis

Specimens were scanned in one of two high-resolution micro-tomographic systems. GOH specimens were scanned at a nominal resolution of 20 μm (μCT 40, Scanco Medical AG.). After scanning, a 5 mm cube was selected from the center of the sample for the subsequent analysis. A low-pass gaussian filter was used to remove noise before segmenting the gray scale images using individual thresholds as determined using Archimede’s principle(63). BIOMED specimens were scanned at a nominal resolution of 14 μm (μCT 20, Scanco Medical AG.) and a 4 mm cubic volume of interest was chosen for analysis. A low-pass gaussian filter was used to remove noise before segmenting the gray scale images using a fixed threshold. The three-dimensional mean intercept length (MIL) tensor was defined as determined for each specimen using the method of directed secants (43, 44).

Finite element analysis

Finite element (FE) models were used to calculate the orthotropic apparent stiffness tensor for each sample. Voxel based models were created with a voxel size of 20 μm for the GOH specimens and 28 μm for the BIOMED specimens. For all elements, linear elastic and isotro-

pic material properties were assigned with a Young's Modulus of 10 GPa and a Poisson's ratio of 0.3. A series of six finite element problems were solved for six uniaxial strain cases using the preconditioned conjugate gradient method. The nearest orthotropic stiffness tensor could then be determined for each sample(20-22).

Morphology-elasticity relations

Three morphometry based relations were evaluated for their ability to predict the mechanical properties derived by FE analysis. The first, proposed by Yang et al. (217, 222), uses a power relation to fit the components of the stiffness matrix (c) based on volume fraction alone.

$$\begin{aligned} c_{iiii} &= \lambda_{0ii} \rho^{k_{ii}} \\ c_{ijij} &= \lambda_{0ij} \rho^{k_{ij}} \\ c_{ijji} &= \mu_{0ij} \rho^{k_{ij}} \end{aligned} \quad (1)$$

where $i, j = 1, 2, 3$; $i \neq j$. Thus, 9 multiplicative ($\lambda \times 6$, $\mu \times 3$) and 9 exponential (k) constants were required to determine the mechanical properties. The value of ρ used in this study was not the true apparent density, but the bone volume fraction (BV/TV).

The Zysset relation (220, 221) also utilizes both fabric and bone volume fraction. However, in this relation, the eigenvalues of the fabric tensor (m_1, m_2, m_3) are again sorted then normalized such that $m_1 + m_2 + m_3 = 3$. In this relation, there are 5 constants ($\lambda_0, \mu_0, \lambda'_0, k, l$).

$$\begin{aligned} c_{iiii} &= (\lambda_0 + 2\mu_0) \rho^k m_i^l m_i^l \\ c_{ijij} &= -\lambda'_0 \rho^k m_i^l m_j^l \\ c_{ijji} &= 2\mu_0 \rho^k m_i^l m_j^l \end{aligned} \quad (2)$$

The relations presented by Cowin et al. (56, 191, 219) combine the fabric tensor and a power relation for volume fraction (ρ) resulting in 18 constants (k). A value of 1.45 for the power relation (n) was determined most appropriate during pilot testing. In this relation, the eigenvalues of the fabric tensor (m_1, m_2, m_3) were derived from inverse of the square root of the MIL tensor then sorted such that $m_1 > m_2 > m_3$ and normalized such that $m_1 + m_2 + m_3 = 1$.

$$\begin{aligned} c_{iiii} &= k_1 + 2k_6 + k_2 + k_7 II + 2k_3 + 2k_8 m_i + 2k_4 + k_5 + 4k_9 m_i^2 \\ c_{ijij} &= k_1 + k_2 II + k_3 (\lambda_i + \lambda_j) + k_4 (m_i^2 + m_j^2) + k_5 m_i m_j \\ c_{ijji} &= k_6 + k_7 II + k_8 (m_i + m_j) + k_9 (m_i^2 + m_j^2) \\ II &= m_2 m_3 + m_3 m_1 + m_1 m_2 \\ k_i &= k_{i1} + k_{i2} \rho^n \end{aligned} \quad (3)$$

The constants for each relation were fit to the results from the FE analysis (\mathbf{c}) using the multiple regression method described in detail by Zysset (55). Briefly, the equation:

$$\mathbf{c} = \mathbf{X}\mathbf{b} + \mathbf{e} \quad (4)$$

was constructed where \mathbf{c} was a $9n$ vector containing the 9 components of the compliance matrix for n specimens, \mathbf{X} was the $9n \times p$ matrix containing the volume fraction and fabric data, \mathbf{b} was a vector containing the p constants in the model and \mathbf{e} was the vector of the residuals. Equation (4) could then be solved for \mathbf{b} using singular value decomposition to obtain the pseudo-inverse \mathbf{X}^+ of \mathbf{X} :

$$\mathbf{b} = \mathbf{X}^+ \mathbf{c} \quad (5)$$

Statistical analysis

For each data set, a rigorous analysis was performed using each of the three previously described relations. Models were fit to each of the two data sets and the fit was evaluated by examining both magnitude of the residuals and the coefficient of determination. Where applicable, the coefficient of determination was adjusted for the number of observations ($9n$) and the number of model constants (p) as follows(224):

$$R_{adj}^2 = 1 - (1 - R^2) \frac{(9n - 1)}{9n - p - 1} \quad (6)$$

The models were then further examined using two further evaluations to examine the assumption that a ‘general fit’ was appropriate for a varied population from multiple skeletal sites. First, the models were fit using a separate fit for each skeletal site in the BIOMED data and each donor in the GOH data. This resulted in models with $4p$ and $35p$ constants for the GOH and BIOMED sets. By comparing site-specific fits to the general fits we could determine how much accuracy was lost when we imposed a generalized model on the data. The presence of a statistically significant improvement in the model fit was evaluated by evaluating the change in R^2 using an F -test as follows(224):

$$F = \frac{(R_{extended}^2 - R_{general}^2)(9n - p_{extended} - 1)}{(1 - R_{extended}^2)(p_{extended} - p_{general})} \quad (7)$$

where F had $(p_{extended} - p_{general})$ and $(9n - p_{extended} - 1)$ degrees of freedom.

The second additional evaluation that we performed was a cross-validation. This was used to assess the model’s stability (i.e. are there some sites/donors who have a large influence

on the model results) and its ability to be used with novel data. For these analyses, we used a modification of the ‘leave one out’ method (225). Again, we constructed 4 models for the BIOMED and 35 for the GOH set. But this time, instead of constructing models for each individual site/donor, the models were constructed using only the data from the other sites/donors and applied to the morphometry data from the site/donor of interest. For this analysis, the coefficient of determination required no adjustment because the model was evaluated on different data than was used to construct it.

Results

Morphometric and mechanical data

The first step in the analysis was to examine the relationships between the input variables, BV/TV, the fabric eigenvalues and the results of the simulated mechanical tests. In the BIOMED data there was a wide range of BV/TV, from 0.04 to 0.48 with the lowest at L2 and the highest at the femoral neck. In the GOH data, BV/TV ranged from 0.01 to 0.24. There was a large variation of this range between donors where female donors tended to have a lower BV/TV that declined with age compared to males who displayed little age related variation (Figure 8.1). BV/TV data and the normalized MIL eigenvalues are summarized by skeletal site in Table 8.1 and Figure 8.1.

The computed Young’s moduli and shear moduli were clearly a function of BV/TV in both sets. While these variables generally exhibited a power relation, it appeared that the E11 Young’s Modulus was more linear, especially at values of BV/TV greater than 0.15 (See Figures 8.2A and 8.2B). There also appeared to be a subtle site-specific effect, especially with respect to samples from the femoral neck (Figure 8.2A). The Poisson’s ratios varied from 0.06 to 0.83 with the proximal tibia exhibiting the widest range. The Poisson’s ratios in both data sets varied widely at low volume fractions but began to converge as BV/TV increased (Figure 8.2). The median values and range of the computed mechanical data are displayed in Table 7.2.

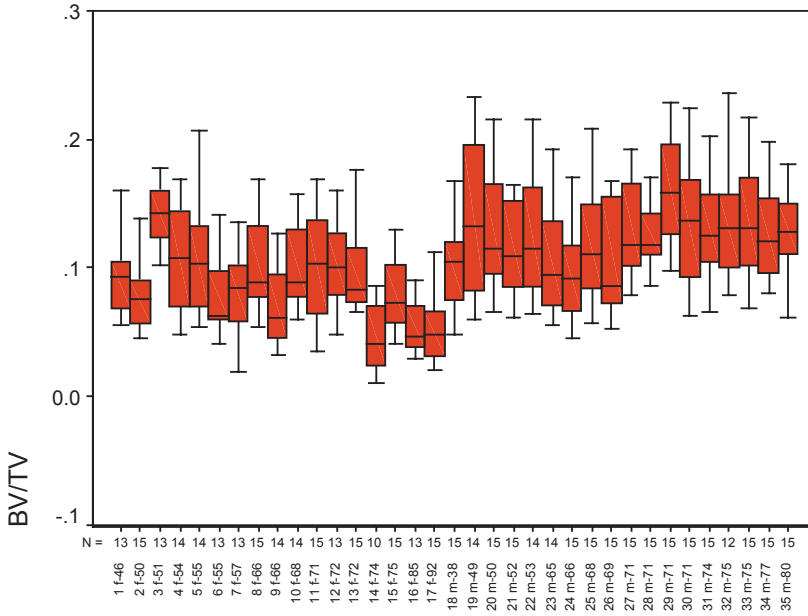
When plotted against the BV/TV the degree of mechanical anisotropy (E_{11}/E_{33}) increased greatly with decreasing volume fractions. However, there was a wide spread in the data, especially that from the proximal tibia. The relation between the morphometric anisotropy (m_1/m_3) and BV/TV was similar to that observed for the mechanical degree of anisotropy. When the mechanical anisotropy was plotted against the morphometric anisotropy there were clear site dependant effects, most notably that the specimens from L2 seemed to plot in a separate cloud than the others from the BIOMED data set. It was also notable that there was a substantial spread in the data (Figure 8.3).

BIOMED	<i>n</i>	BV/TV	<i>m</i> ₁	<i>m</i> ₂	<i>m</i> ₃
Calcaneus	59	0.12 (0.05,0.19)	0.41 (0.38,0.44)	0.32 (0.29,0.36)	0.27 (0.25,0.31)
Femoral Neck	63	0.26 (0.12,0.48)	0.39 (0.35,0.43)	0.33 (0.30,0.34)	0.29 (0.26,0.31)
Iliac Crest	51	0.14 (0.06,0.27)	0.38 (0.36,0.41)	0.33 (0.31,0.35)	0.29 (0.27,0.31)
L2	62	0.09 (0.04,0.17)	0.38 (0.35,0.43)	0.32 (0.29,0.35)	0.30 (0.26,0.32)
GOH					
Proximal Tibia	498	0.10 (0.01,0.24)	0.40 (0.34,0.47)	0.32 (0.27,0.37)	0.28 (0.22,0.32)

Table 8.1: Morphometric data summarized by site (median values and range). *H1-H3* are the summarized normalized eigenvalues of the MIL derived fabric ellipsoid.

BIOMED	<i>E</i> ₁₁	<i>E</i> ₂₂	<i>E</i> ₃₃	<i>v</i> ₁₂	<i>v</i> ₁₃	<i>v</i> ₂₃	<i>G</i> ₂₃	<i>G</i> ₃₁	<i>G</i> ₁₂
Calcaneus	494 (155,975)	260 (86,698)	141 (42,408)	0.16 (0.06,0.51)	0.40 (0.24,0.59)	0.40 (0.22,0.53)	59 (15,184)	81 (26,237)	104 (21,229)
Femoral Neck	1516 (516,3093)	982 (291,2726)	619 (164,2240)	0.29 (0.23,0.37)	0.32 (0.27,0.42)	0.34 (0.19,0.46)	281 (76,638)	350 (90,996)	482
Iliac Crest	613 (210,1353)	379 (118,1254)	294 (74,848)	0.24 (0.13,0.49)	0.30 (0.19,0.46)	0.30 (0.18,0.48)	127 (30,358)	140 (41,404)	203 (49,482)
L2	347 (182,776)	137 (42,418)	91 (27,365)	0.22 (0.10,0.45)	0.39 (0.24,0.63)	0.36 (0.21,0.56)	46 (14,148)	51 (19,188)	54 (17,241)
GOH									
Proximal Tibia	425 (21,1518)	186 (10,982)	131 (4,597)	0.26 (0.06,0.83)	0.33 (0.12,0.67)	0.42 (0.14,0.68)	53 (2,223)	67 (3,369)	92 (4,455)

Table 8.2: Summary of finite element results by site (median values and range).



Donor Gender-Age

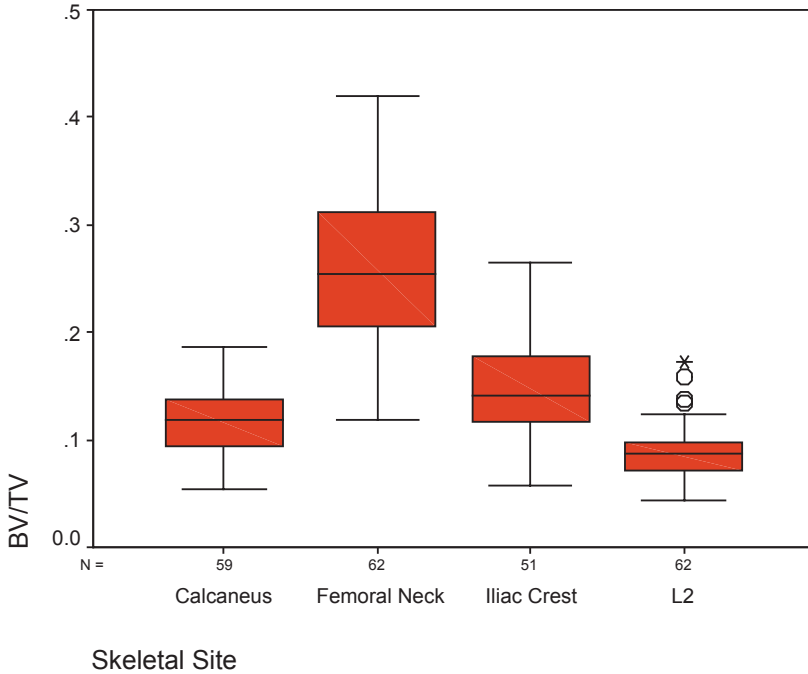


Figure 8.1: BV/TV by donor for GOH data and by skeletal site for BIOMED data.

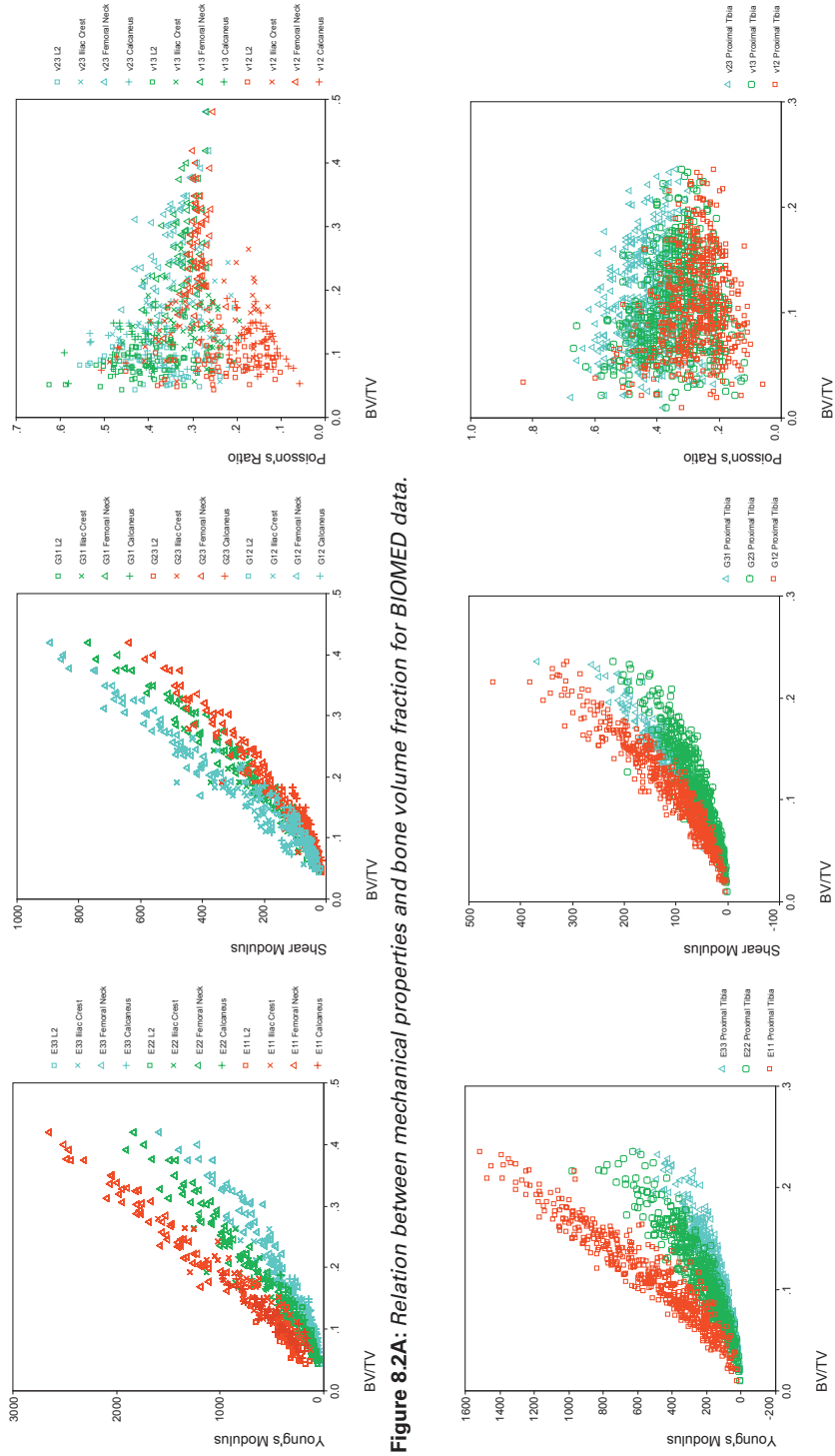


Figure 8.2A: Relation between mechanical properties and bone volume fraction for BIOMED data.

Figure 8.2B: Relation between mechanical properties and bone volume fraction for GOH data.

Figure 8.2: Finite element results plotted against bone volume fraction

General model fits

When fit to the mechanical data, all three models yielded excellent fits with between 96.0 and 98.5% of the variance explained (Table 8.3). The predicted values have been plotted against those from the FE models in Figure 8.4. The standard deviations of the residuals from the stiffness matrix were examined as an additional criterion for the model fits. The standard deviation of the residuals ranged from 26 to 83 MPa depending on which model and set were used (Table 8.3). Analysis of the residuals confirmed that the estimation errors were roughly normally distributed for all three models. The Cowin model consistently produced the smallest dispersion of the residuals for both data sets. All 3 models occasionally produced spurious results with errors of up to approximately 232 MPa, 467 MPa and 944 MPa for the Cowin, Yang and Zysset models respectively. The Yang and Zysset models tended to produce larger errors for the stiffest samples whereas the residuals from the Cowin model were evenly distributed (Figure 8.4). For this reason the three models seemed much more equal when examined in relative terms (Figure 8.5, left). The Yang model displayed non-linear behaviour that resulted in substantial over-estimation of c_{1111} stiffness matrix component at high values of BV/TV (Figure 8.4 center). The Cowin model produced 14 cases in the GOH data and 1 case in the BIOMED data that were not positive definite. All results that were not positive definite were from samples with low BV/TV (< 0.055). Model constants for the general fits are presented in Table 8.4.

Site effects

Site dependant effects and the stability of the fits with respect to site were examined using site-specific fits and cross-validation. Use of site-specific fits led to small but highly significant improvements in coefficients of determination of all three models ($p < 0.001$). The range of the residual errors was reduced by 30, 50 and 20% for the Yang, Zysset and Cowin models respectively. The reduction of the standard deviation of the residuals varied between 16 and 42% with the largest improvement seen for the Zysset model (Table 8.3A and B). In absolute terms, use of site-specific models led to the greatest improvement for the estimates of stiffness at the femoral neck (Figure 8.4B), especially with respect to the Yang and Zysset models. However, in relative terms these improvements were minor since the femoral neck was the stiffest of the sites tested. In relative terms, the Cowin model fit poorly at L2, although this was slightly improved by using a site-specific model (Figure 8.4B). The model constants, calculated by fitting the entire data sets as well as the individual skeletal sites, are displayed in Table 8.4. The model constants varied considerably between sites. Generally the exponential modifier varied between 1.2 and 1.8 in the Yang and Zysset models with the exception of k_1 for the L2 specific fit of the Yang model, which was 0.88. k_1 values were consistently lower than the other k values for the Yang model. In the cross-validation there was a larger inflation of errors for the Yang and Cowin models than for the Zysset model (i.e. the Zysset model was more stable). This was true in both relative and absolute terms (Figure 8.4). For the Yang

	Coefficient of Determination				Residuals			
	Stiffness Matrix	E (MPa)	G (MPa)	ν	Average	Max.	Min.	St. Dev
	R^2_{adj}	R^2	R^2	R^2	(MPa)	(MPa)	(MPa)	(MPa)
<i>BIOMED</i>								
Yang	0.974	0.962	0.960	0.255	3.1	423	-467	64
Zysset	0.974	0.964	0.966	0.003	-4.6	339	-944	83
Cowin	0.985	0.978	0.972	0.221	-2.0	363	-220	49
<i>GOH</i>								
Yang	0.960	0.937	0.922	0.292	3.3	391	-386	43
Zysset	0.974	0.964	0.937	0.064	1.6	235	-431	35
Cowin	0.984	0.976	0.933	0.031	-2.0	232	-135	26

Table 8.3A: General model fits. Also presented are the raw coefficients of determination for the Young's moduli, Shear moduli and Poisson ratios.

	Coefficient of Determination		Residuals			
	Stiffness Matrix	Stiffness Matrix	Average	Max.	Min.	St. Dev
	R^2_{raw}	R^2_{adj}	(MPa)	(MPa)	(MPa)	(MPa)
<i>BIOMED</i>						
Yang	0.986	0.985	2.6	320	-302	48
Zysset	0.986	0.986	2.5	346	-320	48
Cowin	0.990	0.989	-1.7	268	-209	41
<i>GOH</i>						
Yang	0.971	0.966	2.2	361	-301	38
Zysset	0.982	0.981	3.2	265	-386	30
Cowin	0.990	0.989	-1.8	217	-92	21

Table 8.3B: Summarized errors from site/donor specific fits.

	Coefficient of Determination		Residuals			
	Stiffness Matrix		Average	Max.	Min.	St. Dev
	R^2		(MPa)	(MPa)	(MPa)	(MPa)
<i>BIOMED</i>						
Yang	0.927		7.0	817	-765	108
Zysset	0.971		-4.6	335	-1019	91
Cowin	0.972		-3.1	448	-346	69
<i>GOH</i>						
Yang	0.959		3.3	391	-395	43
Zysset	0.973		1.6	229	-431	36
Cowin	0.984		-2.0	233	-136	27

Table 8.3C: Cross-validation fits.

Table 8.3: Adjusted coefficients of determination and residual values for model fits. Coefficients for the stiffness matrix were determined in normal space (i.e. Yang and Zysset data were converted back from log space). Summarized residual statistics are presented on the right.

model there was a large inflation of errors for estimates at the femoral neck. It should be noted, however, that this this particular cross-validation involved considerable extrapolation with respect to the BV/TV.

Donor effects

In a similar manner to the method used to examine site-specific effects in the BIOMED set, cross-validation and donor-specific models were used in the GOH set to examine the influence of individuals on model behaviour. Use of donor specific fits led to an overall 15, 20 and 22% decrease in the estimate error for the Yang, Zysset and Cowin models ($p < 0.001$ by F -test). However, for specific donors it was possible to reduce the error by half, especially in the case of the Zysset model (Figure 8.4B left). However, as was the case in the BIOMED set, the errors in the Zysset model tended to be largest when the stiffness was highest and thus the reduction of errors was minimal in relative terms (Figure 8.4B right). The relative errors of the general fit were rather large for three of the donors (#7, 14 and 17). The results for these three donors could be partly salvaged by performing donor specific fits except in the case of donor #7 for the Cowin model. These three donors happened to include the lowest BV/TV values in the entire set (Figure 8.1). The cross-validation of the GOH data sets indicated very robust behaviour of all three models. The maximum change in the estimates ranged from 9 MPa with the Cowin Model to 17 MPa with the Zysset model. The average change in the residual was less than 0.5 MPa for all three models and no individuals exerted undue influence on the model fits during cross-validation (Figure 8.4B).

Discussion

In the present study we have examined the performance of three morphology-based constitutive equations used to predict the orthotropic elastic properties of trabecular bone. We have focused particularly on inter-subject and inter-site influences on model fits and stability. By comparing site/donor-specific fits to general fits we could quantify how accuracy was sacrificed by generalizing the models with respect to skeletal site and donor. Fitting the morphology-elasticity relations using general fits led to mean errors in the range of 15-30%. However, approximately ½% of the specimens produced errors of greater than 100% of the estimated value. This is in the range reported previously using these morphology-elasticity relations in conjunction with FE derived mechanical properties (55, 190, 215). To our knowledge there has only been one previous study that investigated the use of a fabric based relation to examine the effect of site and donor (38). Although they reported significant influence of site and donor on the model fit, their sample size was limited and they did not quantify these effects. In the present study, the accuracy of all three morphometry-elasticity relations could be improved by using site-specific or donor-specific fits with a reduction in the standard deviation

	λ_{011}	λ_{022}	λ_{033}	λ_{012}	λ_{013}	λ_{023}	μ_{023}	μ_{031}	μ_{012}
BIOMED	9500	11400	8245	4606	3021	3503	3007	3462	4981
Calcaneus	11048	8866	7480	3569	2893	4146	1349	1615	1551
Femoral Neck	8866	7785	6311	2752	2345	2345	1220	1335	1404
Iliac Crest	7864	9414	9136	2345	3294	3328	1309	1362	1196
L2	3395	11271	9701	2368	2018	4024	1697	950	989
GOH	14449	7816	5981	2368	2180	2551	1705	2810	3457

	k_1	k_2	k_3	k_4	k_5	k_6	k_7	k_8	k_9
BIOMED	1.32	1.68	1.74	1.79	1.64	1.75	1.73	1.69	1.76
Calcaneus	1.42	1.56	1.77	1.75	1.67	1.88	1.80	1.72	1.62
Femoral Neck	1.21	1.41	1.57	1.36	1.44	1.47	1.56	1.48	1.30
Iliac Crest	1.26	1.52	1.68	1.38	1.63	1.65	1.56	1.50	1.29
L2	0.88	1.72	1.80	1.53	1.47	1.80	1.75	1.45	1.43
GOH	1.50	1.55	1.62	1.46	1.52	1.58	1.54	1.65	1.58

Table 8.4A: Yang model.

	λ_0	λ'_0	μ_0	k	l
BIOMED Total	5090	3383	3436	1.67	1.39
Calcaneus	5945	3071	2976	1.69	1.26
Femoral Neck	2814	2483	2550	1.41	1.32
Iliac Crest	3244	2628	2794	1.48	1.21
L2	3747	2170	2196	1.51	1.93
GOH	4465	2781	2545	1.58	1.39

Table 8.4B: Zysset model.

	k_{-11}	k_{12}	k_{21}	k_{22}	k_{31}	k_{32}	k_{41}	k_{42}	k_{51}	k_{52}
BIOMED	-1163	24067	12967	-32800	-9432	-39518	9780	-1756	8460	145770
Calcaneus	542	-3453	2944	132100	-4736	-117280	4043	99980	6454	159670
Femoral Neck	-330	15994	11745	-20255	-10687	-28309	11543	-17312	8889	143710
Iliac Crest	-1350	36383	4080	85806	-126	-190630	98	158910	455	262660
L2	-1055	54916	1139	485140	2001	-653580	-1332	569860	-3259	849060
GOH	-447	5623	6154	108000	-4862	-121720	4864	95422	5017	187260

	k_{61}	k_{62}	k_{71}	k_{72}	k_{81}	k_{82}	k_{91}	k_{92}
BIOMED	-149	2781	-2737	-78600	3052	67659	-4440	-85263
Calcaneus	843	-5931	-4575	-73220	1931	88747	-2839	-117710
Femoral Neck	3207	-17194	-12734	-14915	2777	64974	-3741	-82717
Iliac Crest	2497	-20206	-5701	-78179	-1927	136440	2927	-187550
L2	233	-2283	-382	-239160	-395	237040	722	-332580
GOH	-330	8977	83	-119330	814	88597	-1108	-115340

Table 8.4C: Cowin model.

Table 8.4: Model constants for generalized and site-specific fits.

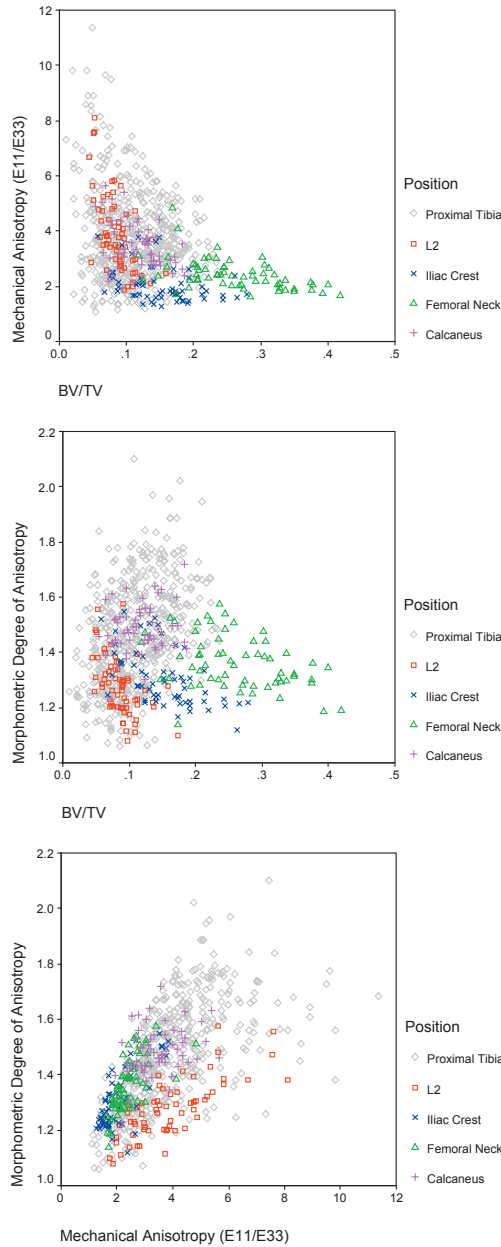


Figure 8.3: Site dependant effects in the relation between BV/TV and anisotropy. The relation between the degree of anisotropy of the major and minor Young's Moduli (E_{11}/E_{33}) is plotted against BV/TV (top). This can be contrasted with morphometric anisotropy from the fabric tensor (m_1/m_3 ; center). When the relation between the mechanical and morphometric anisotropy were plotted against each other there were clearly site-dependant relations (bottom). A similar donor-dependant effect was seen in the proximal tibia.

of the residuals that varied from 15 to 42%. Cross-validation was used to assess the stability and performance of general fits when applied to new data. In our study of donor effects, we had a large number of donors with overlapping ranges of both BV/TV and anisotropy. We found that with this data an excellent degree of model stability could be reached with less than 35 donors. In the cross-validation by skeletal site, there was a large amount of overlap in morphometry at the calcaneus, iliac crest and L2 but not for the femoral neck. The resulting models were more volatile when they were used to extrapolate results at the femoral neck. This implies that it may be necessary to use a wider range of input data to obtain general fits that are stable respect to skeletal site.

In the present paper we have examined whether a global relation between either BV/TV alone or BV/TV in conjunction with fabric was appropriate when applied to trabecular bone. While global models provided reasonable results, the model fits could be substantially improved by including either donor or skeletal site. A clear example of the site effect is illustrated in Figure 8.6, where we have plotted a small subset of the data from the general fit of the Cowin model. In order to understand the source of the site-specific or donor-specific effects, we must further consider the modelling assumptions. One possibility that we had to rule out was that apparent site or donor-dependant effects were artefacts of non-linearity in the regression model (i.e. the effect of trying to fit the data an inappropriate mathematical model). For this reason we performed an analysis of the residuals. For the Yang and Cowin models we found no obvious sign of non-linearity in our residual analysis. However, there was clearly non-linearity in the Zysset model, associated with the difficulties fitting the c_{1111} stiffness entries. We examined this further using three-dimensional visualization of the data with respect to the log transformed stiffness, BV/TV and fabric from multiple views (unpublished analysis). From this inspection we could clearly see that although there was non-linearity, data points from L2 lay on a different plane than those from the calcaneus or iliac crest. This assured us that the site-specific differences noted in Figure 8.3 (right) were not related differences in BV/TV alone. Having established that the observed differences were not an artefact of ill-fitting models, we considered other possible explanations. One possibility was that of a ‘lurking variable’ that was not included in the analysis. An obvious example of this can be seen with the Yang model. It has previously been demonstrated that the relation between the mechanical properties of bone and BV/TV vary depending on donor and anatomic site and that this is also related to the degree of mechanical anisotropy (37, 40, 41, 53). We have demonstrated in the current data that the residuals from the Yang model were correlated to the fabric. Therefore, with the Yang model it is likely that at least part of the site or donor-specific differences were due to differences in anisotropy between sites and/or donors. In the Zysset and Cowin models, fabric was incorporated in the analysis. However, we have previously demonstrated that a number of other morphometric parameters such as connectivity, structure model index, trabecular thickness and trabecular spacing vary widely between BV/TV adjusted sites and

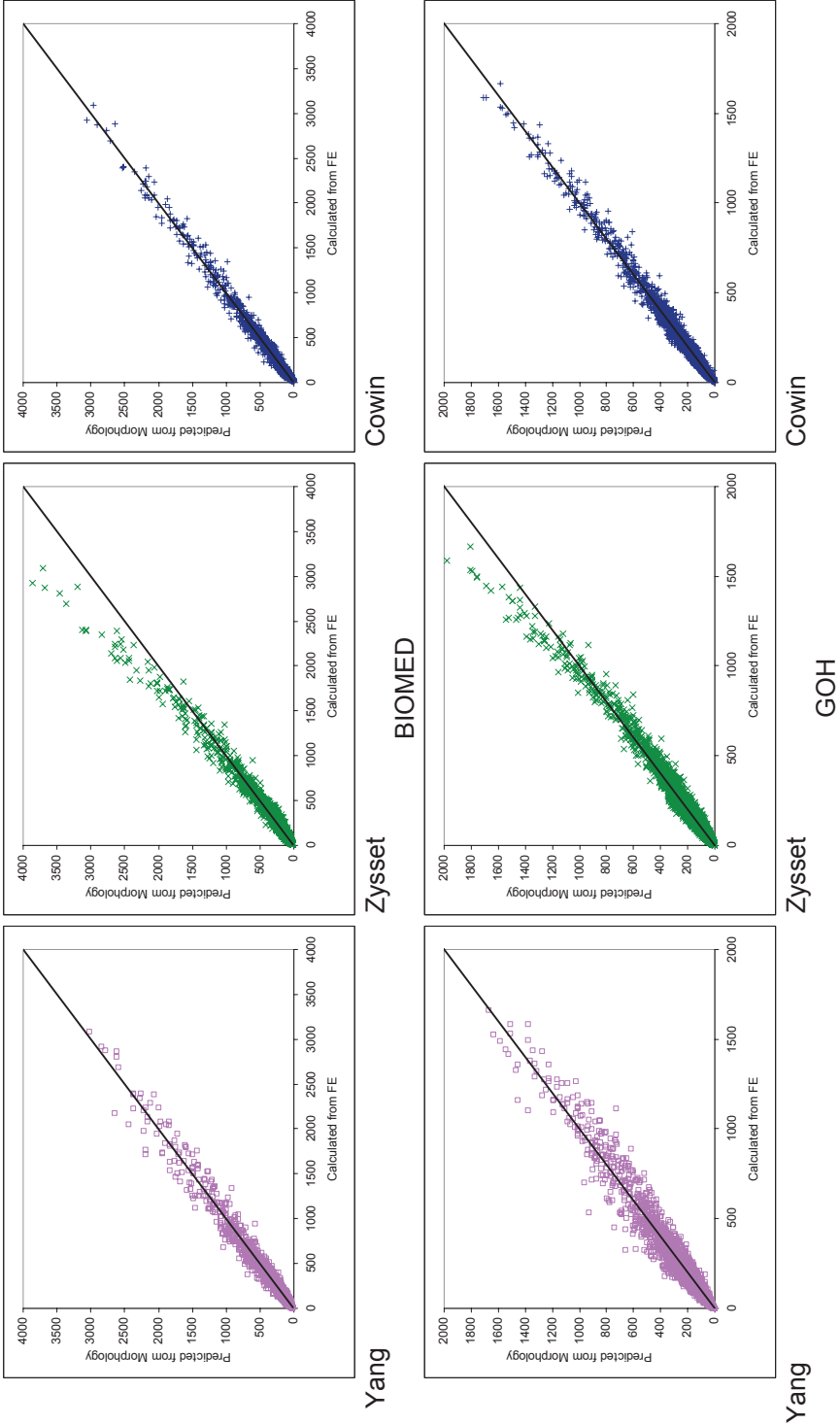


Figure 8.4: Observed and predicted elements of the stiffness matrix for BIOMED and GOH data using the generalized fit for each of the three models. Solid line indicates $y=x$.

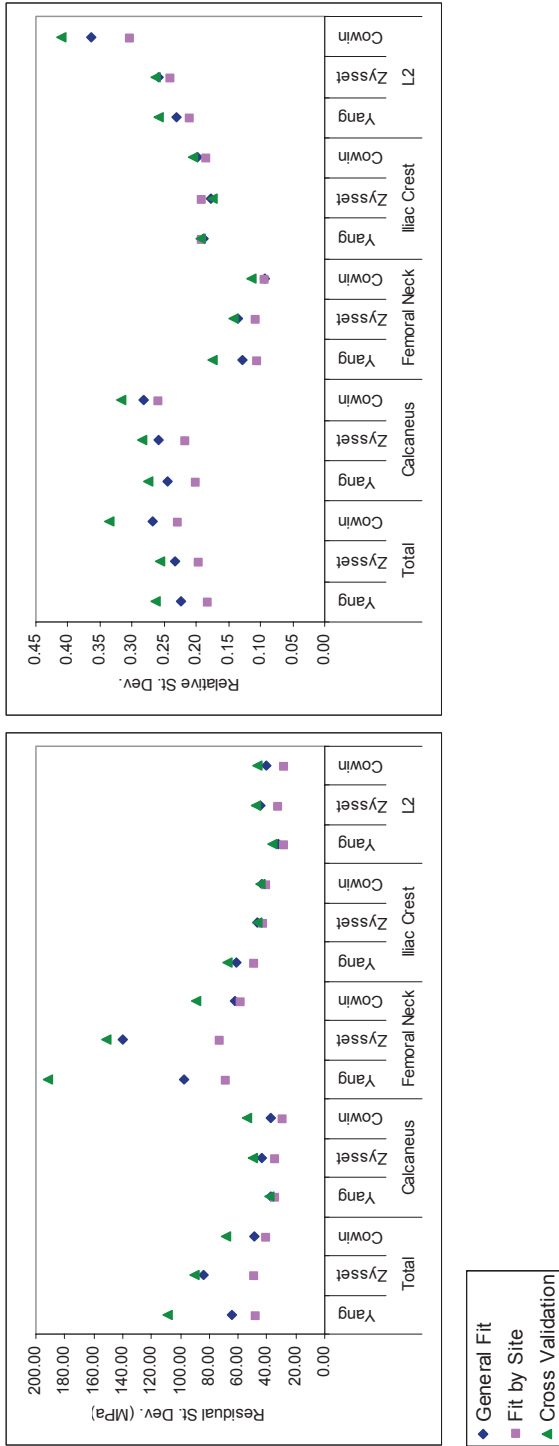
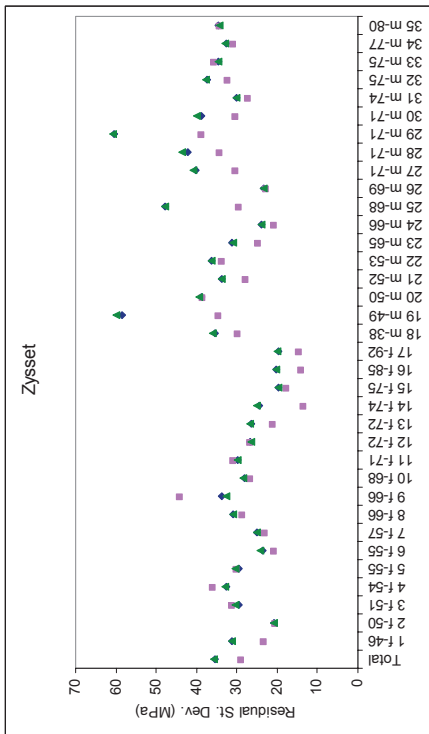
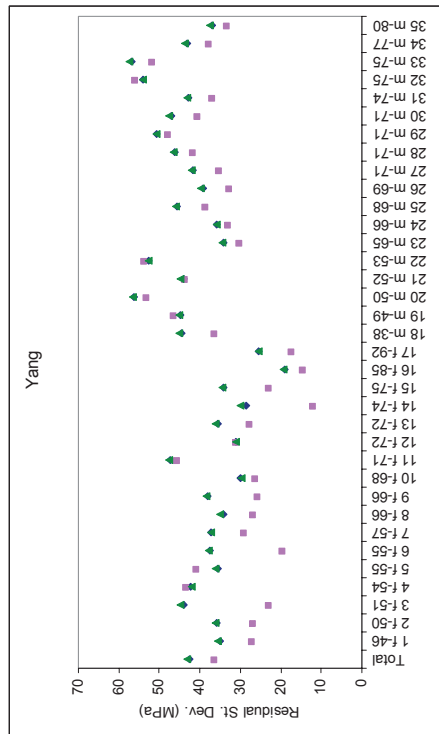
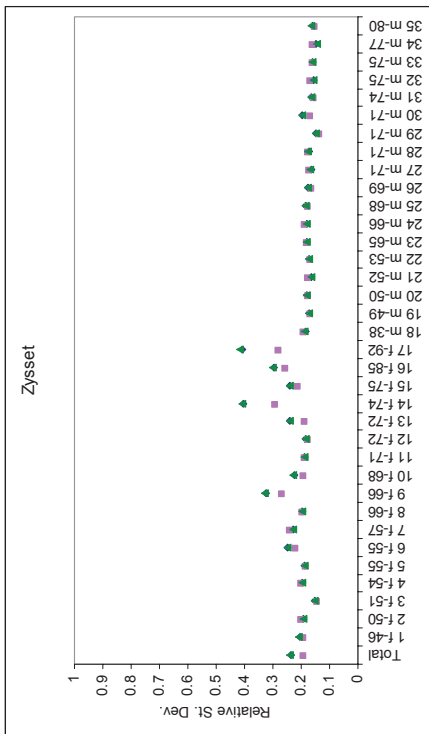
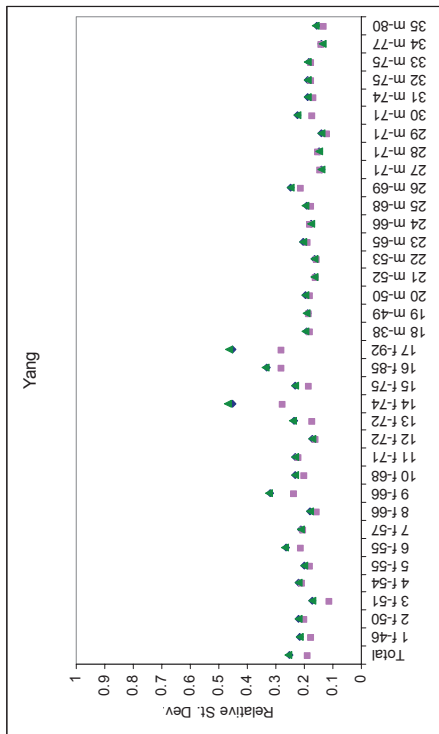


Figure 8.5A: Generalized fits, site-specific fits and cross-validation by site (BIOMED data). Standard deviation of the residuals (left) and standard deviation of the residuals normalized to magnitude of the predictor variable (right).



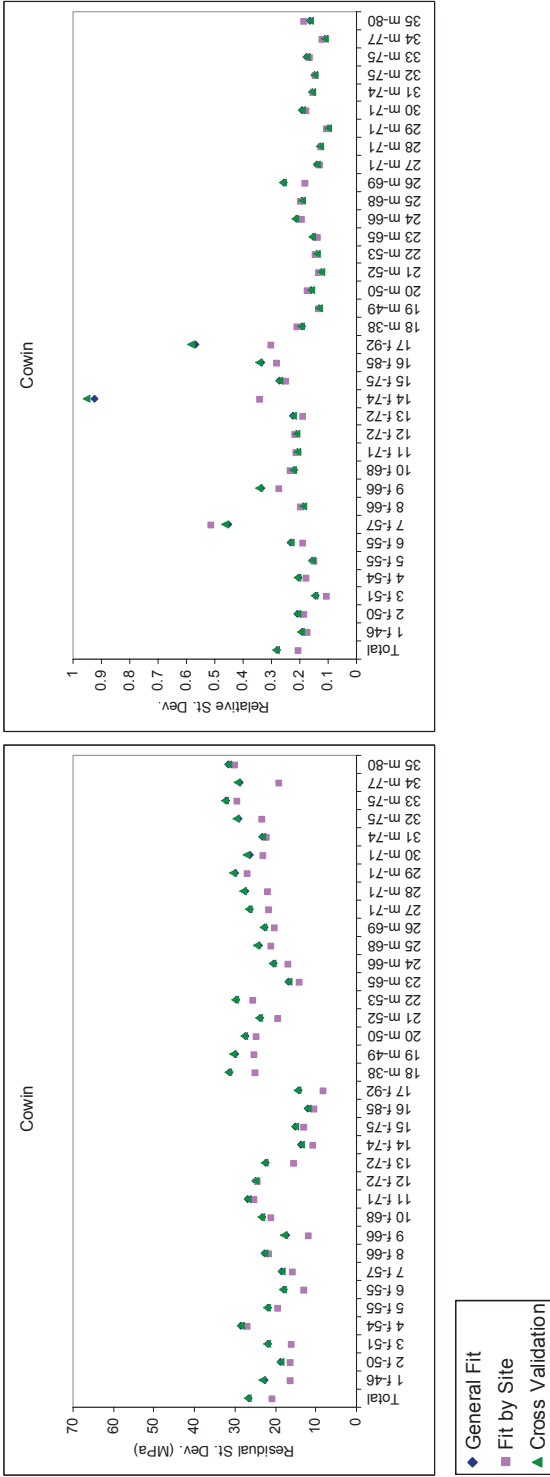


Figure 8.5B: Generalized fits, site-specific fits and cross-validation by donor (GOH data). Standard deviation of the residuals (left) and standard deviation of the residuals normalized to magnitude of the predictor variable (right).

Figure 8.5: Summarized results for multiple fits by site and by donor. Multiple regression models were fit using one of three sets of previously published constitutive equations. Each of these models was fit in three ways; a generalized fit where all samples were pooled for analysis, a site/donor-specific fit where each site/donor was fit individually or a cross-validation where $(n-1)$ sites/donors were used to construct the model which was then tested on site/donor n .

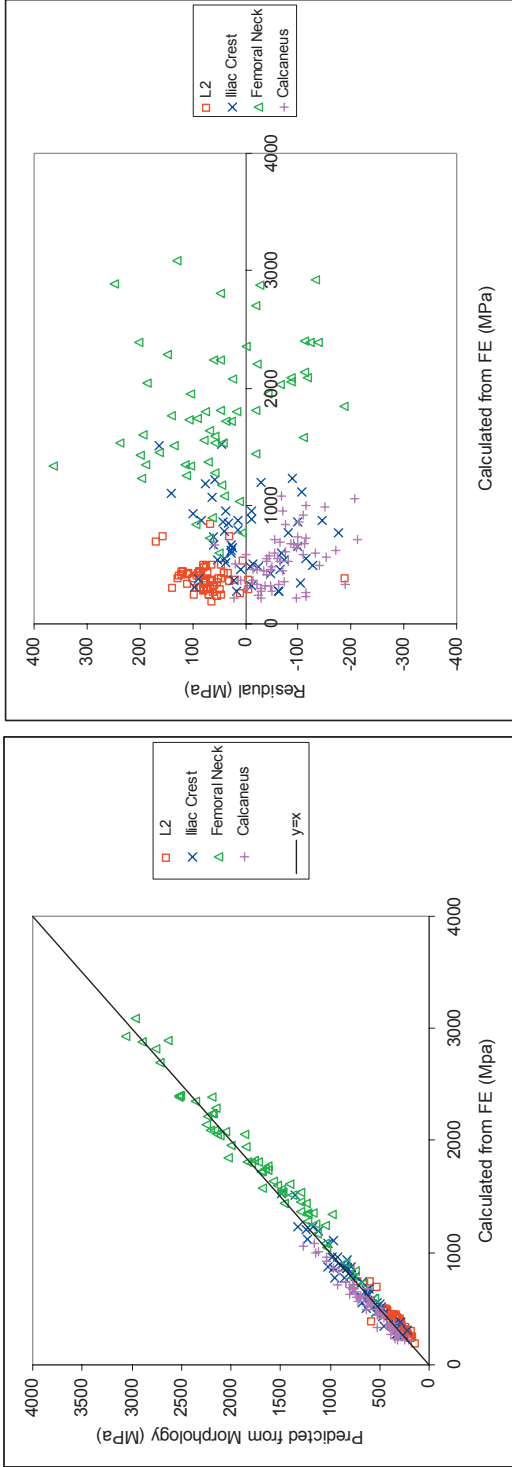


Figure 8.6: An example of site-specific effects on model fit. Illustrated above are the subset of only the c1111 stiffness matrix entries from the BIOMED data as fit by the general Cowin model. The predicted models are plotted against the FE values on the left and the residuals are plotted against the FE values on the right. Note that the estimated values for L2 plot underneath and those for the calcaneus plot above the line $y=x$ (left). This effect is more obvious when the residuals are plotted (right).

donors. It is possible that the relation between morphometric and mechanical anisotropy is modulated by these other morphometric parameters.

Although all three of the morphology elasticity relations performed reasonably, each had unique qualities. Therefore it is not possible to discuss the presence of site-specific or donor-specific effects without considering the context of which relation was being used at the time. In absolute terms, the Cowin model consistently outperformed the others, producing a higher coefficient of determination and smaller residuals. However, it also suffered from several limitations. At the lowest values of BV/TV it produced both large relative errors and, occasionally, stiffness matrices that were not positive definite. This was true for the skeletal site L2 (Figure 8.5A left) as well as for three donors with low BV/TV (Figure 8.5B bottom left). While the relative errors for two of the donors with low BV/TV could be improved substantially by using donor-specific fits, this was not effective for either donor 7 or L2. While the problem of invalid stiffness matrices could be corrected when using the Cowin model, it was avoided in the Yang and Zysset models because of their use of log transformed data. This resulted in smaller errors at low BV/TV and thus smaller relative errors, especially in the case of the Zysset model (Figure 8.5). The major disadvantages of these two models were over-constraint in the case of the Zysset model and a lack of constraint for the Yang model. As opposed to the 18 constants in the Yang and Cowin models, the Zysset model was highly constrained with only 5. Because of the increased constraint, the Zysset model was very stable in the cross-validation. However, it did not have the flexibility necessary to model the relatively linear behaviour of E_{11} as a function of BV/TV, resulting in severely overestimated c_{1111} entries of the stress matrix (Figure 8.4, center). This was especially apparent for the magnitude of the absolute errors when fitting the data from the femoral neck (Figure 8.5A). In contrast to the Zysset model, the Yang model offered a great deal of freedom for the model fit. This model used only one dependent variable (BV/TV), but fit each stiffness matrix entry using two constants that were independent of the other stiffness entries. Although the Yang model was the only model that could consistently predict the Poisson's ratios (Table 8.3B) and did not suffer from the limitations of the Zysset model with respect to the behaviour of E_{11} , it still exhibited the poorest performance of the three models. This was not surprising since both of the other models included fabric as well as BV/TV as inputs. When split by stiffness matrix entry, the residuals of the Yang model were correlated to the fabric term as defined in the Zysset model with R^2 values of up to 0.54 for the c_{1111} matrix entry. The Yang model could also produce nonsensical results when used to extrapolate with respect to BV/TV. For example, if the fit from L2 were extrapolated to values of BV/TV greater than 0.24 the predicted value for E_{11} was actually smaller than that for E_{22} . Another example of this point can be seen where there was a large inflation of the estimation error in the cross-validation for the femoral neck.

In the present study we used finite element models derived from microCT scans to fully characterize the mechanical properties of our specimens. This has certain advantages as well as limitations. The greatest advantage of this method is that it is possible to fully characterize the mechanical properties of a small specimen using six simulated tests. This avoids many of the known limitations of mechanical testing such as artefacts due to end effects, the need for a priori knowledge of the material's principal directions, and the possibility of accumulating damage of the sample during sequential testing. However, because of the necessary assumptions that the bone tissue is a homogeneous isotropic material it is only possible to compare the mechanical behaviour of the trabecular architecture between donors or skeletal sites. It has been previously demonstrated in the BIOMED data set that mineralization varied both between donors and skeletal sites with the lumbar spine being the least mineralized and the femur most(198). This implies that subtle variations in bone tissue properties existed that were neglected in the current study.

A fundamental requirement for both finite element homogenization and traditional mechanical testing is that the specimens should be small enough to avoid heterogeneity of the structure yet still contain enough trabecula to act as a continuum. It has been previously demonstrated that these requirements are met when cubes are used where there are at least 5 trabeculae across the specimen in each direction. This is normally satisfied for a 5 mm block of human bone(220, 226). However, in the current study we analyzed a number of specimens with very low BV/TV. For these specimens the accuracy of the finite analysis may be limited due to the failure to meet the continuity assumption.

Although intuitive interpretation of the compliance matrix is easier, we chose to use the stiffness matrix for our analysis. It has been previously demonstrated that the Cowin model performs better when used with the stiffness matrix(55, 215) and this observation was repeated in our pilot testing. When fitting to the compliance matrix, the inversion of the elastic moduli tended to create large errors for the samples with low BV/TV where the finite element results were not as reliable.

Trabecular bone is an anisotropic material. Understanding the orthotropic behaviour of trabecular bone could lead to improved modelling of bone for device design or patient specific FE models. It could also improve understanding of adaptive bone remodelling and the response of bone to mechanical stimulus. The incorporation of measures bone anisotropy may improve failure criterion or improve the predictive power of existing measures of fracture risk. When it is not possible to obtain a measure of morphometric fabric, the model presented by Yang et al. provides a reasonable estimate bone's orthotropic mechanical properties. However, this model is not suitable for extrapolation with respect to skeletal site. Incorporating a measure of bone fabric into estimates results in a more accurate model, especially when the model is

trained using a set derived from the skeletal site of interest. However, donor-specific effects do exist and may degrade model performance for donors with low bone density.

Acknowledgements

The authors of this study would like to thank the Gift of Hope Organ and Tissue Donor Network and the BIOMED I project for the material used in this study. We would also like to thank Dr. Ada Cole, Dr. Arkady Margulis and Eileen Broderick for help in obtaining and preparing specimens. This work was funded by EU Grant QLRT-1999-02024 and NIH grants AR39239 and RR16631.

Chapter 9

Trabecular bone micro-architecture and orthotropic mechanical properties

Day JS, Waarsing JH, Sumner DR, Weinans H

Abstract

While bone mass is a major predictor of the mechanical properties of trabecular bone it is believed that trabecular micro-architecture is also important. In the present study we have investigated the contribution of micro-architecture to the orthotropic mechanical properties of human trabecular bone from two large datasets. The first set consisted of 487 trabecular bone specimens from the proximal tibia of 35 donors. The second set consisted of 235 specimens from the calcaneus, femoral neck, iliac crest, and second lumbar vertebra of 70 donors. MicroCT scans were used to quantify the following morphometric parameters BV/TV, BS/BV, Tb.Th, Tb.Sp, connectivity density, structure model index and the fabric tensor (by mean intercept length). Finite element models, created from the microCT images, were used to fully characterize the mechanical properties of each specimen. A principal components analysis revealed that the majority of variance in morphometry could be described by three components: density related (BV/TV, BS/BV, Tb.Th, structure model index), connectivity related (Tb.Sp, connectivity density) and anisotropy related variance. A fabric-based relation between morphometry and the elastic properties of trabecular bone was extended to include further variables. This resulted in a 13-16% reduction of the standard error of the estimate for these relations.

Introduction

Osteoporosis is described as, “a systemic disease characterized by low bone mass and microarchitectural deterioration of bone tissue, with a consequent increase in bone fragility and susceptibility to fracture (227).”. Because bone mass can be quantified directly using clinical tools such as DEXA, its link to fracture risk can be demonstrated directly. For women, the age-matched relative risk of fracture is between 1.3 and 2.6 for each standard deviation of bone density below the age-matched mean (26). The concept of bone quality, however, is multifaceted and includes degeneration of bone micro-architecture, quality of the collagen matrix, mineralization and the accumulation of microdamage. At this time, there are no widely accepted clinical tools to measure these parameters. As a result, the importance of bone quality for the resistance to fracture must be either measured in the laboratory or inferred from epidemiological evidence after correcting for bone mass.

The epidemiological case for the importance of bone quality is compelling. Independent of bone mass, risk factors for fragility fractures include: age, family history of fragility fractures, presence of a previous fracture, smoking, high levels of alcohol consumption, use of corticosteroids, and low body mass index. Further, the majority of fractures occur in patients who are not osteoporotic but osteopenic (227). While some of the aforementioned risk factors may be associated with an increased risk for falls, a case for the importance of bone quality remains strong.

The concept that bone micro-architecture may be a determinant of fracture risk is not new. It has long been noted that degeneration of the continuity of the trabecular structure in the proximal femur, as observed on radiographs, provides a useful index of osteoporosis (2). Multiple *in vitro* studies have been performed to quantify the relation between micro-architecture and either fracture or the mechanical properties of bone. Histological studies of biopsies of trabecular bone from subjects with fractures indicate that there is a decreased connectivity (186, 210, 228-230) and increased anisotropy (177, 212) compared to age matched or BMD matched controls. This is further supported by studies that apply multiple regression models to demonstrate that the mechanical properties of trabecular bone specimens are related to various architectural parameters such as connectivity, thickness, spacing or material anisotropy even after correction for bone mass (55, 171, 189-191). Of these regression models, none have performed consistently as well as the ‘fabric’ based models. These are models that predict the multiaxial mechanical properties of trabecular bone based on measures of bone mass and a description of the material anisotropy (or fabric), usually derived using the Mean Intercept Length (MIL) (44).

In the current study, we have investigated the importance of micro-architecture on mechanical stiffness using a unique data set of trabecular bone from a large number of donors and skeletal sites. First, using a principal components analysis we have investigated the structure of the variance within the morphometric data in order to identify architectural parameters that were likely to contain unique information. Next, we evaluated the improvement in performance of a fabric-based model to predict stiffness after incorporating further architectural variables. Finally, we investigated the ability of morphometric parameters to predict inter-subject and inter-site variations of the mechanical properties of trabecular bone.

Materials and Methods

Donor populations

Trabecular bone specimens were cut from the proximal tibia of 35 donors supplied by the Gift of Hope (GOH) Organ and Tissue Donor Network (male: $n = 18$, $\text{age}_{\text{mean}} = 65$ $\text{age}_{\text{sd}} = 12$; female: $n = 17$, $\text{age}_{\text{mean}} = 67$ $\text{age}_{\text{sd}} = 12$). Samples were prepared by cutting a transverse bone slab from the proximal tibia. The first cut was taken immediately distal and parallel to the subchondral bone plate at the proximal aspect of the tibial tuberosity. The thickness of the slab was scaled to 16% of the medial-lateral width of the tibia resulting in thicknesses that varied between 10-14mm. A rectangular grid of 7.5mm cylindrical specimens was drilled from this slab using a diamond core drill. This grid contained 3 samples in the anterior-posterior direction and 5 samples in the medial lateral direction, yielding ~15 samples per donor.

A second set of human trabecular bone specimens was obtained from European Union BIOMED I Concerted Action "Assessment of Bone Quality in Osteoporosis". This population, including cause of death, has been previously described in detail(198, 223). Briefly, trabecular bone samples originated from 70 human cadavers with ages ranging from 23-92 years (male: $n = 38$, $\text{age}_{\text{mean}} = 67$ $\text{age}_{\text{sd}} = 15$; female: $n = 32$, $\text{age}_{\text{mean}} = 73$ $\text{age}_{\text{sd}} = 15$). For the present study, 235 specimens from the right femoral neck, center of the second lumbar vertebral body, calcaneus, and anterior-superior part of the iliac crest were used. Samples were excluded if they contained compact bone, could not be harvested in one piece or contained large voids. A portion of the analysis of this data has been previously reported (189).

All samples were subjected to screening wherein samples were excluded from further analysis if they included compact bone, could not be harvested in one piece, had a BV/TV of less than 0.03 or contained large voids.

Micro-CT analysis

Specimens were scanned in one of two high-resolution micro-tomographic systems. GOH specimens were scanned at a nominal resolution of 20 μm (μCT 40, Scanco Medical AG.). After scanning, a 5mm cube was selected from the center of the sample for the subsequent analysis. A low-pass Gaussian filter was used to remove noise before segmenting the gray scale images using individual thresholds as determined using Archimede's principle (63). BIOMED specimens were scanned at a nominal resolution of 14 μm (μCT 20, Scanco Medical AG.) and a 4mm cubic volume of interest was chosen for analysis. A low-pass gaussian filter was used to remove noise before segmenting the gray scale images using a fixed threshold. The three-dimensional mean intercept length (MIL) tensor was defined as determined for each specimen using the method of directed secants (43, 44).

Finite element analysis

Finite element (FE) models were used to calculate the orthotropic apparent stiffness tensor for each sample. Voxel based models were created with a voxel size of 20 μm for the GOH specimens and 28 μm for the BIOMED specimens. For all elements, linear elastic and isotropic material properties were assigned with a Young's Modulus of 10 GPa and a Poisson's ratio of 0.3. A series of six finite element problems were solved for six uniaxial strain cases using the preconditioned conjugate gradient method. The nearest orthotropic stiffness tensor could then be determined for each sample (20-22).

Principal components analysis

A principal components analysis was performed on the two sets to identify common factors in the morphometry data. In this way, we could determine which of the morphometric parameters shared variance. We used the following parameters as variables: BV/TV, $\ln(\text{BS}/\text{BV})$, SMI(46), CD(49), Tb.Th, Tb.Sp(45), and the degree of mechanical anisotropy (DA) derived from the FE data (E11/E33). We chose to use the FE data to calculate the degree of anisotropy because we feel that the FE model gives the 'gold standard' for anisotropy. The log transformation of BS/BV was necessary to improve linearity in relation to the other variables. After viewing the scree plots (plots of the eigenvalues sorted by relative size) for the two analyses we chose to extract 3 components (231). The analysis was performed on the correlation matrix and employed a varimax rotation. This type of rotation is used to improve interpretation of the results.

Morphology-elasticity relations

The relations presented by Cowin et al. are normally used to predict the entries of the stiffness matrix (c) based on a power relation for the volume fraction (k) and the entries of the fabric tensor (m). In our pilot testing we have determined that 1.45 was the optimal exponent for this power relation. In this relation, the eigenvalues of the fabric tensor (m_1, m_2, m_3) were

derived from inverse of the square root of the MIL tensor then sorted such that $m_1 > m_2 > m_3$ and normalized such that $m_1 + m_2 + m_3 = 1$ (56, 191, 219).

$$\begin{aligned}
 c_{iiii} &= k_1 + 2k_6 + (k_2 + k_7)II + 2(k_3 + 2k_8)m_i + (2k_4 + k_5 + 4k_9)m_i^2 \\
 c_{ijij} &= k_1 + k_2II + k_3(m_i + m_j) + k_4(m_i^2 + m_j^2) + k_5m_im_j \\
 c_{jijj} &= k_6 + k_7II + k_8(m_i + m_j) + k_9(m_i^2 + m_j^2) \\
 II &= m_2m_3 + m_3m_1 + m_1m_2
 \end{aligned} \tag{1}$$

We have extended the original power function (k_{11}, k_{12}) to incorporate a number of linear morphometric terms (k_{13} to k_{17}):

$$k_i = k_{i1} + k_{i2}BV / TV^{1.45} + k_{i3}CD + k_{i4}SMI + k_{i5}Tb.Th + k_{i6}Tb.Sp + k_{i7}BS / BV \tag{2}$$

The terms k_{13} to k_{17} were not entered into this relation in a block, but in a stepwise fashion. The value of 1.45 for the exponent was determined to be appropriate during pilot testing. At each step the term was added that yielded the largest improvement of the Pearson correlation coefficient and the significance of this improvement was evaluated using an F test as follows(224):

$$F = \frac{(R_{extended}^2 - R_{general}^2)(9n - p_{extended} - 1)}{(1 - R_{extended}^2)(p_{extended} - p_{general})} \tag{3}$$

where F had $(p_{extended} - p_{general})$ and $(9n - p_{extended} - 1)$ degrees of freedom.

In addition to the fabric-based relation of Cowin we also included the model presented by Yang et al. which uses a power based relation to fit the components of the stiffness matrix (c) based on volume fraction alone (217, 222).

$$\begin{aligned}
 c_{iiii} &= \lambda_{0ii} \rho^{k_{ii}} \\
 c_{ijij} &= \lambda_{0ij} \rho^{k_{ij}} \\
 c_{jijj} &= \mu_{0ij} \rho^{k_{ij}}
 \end{aligned} \tag{4}$$

where $i, j = 1, 2, 3; i \neq j$. Thus 9 multiplicative ($\lambda \times 6, \mu \times 3$) and 9 exponential (k) constants were required to determine the mechanical properties. The value of ρ used in this study was not the true apparent density, but the bone volume fraction (BV/TV). This model was included so that it would be possible to evaluate the contribution of fabric to the predictive power of the models.

The constants for each relation were fit using the multiple regression method described in detail by Zysset (55). Briefly, the equation:

$$\mathbf{c} = \mathbf{X}\mathbf{b} + \mathbf{e} \quad (5)$$

was constructed where \mathbf{c} was a $9n$ vector containing the 9 unique components of the compliance matrix for n specimens, \mathbf{X} was the $9n \times p$ matrix containing the volume fraction and fabric data, \mathbf{b} was a vector containing the p constants in the model and \mathbf{e} was the vector of the residuals. Equation (4) could then be solved for \mathbf{c} using singular value decomposition to obtain the pseudo-inverse \mathbf{X}^+ of \mathbf{X} :

$$\mathbf{b} = \mathbf{X}^+ \mathbf{c} \quad (6)$$

All of the morphometry-elasticity analyses were performed using custom written Matlab (<http://www.mathworks.com>) code.

Variance Components Analysis

In order to understand the structure of the residual variance after fitting the morphometry-elasticity relations, we performed a variance components analysis. For each of the Yang, Cowin and extended Cowin analyses the residuals were used as a dependant variable. Donor and skeletal site (BIOMED only) were entered as random factors and the variance structure was extracted using the maximum likelihood method.

Results

Principal components

In the principal component analysis it was possible to account for over 92% of the total variance in morphology using 3 principal components. The scores of the first principal component were dominated by BV/TV, BS/BV, Tb.Th and SMI. The second component was dominated by CD and Tb.Sp and the third component was dominated by the DA. Generally, we considered the components to represent ‘density related’, ‘connectivity related’ and ‘anisotropy related’ variance, respectively. These results were very similar for the two data sets (Table 9.1).

Morphology-elasticity relations

All of the morphology-elasticity relations tested in the current study gave excellent prediction of the components of the stiffness matrix for both data sets with Pearson’s correlation coefficients that ranged from 0.96 to 0.99 (Table 9.2, Figure 9.1). Moving from the Yang model, which used only BV/TV as an independent variable, to the Cowin model, which included

BIOMED DATA	Component		
	1	2	3
Cumulative % of Total Variance	51.8	78.5	93.8
BV/TV	-0.904	-0.364	-0.191
ln(BS/BV)	0.971	-0.046	0.197
Tb.Th	-0.956	0.075	-0.112
SMI	0.861	0.209	0.318
CD	0.128	-0.920	-0.181
Tb.Sp	0.298	0.898	0.047
DA _{mech}	0.329	0.183	0.920
GOH DATA	Component		
	1	2	3
Cumulative % of Total Variance	48.4	78.1	92.7
BV/TV	-0.879	0.454	-0.047
ln(BS/BV)	0.979	0.001	0.110
Tb.Th	-0.943	-0.070	-0.145
SMI	0.841	-0.262	-0.001
CD	-0.023	0.966	-0.027
Tb.Sp	0.212	-0.932	-0.054
DA _{mech}	0.126	0.014	0.990

Table 9.1: Rotated components from principal components analysis of morphometry data. The three principal components represent over 90% of the variance in the morphometry data in a more compact form. The first component represents the 'density related' portion of the variance. The second component represents 'connectivity related' variance and the third represents 'anisotropy related' variance. Component loadings of less than 0.3 were considered of lesser importance and are greyed out to facilitate interpretation of the results.

fabric as an independent variable, resulted in a 15% reduction of the standard error of the estimate (SEE) for the BIOMED data and a 37% decrease in the SEE for the GOH data. Extension of the Cowin model resulted in a further 16% decrease of the SEE for the BIOMED data and a 13% decrease of the SEE for the GOH data (Table 9.2). In both the BIOMED and GOH data, the two morphometric parameters that gave the best improvement of the model in the first step of the regression were CD and Tb.Sp. In the BIOMED data, CD performed slightly better than Tb.Sp and this was reversed in the GOH data (Table 9.2). In both data sets SMI was the second parameter included in the extended model. Although all of the architectural parameters gave significant improvement to the model fit (as assessed by F tests for

	BIOMED		GOH	
	R ²	SEE	R ²	SEE
Yang (BV/TV)	0.9796	56.5	0.9600	41.6
Cowin (BV/TV + Fabric)	0.9852	48.3	0.9842	26.3
Cowin + BS/BV	0.9868	45.7	0.9859	24.9
Cowin + CD	0.9880	43.6	0.9875	23.5
Cowin + SMI	0.9874	44.6	0.9865	24.3
Cowin + Tb.Th	0.9872	45.0	0.9862	24.6
Cowin + Tb.Sp	0.9879	43.8	0.9873	23.6
Cowin + CD + SMI	0.9894	41.0		
Cowin + Tb.Sp + SMI			0.9882	22.8
Cowin + CD + SMI + Tb.Th	0.9898	40.2		
Cowin + Tb.Sp + SMI + CD			0.9888	22.2
Cowin + CD + SMI + Tb.Th + BS/BV	0.9903	39.3		
Cowin + Tb.Sp + SMI + CD + Tb.TH			0.9898	21.3
Cowin + All	0.9904	39.0	0.9900	21.1

Table 9.2: Summarized results of multiple regression analysis. A stepwise multiple regression analysis was performed to determine whether the addition of morphometric parameters could improve the prediction of the components of the stiffness matrix compared to a fabric based morphometry-elasticity model (Cowin). A density-based model (Yang) was also included to assess the contribution of fabric. Models were evaluated based on goodness of fit (R²) and the standard error of the estimate (SEE).

BIOMED Data						
Variance Component	Yang	Cowin	Extended	Yang	Cowin	Extended
Skeletal Site	246	146	13	7.5%	6.1%	0.8%
Donor	122	139	24	3.7%	5.8%	1.6%
Donor-Site Interaction	209	313	46	6.3%	13.1%	3.0%
Unexplained Error	2715	1793	1464	82.5%	75.0%	94.6%
GOH Data						
Variance Component	Yang	Cowin	Extended	Yang	Cowin	Extended
Donor	110	117	14	6.1%	16.4%	3.1%
Unexplained Error	1697	598	442	93.9%	83.6%	96.9%

Table 9.3: Variance components analysis of the residuals. After fitting the morphology-elasticity relations, a variance components analysis was used to identify structure within the residuals. Residual variation was partitioned into skeletal site (BIOMED only), donor, interaction (where appropriate) terms, and unexplained error. The results are expressed in raw variance (left) and percent of total variance (right).

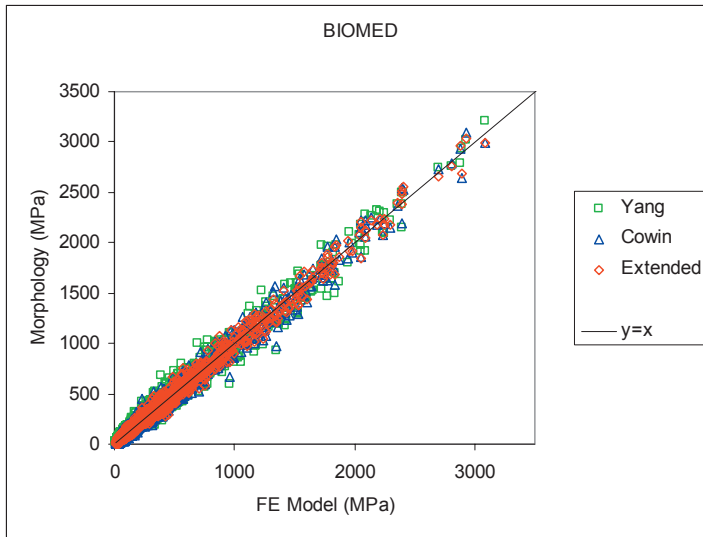


Figure 9.1A: BIOMED data.

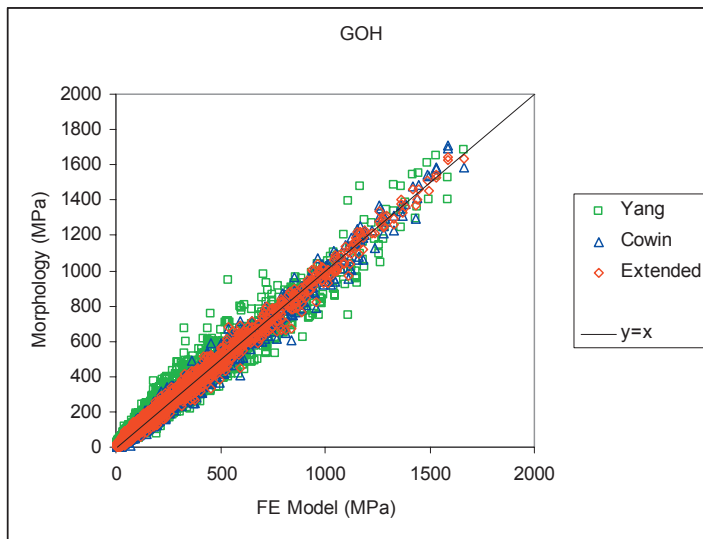


Figure 9.1B: GOH data.

Figure 9.1: Predicted stiffness matrix entries plotted against FE derived values for 3 morphology-elasticity models. The Yang model was used to predict elasticity based on only density (BV/TV). The Cowin model utilized a combination of density and fabric ($BV/TV + fabric$). The extended model was an extension of the Cowin model that included (BV/TV , fabric, BS/BV , connectivity density, structure model index, $Tb.Th$ and $Tb.Sp$).

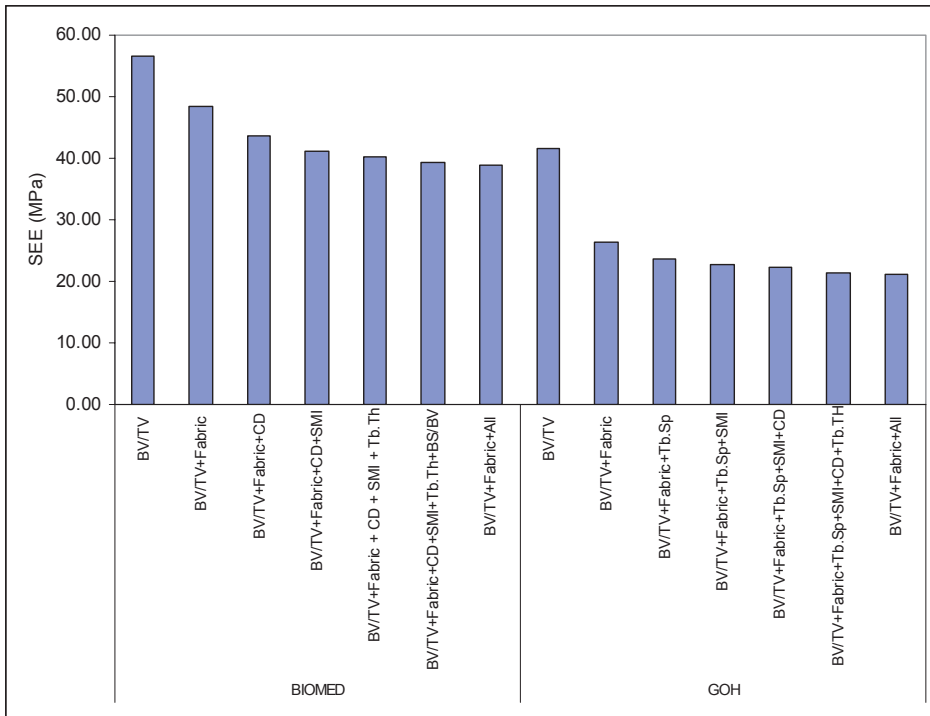


Figure 9.2: Regression results summarized as the standard error of the estimate (SEE). Step-wise multiple regression models were used to assess whether the additional morphometric variables would result in significant improvement for the estimation of the components of the stiffness matrix compared to a fabric-based model (Cowin: BV/TV + Fabric). These results of these analyses are summarized above for each step in the regression as the standard error of the estimate. A density-based model (Yang: BV/TV) was included to assess the contribution of fabric to the overall model fit.

change in R^2), the majority of the improvement was seen after the entry of the first one or two architectural parameters (Figure 9.2; Table 9.2).

Variance Components

In the analysis of the residual variance similar patterns were seen in both data sets. Moving from the Yang model (BV/TV) to the Cowin model (BV/TV + fabric), there was little reduction of the donor-dependant error. There was, however, a 40% reduction in the site dependant error in the BIOMED set and a large reduction of the unexplained variance in both sets. Moving from the Cowin model to the extended model (BV/TV + fabric + architecture) virtually eliminated both the site dependant and donor dependant portions of the residual error (Figure 9.3; Table 9.3).

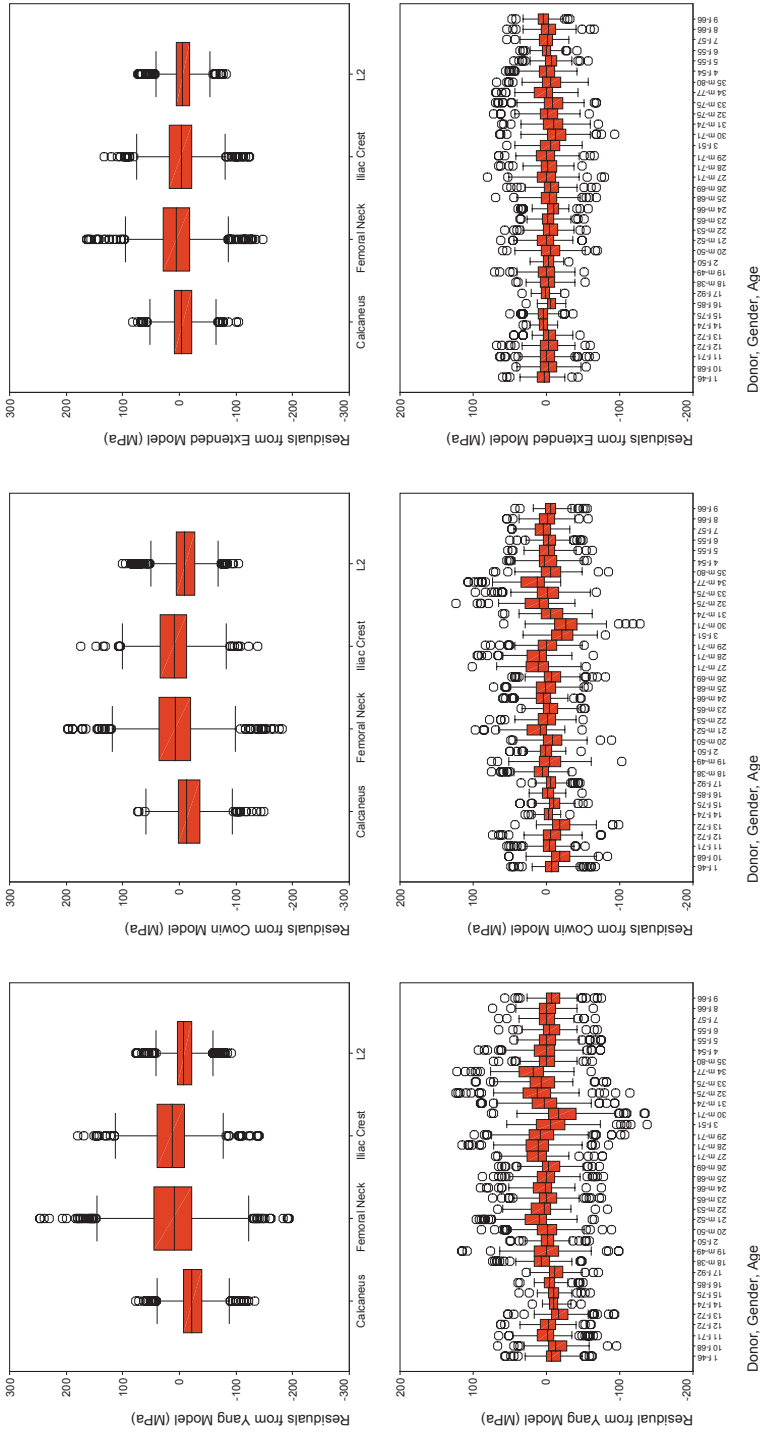


Figure 9.3: Boxplots of the residuals from the BIOMED data by skeletal site (left) and GOH data by donor (right) for the Yang model (top), Cowin model (middle) and extended Cowin model (bottom). Extending the Cowin model by adding other architectural parameters was effective at reducing the magnitude of the residuals, as well as site-related and donor related effects.

Discussion

In the current study, our aims were to investigate whether additional aspects of micro-architecture information would improve the prediction of the orthotropic mechanical properties of trabecular bone. We used a principal components analysis to identify likely candidates from a pool of morphometric parameters. We found that much of the variance in morphology could be described by 3 components: a 'bone mass' component, a connectivity (or spacing) component, and an anisotropic component (Table 9.1). Our results are similar to those reported in a previous principal components analysis of the mandibular condyle (19). In our previous study we observed that the morphology-elasticity relation proposed by Cowin (56, 191) provides excellent prediction of the components of the orthotropic stiffness matrix. This relation already included bone density and fabric as independent variables and we considered that it was an excellent candidate for extension to include further architectural terms. We used a stepwise approach to extend the Cowin model, at each step adding the morphometric parameter that yielded the largest significant improvement in the fit between morphology and elasticity. As was inferred by the principal components analysis, connectivity density and trabecular spacing both gave excellent improvements in the first step of the model extension. Structure model index was chosen as the second extended variable in both data sets. While addition of further variables did result in significant improvement of the model, these improvements were rather modest (Table 9.2).

Because bone density is the current clinical gold standard, we compared our results to a morphology-elasticity relation that used only bone density (BV/TV) as an independent variable (217). We used a variance components analysis of the residuals to partition the variance between random effects for donor and site as well as error term. We found that moving from a density-based relation to one that also included fabric reduced a great amount of the site-related variance and much of the unexplained variance (error term) but not the donor effect. Extension of the relation to include further aspects of micro-architecture reduced the amount of donor-related residual variance to negligible levels (Figure 9.3).

It has been extensively reported that the uniaxial mechanical properties of trabecular bone are strongly related to the apparent density (52, 53). The relation between density and Young's modulus varies widely between skeletal sites. This is also the case for both the shear properties and the degree of mechanical anisotropy (37, 40, 41, 232). The importance of mechanical anisotropy and its relation to the morphometric fabric has been previously noted, and multiple relations have been proposed to relate the mechanical properties to density and fabric (55, 56, 171, 191, 218-220, 233). In the present study we have demonstrated that the addition of fabric to the density relations (i.e. moving from the Yang model to the Cowin model) resulted in a substantial reduction of the residual variance associated with skeletal site. In addition to the

reduction of the site-related component, there was also a large reduction in the ‘unexplained’ component of the residual variance. It is likely that the addition of fabric to the model was also able to correct for the wide range of bone anisotropy observed within a single skeletal site. In this case, the reduction of the unexplained error was due to within-site variation of the sampling location. This can explain why this reduction was so large in the GOH data where we intentionally took samples from a variety of locations within one skeletal site as opposed to the BIOMED data where the sampling location was controlled as strictly as possible

In the current study we have extended a fabric based morphology-elasticity relation to include further architectural variables. We chose to use fabric-based models because they are known to give excellent predictions for the full orthotropic stiffness matrix (55, 191). Previous studies have used one of two methods to investigate the effects of micro-architecture on trabecular bone mechanics. In the first approach, similar to ours, the mechanical properties of a number of samples were characterized either by mechanical testing or finite element modeling. Multiple regression methods were then used to construct predictive models based on the morphology (171, 174, 175, 215). In the other approach, a population of pathological donors were compared to an age matched or BMD matched control group. This approach has been used frequently to assess bone quality in groups that have experienced fractures (i.e. exhibit inferior mechanical properties) (170, 177, 186, 209, 210, 229, 230, 234). While the two approaches tend to yield similar results, there is considerable disagreement on the role of connectivity. Studies that compare fracture patients to controls seem to consistently indicate that fracture is associated with lower bone connectivity. However, a recent study of the effect of connectivity on bone stiffness after controlling for bone mass indicated a decline in stiffness was associated with increased connectivity. In addition, it has recently been demonstrated that reduced mechanical stiffness can be accompanied by either an increase or decrease of connectivity (132). This is because during bone loss, connectivity can be increased when a trabecular plate is perforated or decreased when a strut is severed. In the current study we found that ‘connectivity related’ parameters (CD and Tb.Sp) were important for the reduction of donor-dependant residuals. While this indicated a potential for ‘connectivity related’ parameters to identify patients with a propensity to fracture, we also observed a negative relation between connectivity and adjusted stiffness (observed by examining the residuals from the basic Cowin model).

In the current study we used finite element models to estimate the orthotropic mechanical properties of 4-5 mm cubes of trabecular bone. Our morphometric analysis was performed using true three-dimensional parameters. While we feel that these methods are the best available for this type of analysis they still have limitations. For the finite element analysis it was necessary to assume that the Young’s Modulus of bone at the matrix level was isotropic, homogenous, and was the same for all of the donors. Thus, we examined the contribution

of only micro-architecture to the mechanical properties and ignored all tissue and matrix level effects such as mineralization or microdamage. A second assumption, required for the homogenization of the finite element results was that the samples of trabecular bone were sufficiently large as to approximate the apparent mechanical properties as a continuum. This is normally satisfied for a 5 mm block of human bone(220, 226). However, in the current study this limit may have been exceeded for specimens with low bone volume fractions. Our use of three-dimensional model free morphometric parameters was intended to reduce biases that can be introduced when using the parallel plate model (43, 45, 54, 193, 233). This is of particular concern in the present study where trabecular spacing was an important parameter. Because the plate model calculates the trabecular thickness, spacing and number based on a measured surface and bone volume fraction it severely constrains the solution, especially for the trabecular spacing (193). In the present study, we have demonstrated that the connectivity and trabecular spacing contain important information that is independent of the specific surface (BS/BV) and the bone volume fraction. Similar to the finite element models, the measurement of morphometric parameters requires large enough samples to be representative of the structure with minimal edge effects (235). While we have demonstrated interesting findings in the current study, we feel that it is likely that much of the unexplained variance is due to sampling noise in our relatively small specimens.

We recommend that a description of trabecular micro-architecture requires one measure of bone mass, one measure of anisotropy and one of connectivity related parameters. Using a combination of these three measures seems to provide enough information to predict the orthotropic mechanical properties of trabecular bone. After correcting for bone mass, accounting for morphometric anisotropy is necessary for the prediction of the mechanical properties of bone from multiple skeletal sites. For differences between people, a measure of connectivity is necessary.

Acknowledgements

The authors of this study would like to thank the Gift of Hope Organ and Tissue Donor Network and the BIOMED I project for the material used in this study. We would also like to thank Dr. Ada Cole, Dr. Arkady Margulis and Eileen Broderick for help in obtaining and preparing specimens. This work was funded by EU Grant QLRT-1999-02024 and NIH grants AR39239 and RR16631.

Chapter 10

Final Discussion

In the current body of work, we have examined many aspects of the concept of ‘bone quality.’ Curiously, ‘bone quality’ is defined not by what it is, but by what it is not; i.e. bone quality describes all of the properties of bone that are not bone mass. In essence, quality is a combination of micro-architecture, collagen quality, mineralization, mineral quality, and microdamage.

Bone as a material has many hierarchical levels of organization. Thus, any discussion of its mechanical properties should also take into account the level of organization that is under investigation (67). At the nanostructural scale, the Young’s modulus of bone is determined by the material composition, matrix quality, and lamellar structure and varies between 12 and 30 GPa (65, 236, 237). At the microstructural level (micron scale) material discontinuities such as microcracks, osteocyte lacuna and osteonal boundaries disrupt the material continuity. The resulting Young’s modulus is therefore reduced, usually in the range from 5 to 20 GPa (20, 52). At the structural level (or apparent level in trabecular bone), the mechanical properties of bone are influenced by all of the underlying material properties plus the effects of porosity and micro-architecture. At this level of scale, the Young’s modulus can vary widely in the mega to gigapascal range.

We have been able to take advantage of recent developments in microcomputed tomography, finite element modeling, and three-dimensional morphometry to both characterize bone micro-architecture and evaluate its contribution to the elastic properties at the apparent level. Using a variety of methods we have also investigated the properties of the calcified tissue at the microstructural level. While our use of highly detailed finite element models allowed us to uncouple the effects of micro-architecture from the material properties, there were some limitations. The modeling assumptions required the properties of the calcified tissue to be approximated as an isotropic homogenous medium. This is a simplification of the true material properties (158, 159). The resolution of the model, sample size and the applied boundary conditions can also affect the results of finite element analyses (15, 70). Additionally, non-ideal behaviour such as buckling could not be represented by the models’ linear brick elements (16). We have taken care to minimize these errors during our experiments by using bone samples that were of adequate size to represent the true continuum(226), by ensuring that scans and finite element models were of sufficient resolution to minimize errors, and by using mechanical testing protocols that produced only limited end-effects (17). However, we feel that there were limitations to the accuracy of the models for bone samples with very low bone volume fractions.

Morphometric parameters and bone micro-architecture

Recent advances in imaging and image analysis have led to an explosion of the number of morphometric parameters that can be quickly and conveniently measured. In chapter 6, we demonstrated that the use of 3D methods eliminate the biases introduced by 2D model-based methods. However, it should be noted that many parameters are introduced with little consideration of how they relate to previously existing parameters or whether they actually offer new or better information. In our study of a limited number of parameters (chapter 9) we found that the information from seven morphometric parameters could be represented by three principal components that broadly represented density-related, connectivity-related, and anisotropy-related variance. These findings were in agreement with a previously published study (19) and will be discussed further in the following sections.

In addition to the baffling number of available morphometric parameters, the results of many morphometric studies are presented using obsolete techniques. Although a clearly superior direct method exists for the measurement of thickness and spacing of trabecular structures, many researchers still use the plate model, a method that is well known to produce biased results (43, 45, 54, 193). Although there has been some effort towards standardization of the measurement and reporting of two-dimensional histomorphometry (166), this has not yet occurred for three-dimensional methods.

While morphometric parameters are useful for interpreting the mechanisms of bone degeneration with aging or disease, the ‘Holy Grail’ of this field is the search for the perfect parameter, or combination of parameters for the prediction of fracture. We consider micro finite element (FE) models to provide a ‘gold standard’ measure of the contribution of architecture to the mechanical properties of trabecular bone. By assuming that bone is an orthotropic material, its stiffness can be fully described by a mere 9 constants: 3 Young’s moduli, 3 shear moduli and 3 poisson ratios (21, 190, 218). However, use of FE models for the prediction of fracture risk will require an increased knowledge of the forces encountered during fracture. Although it is well known that the strength and stiffness of bone are highly correlated during uniaxial loading there have been few studies of multiaxial loading. Further, the applied loads encountered during clinical fracture are not yet completely understood. Therefore, it is not currently known whether the principal axis strength, off-axis strength, rigidity or a combination of these properties are crucial(238).

While FE modeling provides an ideal method for the examination of bone properties in the lab, there are significant barriers to its clinical use. Achieving a scanning resolution that is sufficient to resolve individual trabeculae requires expensive equipment and, for computed tomography, high doses of radiation. In contrast, DXA, the current clinical standard, provides both a safe and inexpensive method to measure both areal BMD and the macro-geometry of

the skeletal site of interest. For these reasons, it is likely that DXA will continue to be used as the clinical gold standard in the near future.

Structural anisotropy

Trabecular bone is mechanically anisotropic and its efficiency as a material lies the arrangement of its porous structure. It has long been proposed that the alignment of bone fabric is adapted to the principal stress trajectories (3), and this has been applied to simulations of bone adaptation (9, 239). While there has been intensive study of the factors that influence bone mass, there is little known about the development or control of anisotropy in trabecular bone. In a recent study of the development of structure in porcine bone it was demonstrated that bone density was adapted to mechanical loading early in development and that this was followed by reorganization of the anisotropic structure (240). It has been also suggested that in the vertebrae, the structural anisotropy increases during aging as horizontal trabeculae are preferentially resorbed (214, 241). In our study of bone morphometry, we have confirmed previous observations that the degree of anisotropy was one of the few morphometric parameters that was not highly correlated to the bone mass (38, 199). In our principal components analysis of morphometric parameters, we identified anisotropy as an independent factor. Surprisingly, when we investigated morphometry-elasticity predictive models, we found that the addition of fabric to a model based on bone volume fraction reduced the residual variance significantly, but that this reduction was associated with site-dependant and sampling effects rather than to donor-related effects.

In order to further understand the role of anisotropy, we have investigated a sub-population of the GOH data set. This data set consisted of biopsies of trabecular bone from the proximal tibia of 35 donors. Based on previous suggestions that the loss of horizontal trabeculae plays an important role in aging in females, we selected 5 female donors with low bone mass for further analysis. We found that although these donors tended to have a highly connected trabecular network there was surprising variation in the thickness and spacing of the trabeculae (Appendix B; Figure 10.4). Further, the micro-architecture of the bone from these donors was, after correction for bone volume fraction, much stiffer than the rest of the population in the main direction (E_{11}) and weaker than the rest of the population in the transverse directions and in shear (Appendix B; Figure 10.5). Similar results have been reported previously in both the vertebrae and femoral heads of donors who experienced fractures as compared to controls (242). In this study it was suggested that osteoporosis and the tendency to fracture were actually due to over-adaptation of bone structure to normal mechanical stimulus. While our results do indicate that the donors with low bone mass were over-adapted in the principal loading direction we could not confirm whether this was a cause or effect of bone loss.

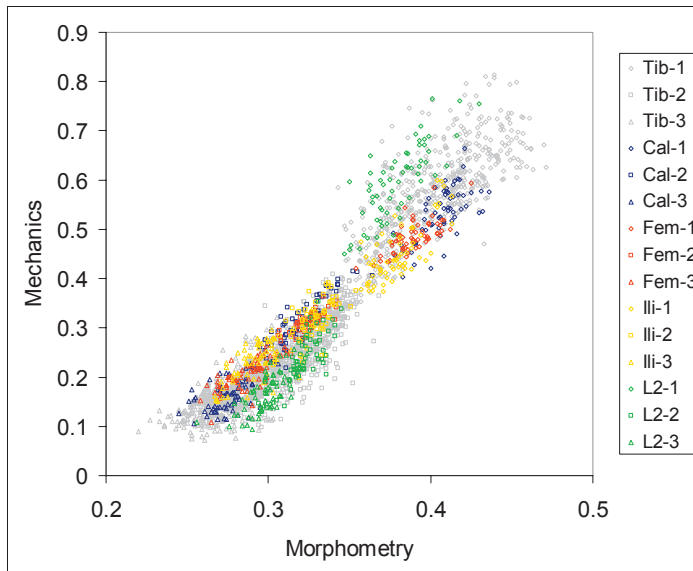


Figure 10.1: A plot of the eigenvalues of the fabric tensor plotted against the normalized principal Youngs Moduli. The ‘strength’ of the fabric in the three principal directions (normalized so that $h_1 + h_2 + h_3 = 1$) was plotted against the normalized Youngs moduli (normalized so that $E_{11} + E_{22} + E_{33} = 1$) for each sample. Samples are grouped by site with the same colour and plotted for all three directions (i.e. Tib-1 is a tibial sample plotted for the main direction). This graph shows that there were clear site-dependent effects on the relation between morphometric and mechanical anisotropy. A further investigation revealed this relation was also influenced by bone volume fraction.

Further, although we didn’t have a large enough sample size to perform a rigorous statistical analysis, it seemed that this ‘over-adaptation’ was common in donors with low bone volume fractions.

In our study of morphometry-elasticity relations we chose to use the mean intercept length for the measurement of fabric (44). This method is surface based and quantifies the number of bone/marrow interfaces in each direction. A number of other volume based methods have been proposed and generally yield similar results (215, 243).

In chapter 8 we saw that the relation between morphological and mechanical anisotropy was site-dependant. We have displayed this relation again in a slightly different format in this chapter (Figure 10.1). A further investigation revealed that part of this effect could be explained by differences in the bone volume fraction between sites (data not shown). It is possible that other architectural differences between the skeletal sites were also involved. It is

also possible that some of the differences were due to a mechanical transition from trabecular bending at the lowest volume fractions to a combination of bending and axial loading at higher volume fractions.

Structural connectivity

Structural connectivity is often considered an important determinant of the strength of trabecular bone. During normal bone remodeling, thin trabeculae may become disconnected during resorption. These trabeculae are often not reconnected during the formation phase and are thereafter ‘lost.’ It is believed that the loss of trabecular connections, especially in the directions that are not routinely loaded, is more pronounced in women than men during aging (207, 208). A decrease of trabecular connectivity has been observed in biopsies from the iliac crest of patients with vertebral fractures (186, 210, Legrand, 1999 #804, 229). This supported the concept that a loss of connectivity during aging can disrupt the trabecular network, resulting in weaker bone. However, this view has been challenged as there have also been a number of studies that demonstrated unchanged or increased connectivity in trabecular bone both from sites of fracture and from the iliac crest (177, 209, 244, 245).

Although many studies have investigated the micro-architecture of patients who have experienced fractures, few studies have tried to directly quantify the contribution of connectivity to the mechanical properties of trabecular bone. Kabel et al. used microFE models to study the contribution of connectivity to the mechanical properties of trabecular bone specimens after correcting for the bone volume fraction (174). They found that adding connectivity to the relation between the Young’s modulus and bone volume fraction reduced the residual error by a modest 8% in a set of multiple biopsies from various anatomic sites of one donor. In a dataset with a smaller number of samples from a multiple donors, the connectivity accounted for 31% of the residual error. It was striking that higher values of connectivity were associated with a decreased Young’s modulus. In a similar study, a simulation model was used to investigate the changes of the mechanical properties in a small number of specimens during bone atrophy and recovery (175). No functional relationship was found between connectivity and elasticity, but there was a linear relation between loss of connectivity and loss of elastic modulus. When considered together, it seems that there may be different mechanisms involved with the loss of connectivity during aging (i.e. within one person) compared to developmental or genetic differences in connectivity between people.

In the current body of work we observed a substantial range in the relation between micro-architecture and bone volume fraction. As we have noted in Chapter 7, the micro-architecture varied widely between donors and we could clearly identify donors with a ‘coarse’ structure

(low connectivity, wide spacing, thick, plate-like trabeculae) and donors with a ‘fine’ structure (high connectivity, close spacing, and thin, rod-like trabeculae). Connectivity was tightly related to the trabecular spacing and the variation of connectivity was somewhat independent of both the bone volume fraction and the degree of anisotropy. Addition of connectivity or trabecular spacing to a fabric-based model for predicting the elastic properties of bone decreased the residual variance by approximately 15%. Much of the donor-specific variance was related to the connectivity (Chapter 9). In order to further investigate the effect the architecture on the mechanics we have plotted data from a subset of ‘coarse structured’ and ‘fine structured’ donors in Appendix C (Figure 10.6). When we examined the FE data, we found that the coarse structures were architecturally more efficient with a higher elastic modulus and rigidity in all of the principal directions with the exception of the main loading axis. The observation that the relative stiffness was not different in the main direction may indicate that although these different donors employed different architectural strategies, the stimulus to which they adapted was the loading in the main direction, thus resulting in similar resultant stiffness of the bone in that direction.

Bone quality, micro-architecture and calcified tissue properties; implications for clinical treatment

In the previous sections of this chapter, we have been presented with what seems to be contradictory evidence. In our examination of trabecular micro-architecture, the donors with a ‘coarse’ trabecular structure had a more efficient architecture than those with ‘fine’ trabecular structure. However, in Chapter 7 we saw that in the BIOMED dataset (biopsies from 70 donors at four skeletal sites), donors who had experienced previous fractures tended to have ‘coarser’ structure i.e. wider trabecular spacing with a lower trabecular number. This suggests that there may be some interaction between the calcified tissue properties and the trabecular micro-architecture. In a recent series of articles, Banse et al. demonstrated that both the mechanical properties of bone and its micro-architecture were related to collagen cross-link profiles, independent of bone mass (33, 129, 246). We did not have information regarding the collagen properties of the specimens in our two data sets (GOH and BIOMED). However, in the GOH data we had determined the calcified tissue density using Archimedes’ principal. This average density provides a rough measurement of tissue mineralization, as we have already demonstrated in our study of bisphosphonate treated dogs (Chapter 5). Using the average density as a proxy for mineralization, we chose the 3 donors with the highest and 3 donors with the lowest tissue density and plotted the relation between bone volume and morphometric parameters (Appendix D; Figure 10.8). We found that the hypermineralized donors had ‘fine’ structured bone and the hypomineralized donors had ‘coarse’ structured bone (Appendix D; Figure 10.9). It is well known that high levels of bone turnover are an

independent risk factor for osteoporotic fracture (247). Because of the methods used to collect samples for the GOH data set, we could not screen the donors' medical histories (i.e. for secondary hyperparathyroidism, renal disease, anti-resorptive therapy etc.). However, it is not unreasonable to suggest that the differences in levels of mineralization seen in our donors may be due to differences in bone remodeling rates between these donors. If this were the case, it suggests that the matrix quality of the hypomineralized donors may be of inferior quality.

In general, our findings support the idea that there is an optimal 'window' for both bone turnover and mineralization. In chapter 5 we demonstrated that hypermineralization related to reduced remodeling after bisphosphonate treatment did not increase the elastic stiffness of the bone and resulted in an accumulation of microdamage. In chapter 7 we demonstrated that donors with similar bone densities can have very different trabecular architectures. In Appendix D of this chapter, we have presented preliminary evidence of a link between the tissue properties at the nanostructural scale and the resulting microstructure. At the present time we do not know if the variation in micro-architecture was due to genetic causes, inherent differences in the matrix properties, differences in remodeling rates between donors independent of the matrix properties, or the donors' medical history and lifetime history of loading. However, the underlying reasons for the differences in both structure and tissue properties should be considered with respect to pharmaceutical treatment for the prevention of fracture.

Bone and the progression of osteoarthritis

It is undeniable that osteoarthritis is a disease that affects all of the tissues of the afflicted joint. In bone, the formation of osteophytes and subchondral cysts as well as sclerosis and densification of the subchondral plate are clearly visible on radiographs. Since Radin introduced his theories regarding the role of subchondral bone in the initiation and progression of osteoarthritis (OA) there has been lively debate on whether initiation of the disease begins in the cartilage or the underlying bone (50, 51). While resolution of this point is of great importance for the understanding of OA etiology, the focus on the role of bone in disease initiation obscures the fact that successful management of the disease will require management of both cartilage and bone degradation. Efficient function of a joint requires both a viable cartilage surface for smooth lubrication as well as stable joint kinematics, provided by the underlying bone. Joint biomechanics can be compromised by the erosion and deformation of the bony structures, while painful impingement of soft tissues by osteophytes can limit the range of motion. It is likely that proceeding with either chondroprotective or cartilage repair treatments without addressing bone related issues would limit the long-term success of any treatment.

In the current body of work, we have investigated the effects of osteoarthritis on the subchondral trabecular bone. In Chapter 2 we observed a reduction of the effective tissue Young's modulus with in the presence of cartilage damage. The donor material that we used for this study was a subset of a larger study where an increased bone volume fraction and decreased apparent Young's modulus were observed in the donors with damaged cartilage (98). We had a further opportunity to examine the association between cartilage damage and the properties of the calcified matrix in a population of donors with varying degrees of cartilage damage. All of the tibiae that were supplied by the Gift of Hope (GOH) Organ and Tissue Donor Network had been scored visually for cartilage damage (Table 10.1). This original intent for the collection of this data was to study the affect of osteoarthritis on the properties of the underlying bone. We have investigated both the density and effective Young's modulus of the calcified tissue from these donors and summarized the results in Appendix A. While this analysis did not lead to any statistically significant findings, there were some interesting trends. Both the density and effective Young's modulus of the calcified tissue were reduced in donors with mild fibrillation of the cartilage surface (Collins grade 1). These properties returned to normal levels in donors with more extreme cartilage damage (Figure 10.2, Figure 10.3). This is interesting because it bears similarity with the findings that we have presented in Chapter 3 where we observed an increased proportion of denatured collagen associated with mild cartilage damage. In our preliminary investigation of severe osteoarthritis of the proximal

Collins 0		Collins 1		Collins 2		Collins 3,4	
Gender	Age	Gender	Age	Gender	Age	Gender	Age
M	38	M	49	M	53	F	51
F	46	M	52	F	55	F	55
F	50	F	57	M	65	M	69
M	50	M	66	F	66	M	71
F	54	M	71	F	68	F	72
M	68	M	75	F	71	M	74
M	71	F	85	M	71	<i>F</i>	<i>66</i>
F	72			F	72	<i>F</i>	<i>75</i>
				F	74	<i>M</i>	<i>75</i>
				M	75		
				M	77		
				F	92		

Table 10.1: Donor list by Collins grade for GOH data osteoarthritis sub-study. Note that Collins Grade 4 donors are denoted in italics and that one extra donor has been included in this study that was not included in the morphometry tests (this donor was missing some data necessary for the morphometry study).

tibia, the levels of denatured collagen were not different than controls. In the femoral head, there were indications that the level of denatured collagen may have been higher in regions where the cartilage was intact than in areas of complete eburation.

Based on our observations we believe that the interaction between the progression of osteoarthritis and the properties of the underlying trabecular bone is transient in nature. Early in the disease progression, the normal mechanical relation between the subchondral bone and overlying cartilage is disturbed (62). As a result, remodeling is stimulated in the underlying trabecular bone (57, 94). Increased remodeling activity results in a lower mean age of the bone by reducing the time available for passive mineralization of the matrix (12). Thus the mean mineralization, and Young's modulus are reduced in osteoarthritic bone (71, 93, 101, 126-128). As the disease progresses, the subchondral plate becomes sclerotic. Although the matrix quality of this bone is poor (79, 248), the apparent stiffness is increased (Chapter 4). This leads to stress shielding of the underlying trabecular bone and local remodeling rates return to normal. The regionalization of stress shielding would depend on the mechanics of the joint in question and would be different in the femoral head than in the proximal femur. Our data suggests that there was stress shielding of the trabecular bone underneath the subchondral plate. A previous study of osteoarthritis in the femoral head has provided evidence of possible stress shielding in the inferior region of the femoral head in advanced osteoarthritics (99, 249).

Obviously, the involvement of bone in osteoarthritic disease progression is complex. Bone remodeling in the arthritic joint is likely to be influenced by both biological (i.e. growth factors, cytokines) and mechanical stimuli (i.e. limb disuse, joint alignment). However, osteoarthritis should not be viewed as only a disease of the cartilage, but of the entire affected joint.

Concluding remarks

In the current body of work, we have examined bone quality in its interaction with the apparent mechanical properties of trabecular bone. By using microCT to obtain a full three-dimensional representation of the structure, we could separately evaluate the influence of architecture and matrix properties. In osteoarthritis, we found that bone matrix properties were affected early in the disease progression. In a study of bisphosphonate treatment, we found that excessive suppression of bone remodeling resulted in an increase in the accumulated microdamage accompanied with increased mineralization. The increase in mineralization was not associated with a higher effective matrix modulus. In our study of the Gift of Hope and BIOMED donor sample we saw that while architecture was clearly related to the bone volume fraction, there were also independent effects of anatomic location and donor. Currently, little is known

about the biological processes that control either bone architecture or matrix quality. In the future, these processes may provide interesting targets for the management of diseases of the skeletal system.

Appendix A: Investigation of the effects of osteoarthritis on tissue properties in the GOH data set.

In this sub-study, the tibia data from the GOH data set graded for osteoarthritis using the Collins Grade, a visual grading system (197). Briefly the grading system is as follows:

- Grade 0: no cartilage degeneration or osteophytes
- Grade 1: limited fibrillation of the articular surface
- Grade 2: deep fibrillation and fissuring and possible osteophyte formation
- Grade 3: extensive fibrillation fissuring with less than 30% eroded to the bone with osteophytes present
- Grade 4: greater than 30% of the articular surface eroded to the bone with gross geometric changes including osteophytes

Core samples were prepared from the proximal tibia as described in Chapter 7. The density of the calcified tissue was calculated for all of the samples from each donor and then the donor averages were calculated by OA grade and reported in Figure 10.2. Donors were grouped as indicated in Table 10.1 and a one-way ANOVA was used to compare group means. This ANOVA did not reveal any significant differences ($p = 0.18$).

For the tissue modulus study we used only the 6 samples from the medial side and 6 samples from the lateral side (where available). Samples were microCT scanned and then tested mechanically. FE models were prepared from the microCT scans and the scaling factor between microCT and mechanical testing was calculated and designated as the effective tissue modulus, as described in Chapter 2. The median values for each donor were calculated for both the medial and lateral sides. The donor averages were then calculated and are reported in Figure 10.3. These data were analyzed by two-way ANOVA for repeated measures where the group (Collins grade) was used as the between-subjects factor and compartment (medial vs. lateral) as the within-subjects factor. This analysis revealed that neither compartment ($p = 0.86$), Collins grade ($p = 0.372$) or interaction between compartment and Collins grade ($p = 0.267$) were significant.

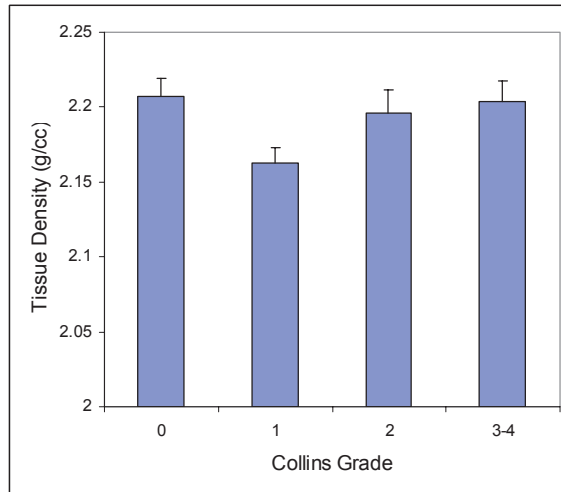


Figure 10.2: Calcified tissue (matrix) density for donors from the GOH data set by Collins grade (mean + SEM).

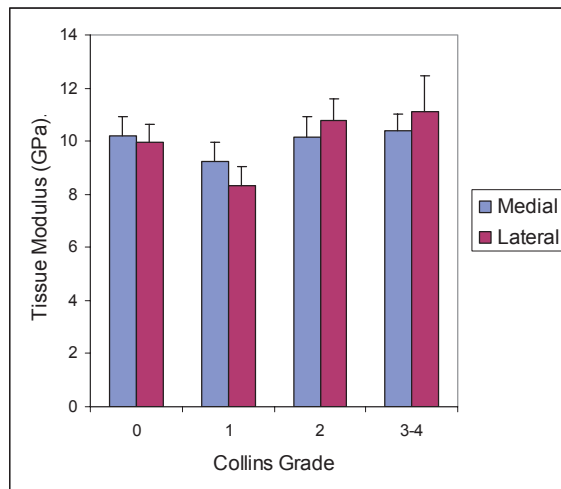


Figure 10.3 Calcified tissue modulus for donors from the GOH data set by Collins grade (mean + SEM).

Appendix B: A sub-study of donors with low bone density

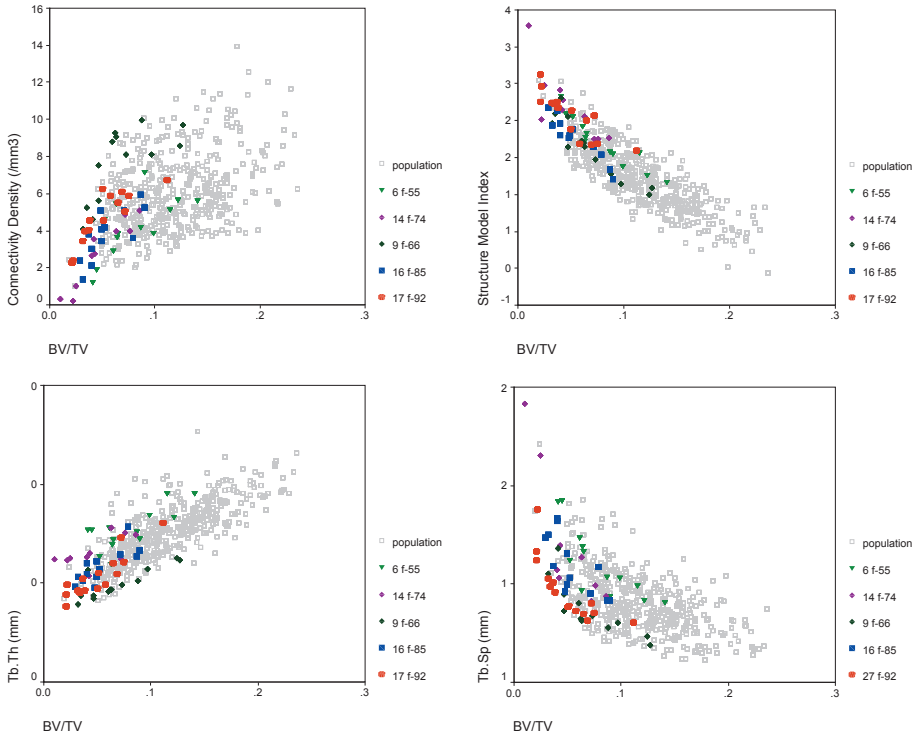


Figure 10.4: Morphometry-bone mass relations for donors with low bone mass. Five donors with low bone density were selected from the GOH data set and the morphometric measures were plotted against the bone volume fraction.

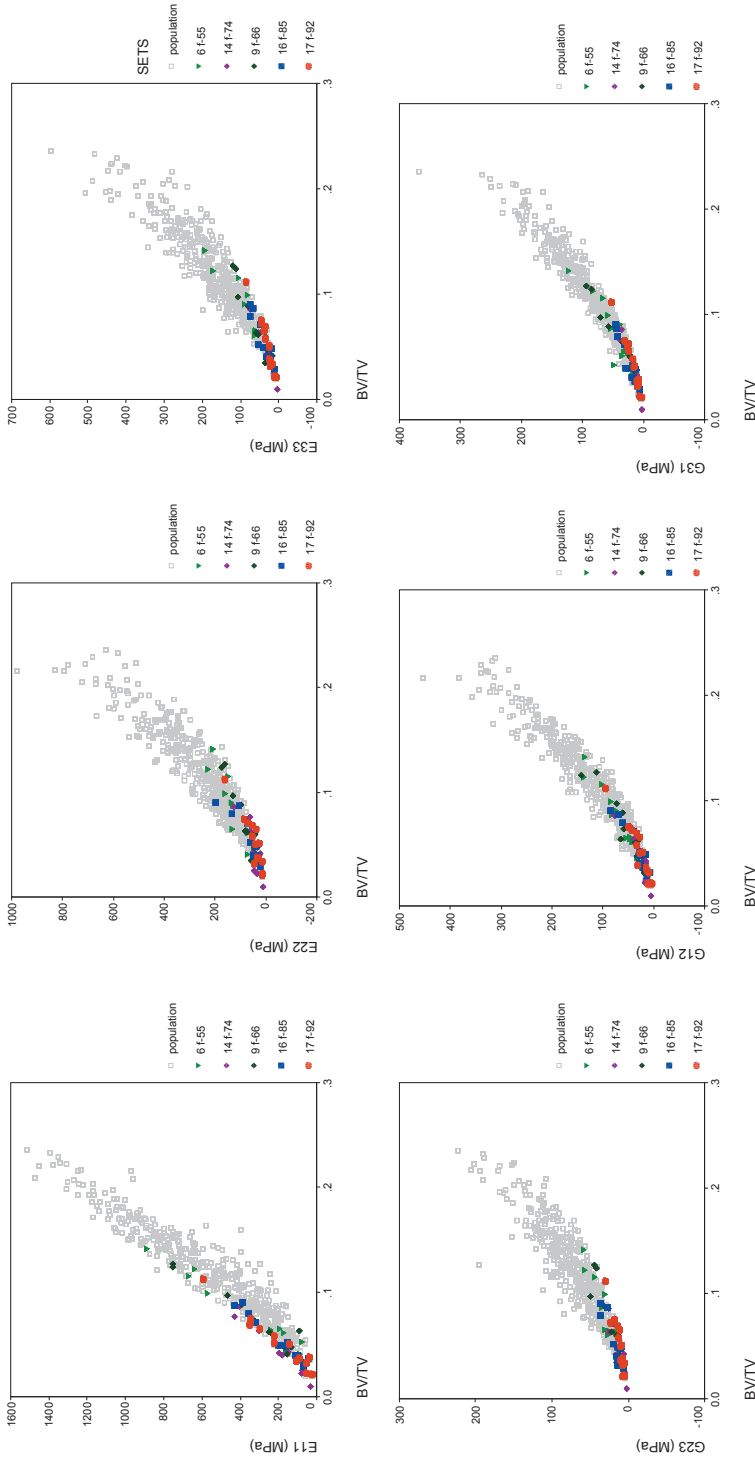


Figure 10.5: Elasticity-bone mass relations for donors with low bone mass. Five donors with low bone density were selected from the GOH data set and the morphometric measures were plotted against the bone volume fraction. Note the clear mechanical anisotropy compared to the rest of the population. The micro-architecture of these donors are stiffer in the primary direction and more compliant in the secondary and tertiary directions than the other donors in the population.

Appendix C: A sub-study of donors with 'fine' and 'coarse' structures

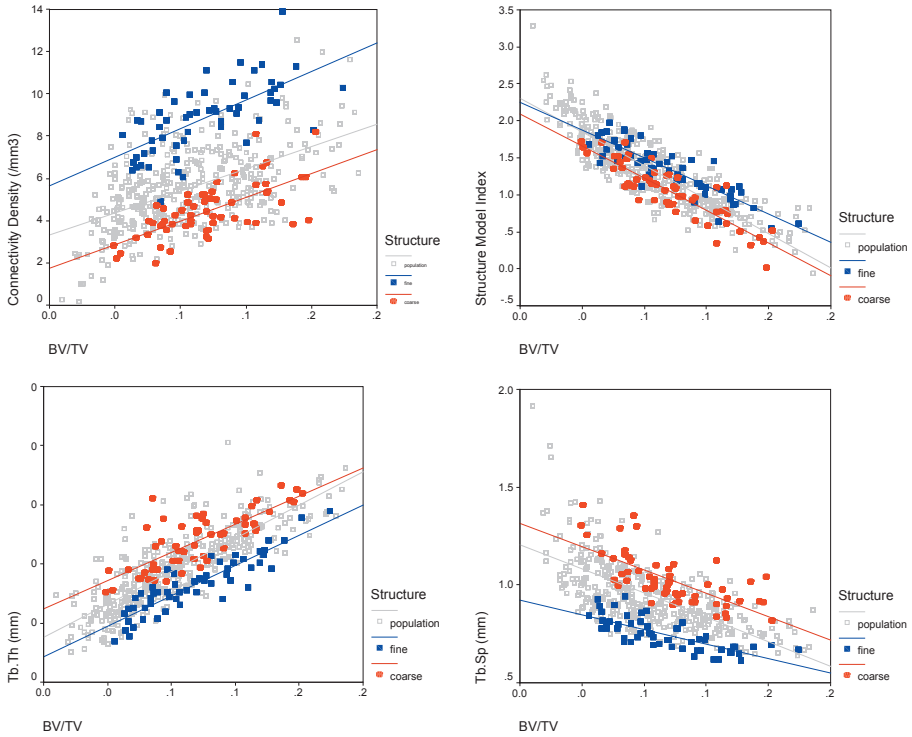


Figure 10.6: Morphometry-bone mass relations for donors with 'fine' and 'coarse' structure. Eight donors (4 x 2) with similar bone densities but very different structures were selected from the GOH data set. 'Coarse' donors had thick plate-like trabecula with wide spacing and 'fine' donors had highly interconnected, thin rod-like trabecula. Here the morphometric variables are plotted against the bone volume fraction by group. The donors by group identification number, gender and age were: coarse: #27 ♂71, #31 ♂74, #18 ♂38, #34 ♂77 fine: #3 ♀51, #1 ♀46, #30 ♂71, #13 ♀72

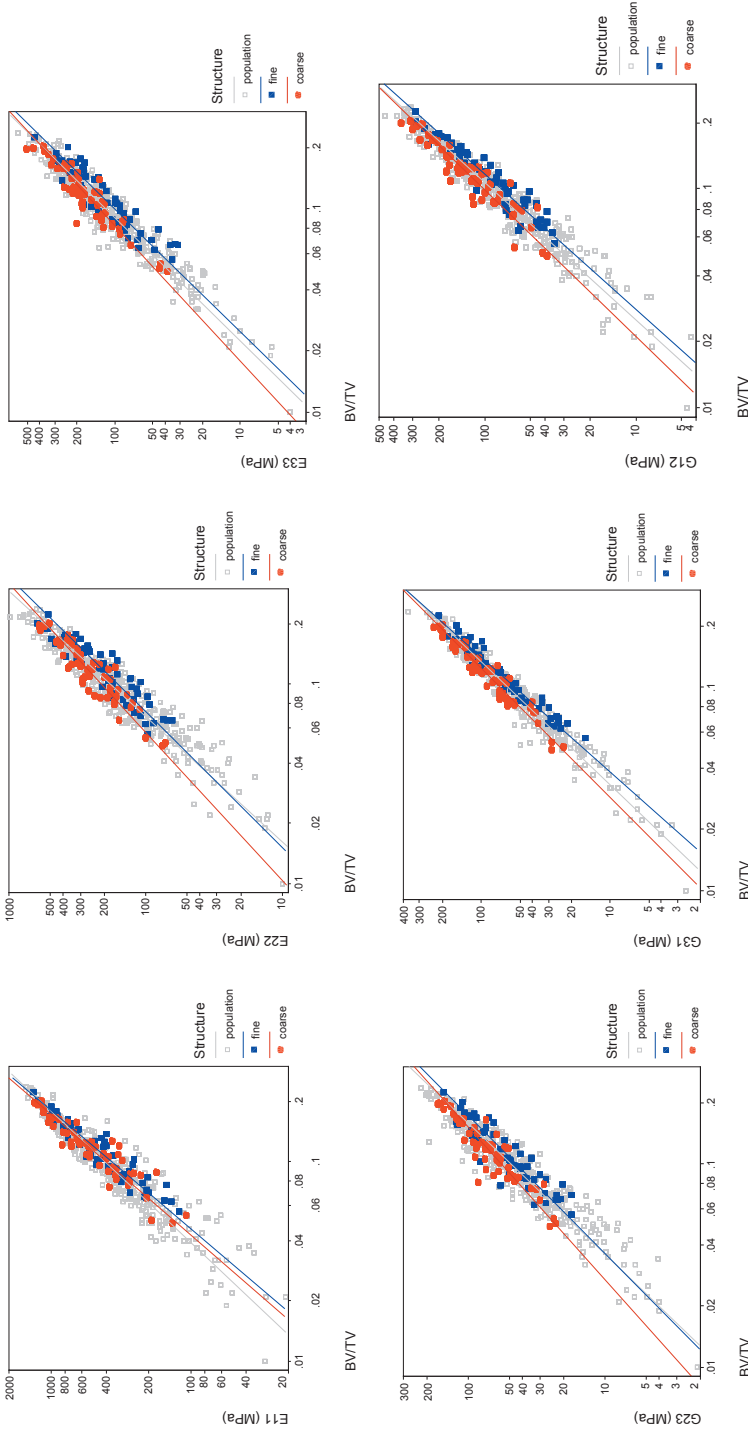


Figure 10.7: Elasticity-bone mass relations for donors with 'fine' and 'coarse' structure. Eight donors (4 x 2) with similar bone densities but very different structures were selected from the GOH data set. 'Coarse' donors had thick plate-like trabecula with wide spacing and 'fine' donors had highly interconnected, thin rod-like trabecula. The micro-architecture-elasticity relations were similar for all donors in the main loading direction (E11). In the other directions, the microarchitecture of the 'coarse' donors was stiffer.

Appendix D: Investigation of the relation between matrix properties and architecture in the GOH data set.

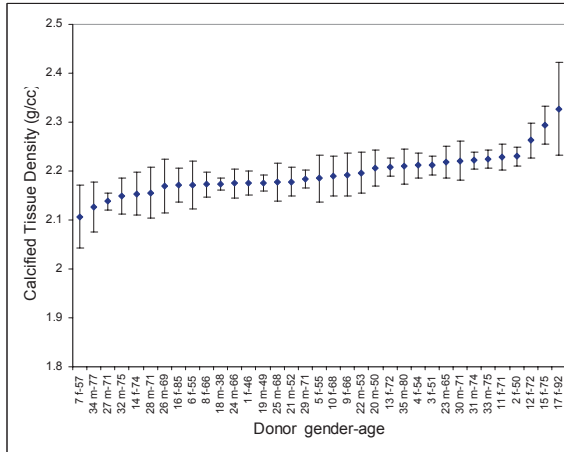


Figure 10.8: Calcified tissue density for samples from the proximal tibia (mean \pm standard deviation). Specimens were dried and defatted before measuring the density of the calcified tissue by Archimedes' principal.

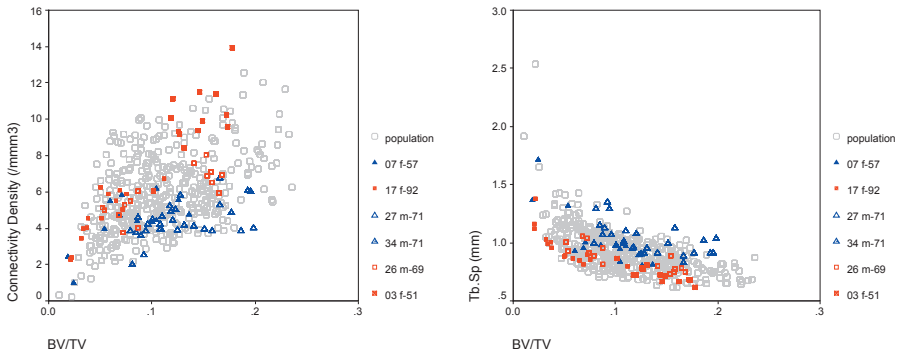


Figure 10.9: Relation between morphometry and bone volume fraction for donors with extreme tissue densities. The three donors with the highest and lowest tissue density were selected and plotted on top of the rest of the population. Donors with high tissue density are plotted with squares and those with low tissue density are plotted with triangles.

Summary

In this body of work we have examined some of the current concepts pertaining to the relation between bone mass, bone quality and the mechanical properties of bone.

In our first series of studies we used a model of human osteoarthritis to investigate the implications of changes in the effective tissue modulus. Having established that the material properties of the trabecular bone were altered in the earliest stages of osteoarthritis, we then investigated a possible cause, namely the breakdown or denaturation of bone collagen. Our original hypothesis was that damage at the micro scale originates at the molecular scale and that an assay of denatured collagen would reflect the first stages of the accumulation of microdamage in bone. Although we found a significant increase in the amount of denatured collagen in early osteoarthritis, our hypothesis regarding its mechanical origin turned out to be unlikely. This points to two alternate possibilities; that either the breakdown of collagen was of an enzymatic nature, or that the quality of the original collagen was poor. In the final investigation of this series we studied the implications of a reduction of the effective tissue modulus in the presence of a normal adaptive bone response. In this study we found that when local bone strain was used as the stimulus for the mechanosensory system a reduction of the local stiffness of the bone material would result in stiffening of the bone material at the organ level. Put in a simpler way, we determined that sclerotic thickening of the subchondral bone plate could result in a stiffer plate, even if the bone material was inferior.

In our second series, we investigated the effects of high dose bisphosphonate treatment in a canine model. This was part of a larger effort to quantify the effects of bisphosphonates on bone quality (150, 164, 250). Our original hypothesis was that, in addition to increasing bone mass and architectural quality, bisphosphonate treatment would result in a more mature (i.e. highly mineralized) bone matrix. This higher level of mineralization would then result in a stiffer material with improved matrix qualities. Again, we were surprised by our results! We found that any improvements in the stiffness that we could detect were due to changes in bone mass and micro-architecture alone. We also found a large, but expected, increase in the amount of microdamage present. It remains to be seen whether a similar accumulation of microdamage will occur in humans treated at clinical dosages. As is often the case in medicine, there is no *easy* way to improve the quality of the bone, and when not considered carefully, side effects of a treatment could be detrimental to its efficacy.

In our third series of studies we focused on the contributions of micro-architecture to bone mechanics. First we evaluated some of the morphometric tools used to quantify architecture. We found that use of the parallel plate model led to volume fraction dependant biases and recommend that direct three dimensional methods should be used whenever possible. Through the BIOMED 1 project and the Gift of Hope Organ and Tissue Donor network (not to mention the generosity of the donor's families and the staff members who collected these specimens)

we acquired a unique selection of trabecular bone specimens. We used these specimens to quantify how bone architecture varied both between people and locations in the body. First, we examined the relation between bone mass and architecture. The general question that we asked could be expressed as; “If you have a certain amount of bone, in how many ways is it typically arranged?” We quantified the arrangement of this bone using microCT in conjunction with standard three-dimensional morphometric measures. By using finite element models of the trabecular structure we could fully characterize the influence of microarchitecture on mechanics without considering possibly confounding matrix-level effects. In the BIOMED dataset we had samples from multiple clinically relevant sites and a wide range of donors. This provided an ideal data set to examine the effect of skeletal site. In the GOH dataset we had a large number of specimens from a small number of sites and a moderately large number of donors (this was particularly true with regards to the proximal tibia). This data set was well suited for investigating how the structure of trabecular bone varied between different people. In this analysis we found that even after correcting for the amount of bone present (BV/TV) there were indeed particular aspects of the architecture that were site specific. We concluded that this was probably due to differences in the mechanical function of the bone at these different sites. We also saw large differences in the bone architecture between people with equal bone mass. We could supply a striking visual representation of this by choosing 4 extreme donors from our data. For these donors, at this anatomic site, it seems that having a highly connected bone structure comes at the expense of having thin trabeculae. A small supplemental study of these four donors led us, once again, to some surprising results. Although the structure of the bone varied widely between these donors, the relation between the amount of bone present and the stiffness in the main loading direction was unaffected. It was only in the minor loading directions and in shear that the differences in architecture seemed to affect the mechanics. It had been previously demonstrated that including a morphometric measure of anisotropy improves the estimation of mechanical properties as opposed to using density alone (38, 171, 189). In our supplemental study, the differences that we observed on the minor axes as opposed to the main loading axis indicate different levels of mechanical anisotropy between these donors. If these differences could be quantified using a measure of morphometric anisotropy alone we should have been able to derive a general constitutive relation for our population i.e. by using a predictive model based on both bone mass and morphometric anisotropy we should be able to predict the mechanical properties for any donor. We tested this hypothesis by evaluating 3 different relations between the morphology and the bone’s elastic properties. Although adding anisotropy resulted in strong increases in the predictive power of the models, there were still strong site-dependant and donor-dependant differences. Unsatisfied with this result we decided to extend the one of the current models to include additional morphometric parameters. A principal components analysis demonstrated the morphology could generally be described by 3 components; one related to bone mass, one to connectivity and the last to anisotropy. We found that by including parameters such

as trabecular spacing or connectivity density in the model we could improve the prediction of the model by about 20% and eliminate much of the residual error that was associated with donor and anatomic site. Although the observed improvement in predicting the mechanical properties was small, it was sufficient to validate the concept that microarchitecture does indeed influence bone mechanics. Concluding this portion of the thesis, we have demonstrated that inter-site and inter-individual differences exist in bone quality as measured by trabecular micro-architecture and that these differences can be, for a large part, quantified using existing morphometric parameters.

Samenvatting

In dit werk hebben we enkele van de huidige concepten onderzocht, welke betrekking hebben op de relatie tussen botmassa, botkwaliteit en de mechanische eigenschappen van bot.

In onze eerste serie studies hebben we een model voor humane artrose gebruikt om de implicaties van veranderingen in effectieve weefselmodulus te onderzoeken. Na het vaststellen van veranderingen in de materiaaleigenschappen van trabeculair bot in de vroegste stadia van artrose, hebben we een mogelijke oorzaak hiervan onderzocht, namelijk de afbraak of denaturatie van het collageen in bot. Onze oorspronkelijke hypothese was dat schade op micro-niveau ontstaat op moleculair niveau en dat een gedenaturiseerd collageen assay een weerspiegeling zou zijn van de eerste stadia van accumulatie van microschade in bot. Hoewel we bij vroege artrose een significante verhoging van de hoeveelheid gedenaturiseerd collageen vonden, bleek onze hypothese betreffende de mechanische oorsprong hiervan onwaarschijnlijk. Dit duidt op twee alternatieve mogelijkheden; of de afbraak van collageen was van enzymatische aard, of de kwaliteit van het oorspronkelijke collageen was laag. In het laatste onderzoek in deze serie hebben we de gevolgen bestudeerd van een verlaging in de effectieve weefselmodulus bij een normale adaptieve botrespons. In deze studie vonden we dat indien de lokale rek in bot gebruikt werd als de stimulus voor het mechanosensore systeem, een verlaging van de lokale stijfheid van het botmateriaal zou resulteren in een verstijving van het bot op orgaaniveau. Eenvoudiger verwoord, we hebben bepaald dat sclerotische verdikking van de subchondrale botplaat zou kunnen resulteren in een stijvere plaat, zelfs als het botmateriaal zelf inferieur (slapper) is.

In onze tweede serie hebben we de effecten van behandeling met hoge doses bisphosphonaten onderzocht in een diermodel met honden. Dit werk vormde een onderdeel van een omvangrijkere poging om de effecten van bisphosphonaten op de botkwaliteit te kwantificeren (150, 164, 250). Onze oorspronkelijke hypothese was dat behandeling met bisphosphonaten, naast het verhogen van de botmassa en van de architecturale kwaliteit, zou resulteren in een meer ontwikkelde (d.w.z hoger gemineraliseerde) botmatrix. Dit hogere mineralisatieniveau zou dan resulteren in een stijver materiaal met een verbeterde matrixkwaliteit. Opnieuw werden we verrast door onze resultaten! We vonden dat elke verbetering in stijfheid die we konden detecteren alleen veroorzaakt werd door veranderingen in botmassa en micro-architectuur. Verder vonden we een grote, maar verwachte, toename in de hoeveelheid microschade in het bot. Het valt nog te bezien of een vergelijkbare accumulatie van microschade zal optreden in mensen die behandeld zijn met klinische doses. Zoals zo vaak het geval is in de geneeskunde is er geen eenvoudige manier om botkwaliteit te verbeteren en zonder zorgvuldige overweging kunnen bijeffecten nadelig zijn voor de doeltreffendheid van een behandeling.

In onze derde serie studies hebben we de aandacht gericht op de bijdrage van micro-architectuur aan botmechanica. Allereerst hebben we een aantal morfometrische methoden geëval-

ueerd die gebruikt worden om architectuur te kwantificeren. We vonden dat het gebruik van het parallele-plaat model leidde tot een fout die afhankelijk is van de volumefractie en adviseerden om waar mogelijk directe 3-dimensionale methoden te gebruiken. Door het BIOMED 1 project en het Gift of Hope Organ and Tissue Donor netwerk (en niet te vergeten door de edelmoedigheid van de familie van de donoren en de stafleden die deze specimens verzameld hebben) hebben we een unieke set trabeculair bot specimens verkregen. We hebben deze specimens gebruikt om te kwantificeren hoe botarchitectuur varieerde, zowel tussen mensen als tussen verschillende locaties in het lichaam. Eerst hebben we de relatie tussen botmassa en architectuur bestudeerd. De algemene vraag die we stelden kan omschreven worden als: "Als je een bepaalde hoeveelheid bot hebt, op welke manieren kan het typisch gerangschikt worden?" We hebben de rangschikking van dit bot gekwantificeerd met microCT door middel van standaard 3-dimensionale morfometrische maten. Door eindige elementen modellen van de trabeculaire structuur te gebruiken konden we de invloed van microarchitectuur op de mechanica volledig karakteriseren zonder rekening te hoeven houden met eventuele 'confounding' matrix-niveau effecten. In de BIOMED data hadden we samples van verschillende klinisch relevante locaties en een groot bereik aan donoren. Dit gaf ons een ideale dataset om het effect van locatie in het skelet te bestuderen. In de GOH dataset hadden we een grote hoeveelheid preparaten van een klein aantal locaties en van een redelijk grote hoeveelheid donoren (dit was speciaal het geval voor de proximale tibia). Deze dataset was goed geschikt voor het onderzoeken hoe de structuur van trabeculair bot varieerde tussen verschillende mensen. Bij deze analyse vonden we dat zelfs na correctie voor de hoeveelheid bot (BV/TV) inderdaad bepaalde aspecten van de architectuur, locatie-specifiek waren. We concludeerden dat dit waarschijnlijk veroorzaakt werd door verschillen in mechanische functie van het bot op deze verschillende locaties. We zagen ook grote verschillen in botarchitectuur tussen mensen met vergelijkbare botmassa's. We konden hier een opvallende visuele presentatie van geven door vier extreme donoren uit de data te nemen. Voor deze donoren leek het dat op deze specifieke locatie een sterk verbonden botstructuur (hoge connectiviteit) samen gaat met het hebben van dunne trabekels. Een kleine aanvullende studie met deze vier donoren leidde, opnieuw, tot enkele verrassende conclusies. Hoewel de structuur van het bot sterk varieerde tussen deze donoren, bleef de relatie tussen de hoeveelheid bot en de stijfheid in de hoofdbelastingsrichting ongewijzigd. Alleen in de overige belastingsrichtingen en in 'shear' leken de verschillen in architectuur van invloed op de mechanica. Er is eerder aangetoond dat het opnemen van een morfometrische maat voor anisotropie de schatting van mechanische eigenschappen verbeterd boven het gebruik van alleen botdichtheid (38, 171, 189). De verschillen die we in onze aanvullende studie zagen bij de overige assen, tegengesteld aan de hoofdbelastingsrichting, geven verschillende maten van mechanische anisotropie aan tussen deze donoren. Als deze verschillen gekwantificeerd konden worden door alleen een maat voor morfologische anisotropie dan hadden we in staat moeten zijn om een algemene wetmatige relatie voor onze populatie te vinden. Oftewel, we zouden met behulp van een

voorspellend model gebaseerd op zowel botmassa als morfometrische anisotropie in staat moeten zijn om de mechanische eigenschappen voor elke donor te voorspellen. We hebben deze hypothese getest door drie verschillende relaties tussen de morfologie en de elastische eigenschappen van bot te evalueren. Hoewel het toevoegen van de anisotropie in een sterke toename van de voorspellende kracht van de modellen resulteerde, waren er nog steeds sterke locatie- en donor-afhankelijke verschillen. Niet tevreden met dit resultaat besloten we één van de modellen uit te breiden met additionele morfometrische parameters. Een ‘Principle Components’ Analyse liet zien dat morfologie over het algemeen kon worden beschreven met drie componenten: Eén gerelateerd aan botmassa, één aan connectiviteit en de laatste aan anisotropie. We vonden dat we door de inclusie van parameters als trabeculaire ‘spacing’ of connectiviteitsdichtheid in het model, de voorspelling door het model met 20% konden verbeteren en veel van de resulterende fout die gerelateerd was aan donor en anatomische locatie konden elimineren. Hoewel de waargenomen verbetering in de voorspelling van de mechanische eigenschappen klein was, was het voldoende om het concept dat microarchitectuur inderdaad de bot mechanica beïnvloedt te valideren. We kunnen dus concluderen dat er inter-locatie en inter-individuele verschillen bestaan in botkwaliteit, zoals gemeten door trabeculaire micro-architectuur en dat deze verschillen voor het grootste deel gekwantificeerd kunnen worden met bestaande morfometrische parameters.

References

References

1. Currey JD. *Bones: Structure and mechanics*. Princeton: Princeton University Press; 2002.
2. Singh I. The architecture of cancellous bone. *J Anat* 1978;127(2):305-10.
3. Wolff J. *Das gesetz der transformation der knochen*. Berlin: A. Hirschwild; 1892.
4. Roux W. *Der kampf der teile im organismus*. Leipzig: Engelmann; 1881.
5. Weinans H, Prendergast PJ. Tissue adaptation as a dynamical process far from equilibrium. *Bone* 1996;19(2):143-9.
6. Frost HM. The mechanostat: a proposed pathogenic mechanism of osteoporoses and the bone mass effects of mechanical and nonmechanical agents. *Bone Miner* 1987;2(2):73-85.
7. Frost HM. Bone's mechanostat: a 2003 update. *Anat Rec* 2003;275A(2):1081-101.
8. Thompson DW. *On growth and form*. Cambridge: Cambridge University Press; 1942.
9. Mullender MG, Huiskes R, Weinans H. A physiological approach to the simulation of bone remodeling as a self-organizational control process. *J Biomech* 1994;27(11):1389-94.
10. Weinans H, Huiskes R, Grootenboer HJ. The behavior of adaptive bone-remodeling simulation models. *J Biomech* 1992;25(12):1425-41.
11. Huiskes R, Ruimerman R, van Lenthe GH, Janssen JD. Effects of mechanical forces on maintenance and adaptation of form in trabecular bone. *Nature* 2000;405(6787):704-6.
12. Parfitt AM. The composition, structure and remodeling of bone: A basis for interpretation of bone mineral measurements. In: Dequeker J, Geusens P, Wahner HW, editors. *Bone mineral measurement by photon absorptiometry*. Leuven: Leuven University Press; 1988.
13. Gibson LJ, Ashby MF. *Cellular solids: Structure and properties*. Cambridge: Cambridge university press; 1997.
14. Boyd S, Shrive N, Wohl G, Muller R, Zernicke R. Measurement of cancellous bone strain during mechanical tests using a new extensometer device. *Med Eng Phys* 2001;23(6):411-6.
15. Jacobs CR, Davis BR, Rieger CJ, Francis JJ, Saad M, Fyhrie DP. NACOB presentation to ASB Young Scientist Award: Postdoctoral. The impact of boundary conditions and mesh size on the accuracy of cancellous bone tissue modulus determination using large-scale finite-element modeling. North American Congress on Biomechanics. *J Biomech* 1999;32(11):1159-64.
16. Ladd AJ, Kinney JH. Numerical errors and uncertainties in finite-element modeling of trabecular bone. *J Biomech* 1998;31(10):941-5.
17. Linde F, Hvid I. The effect of constraint on the mechanical behaviour of trabecular bone specimens. *J Biomech* 1989;22(5):485-90.
18. Cowin SC, Sadegh AM, Luo GM. Correction formulae for the misalignment of axes in the measurement of the orthotropic elastic constants. *J Biomech* 1991;24(7):637-41.
19. Giesen EB, Ding M, Dalstra M, van Eijden TM. Architectural measures of the cancellous bone of the mandibular condyle identified by principal components analysis. *Calcif Tissue Int* 2003;73(3):225-31.
20. van Rietbergen B, Weinans H, Huiskes R, Odgaard A. A new method to determine trabecular bone elastic properties and loading using micromechanical finite-element models. *J Biomech* 1995;28(1):69-81.
21. van Rietbergen B, Odgaard A, Kabel J, Huiskes R. Direct mechanics assessment of elastic symmetries and properties of trabecular bone architecture. *J Biomech* 1996;29(12):1653-7.
22. Hollister SJ, Brennan JM, Kikuchi N. A homogenization sampling procedure for calculating trabecular bone effective stiffness and tissue level stress. *J Biomech* 1994;27(4):433-44.
23. Day JS, Ding M, van der Linden JC, Hvid I, Sumner DR, Weinans H. A decreased subchondral trabecular bone tissue elastic modulus is associated with pre-arthritis cartilage damage. *J Orthop Res* 2001;19(5):914-8.
24. Hou FJ, Lang SM, Hoshaw SJ, Reimann DA, Fyhrie DP. Human vertebral body apparent and hard tissue stiffness. *J Biomech* 1998;31(11):1009-15.
25. Kabel J, van Rietbergen B, Dalstra M, Odgaard A, Huiskes R. The role of an effective isotropic tissue modulus in the elastic properties of cancellous bone. *J Biomech* 1999;32(7):673-80.
26. Ott SM. When bone mass fails to predict bone failure. *Calcif Tissue Int* 1993;53 Suppl 1:S7-13.
27. Black DM, Cummings SR, KarpfDB, Cauley JA, Thompson DE, Nevitt MC, et al. Randomised trial of effect of alendronate on risk of fracture in women with existing vertebral fractures. Fracture Intervention Trial Research Group. *Lancet* 1996;348(9041):1535-41.
28. Zioupos P. Accumulation of in-vivo fatigue microdamage and its relation to biomechanical properties in ageing human cortical bone. *J Microsc* 2001;201(2):270-278.

References

29. Verborgt O, Gibson GJ, Schaffler MB. Loss of osteocyte integrity in association with microdamage and bone remodeling after fatigue in vivo. *J Bone Miner Res* 2000;15(1):60-7.
30. Schaffler MB, Choi K, Milgrom C. Aging and matrix microdamage accumulation in human compact bone. *Bone* 1995;17(6):521-25.
31. Wang X, Bank RA, TeKoppele JM, Hubbard GB, Athanasiou KA, Agrawal CM. Effect of collagen denaturation on the toughness of bone. *Clin Orthop* 2000(371):228-39.
32. Williamson AK, Chen AC, Masuda K, Thonar EJ, Sah RL. Tensile mechanical properties of bovine articular cartilage: variations with growth and relationships to collagen network components. *J Orthop Res* 2003;21(5):872-80.
33. Banse X. When density fails to predict bone strength. *Acta Orthop Scand Suppl* 2002;73(303):1-57.
34. Hannon RA, Eastell R. Biochemical markers of bone turnover and fracture prediction. *J Br Menopause Soc* 2003;9(1):10-5.
35. Heaney RP. Is the paradigm shifting? *Bone* 2003;33(4):457-65.
36. van der Linden JC, Homminga J, Verhaar JA, Weinans H. Mechanical consequences of bone loss in cancellous bone. *J Bone Miner Res* 2001;16(3):457-65.
37. Morgan EF, Bayraktar HH, Keaveny TM. Trabecular bone modulus-density relationships depend on anatomic site. *J Biomech* 2003;36(7):897-904.
38. Goulet RW, Goldstein SA, Ciarelli MJ, Kuhn JL, Brown MB, Feldkamp LA. The relationship between the structural and orthogonal compressive properties of trabecular bone. *J Biomech* 1994;27(4):375-89.
39. Eckstein F, Lochmuller EM, Lill CA, Kuhn V, Schneider E, Delling G, et al. Bone strength at clinically relevant sites displays substantial heterogeneity and is best predicted from site-specific bone densitometry. *J Bone Miner Res* 2002;17(1):162-71.
40. Augat P, Link T, Lang TF, Lin JC, Majumdar S, Genant HK. Anisotropy of the elastic modulus of trabecular bone specimens from different anatomical locations. *Med Eng Phys* 1998;20(2):124-31.
41. Ciarelli MJ, Goldstein SA, Kuhn JL, Cody DD, Brown MB. Evaluation of orthogonal mechanical properties and density of human trabecular bone from the major metaphyseal regions with materials testing and computed tomography. *J Orthop Res* 1991;9(5):674-82.
42. Galante J, Rostoker W, Ray RD. Physical properties of trabecular bone. *Calcif Tissue Res* 1970;5(3):236-46.
43. Odgaard A. Three-dimensional methods for quantification of cancellous bone architecture. *Bone* 1997;20(4):315-28.
44. Whitehouse WJ. The quantitative morphology of anisotropic trabecular bone. *J Microsc* 1974;101 Pt 2:153-68.
45. Hildebrand T, Ruegsegger P. A new method for the model independent assessment of thickness in three-dimensional images. *J Microsc* 1997;185:67-75.
46. Hildebrand T, Ruegsegger P. Quantification of Bone Microarchitecture with the Structure Model Index. *Comp Meth Biomech Biomed Eng* 1997;1(1):15-23.
47. Jinnai H, Watashiba H, Kajihara T, Nishikawa Y, Takahashi M, Ito M. Surface curvatures of trabecular bone microarchitecture. *Bone* 2002;30(1):191-4.
48. Russ JC, Dehoff RT. *Practical stereology*. New York: Kluwer Academic; 2000.
49. Odgaard A, Gundersen HJ. Quantification of connectivity in cancellous bone, with special emphasis on 3-D reconstructions. *Bone* 1993;14(2):173-82.
50. Radin EL, Paul IL, Rose RM. Role of mechanical factors in pathogenesis of primary osteoarthritis. *Lancet* 1972;1(7749):519-22.
51. Radin EL, Rose RM. Role of subchondral bone in the initiation and progression of cartilage damage. *Clin Orthop* 1986(213):34-40.
52. Keaveny TM, Morgan EF, Niebur GL, Yeh OC. Biomechanics of trabecular bone. *Annu Rev Biomed Eng* 2001;3:307-33.
53. Goldstein SA. The mechanical properties of trabecular bone: dependence on anatomic location and function. *J Biomech* 1987;20(11-12):1055-61.
54. Parfitt AM, Mathews CH, Villanueva AR, Kleerekoper M, Frame B, Rao DS. Relationships between surface, volume, and thickness of iliac trabecular bone in aging and in osteoporosis. Implications for the microanatomic and cellular mechanisms of bone loss. *J Clin Invest* 1983;72(4):1396-409.
55. Zysset PK. A review of morphology-elasticity relationships in human trabecular bone: theories and experiments. *J Biomech* 2003;36(10):1469-85.
56. Cowin SC. The relationship between the elasticity tensor and the fabric tensor. *Mechanics of Materials* 1985;4:1937-47.

57. Bailey AJ, Mansell JP. Do subchondral bone changes exacerbate or precede articular cartilage destruction in osteoarthritis of the elderly? *Gerontology* 1997;43(5):296-304.
58. Burr DB, Schaffler MB. The involvement of subchondral mineralized tissues in osteoarthrosis: quantitative microscopic evidence. *Microsc Res Tech* 1997;37(4):343-57.
59. Dequeker J, Mokassa L, Aerssens J, Boonen S. Bone density and local growth factors in generalized osteoarthritis. *Microsc Res Tech* 1997;37(4):358-71.
60. Goker B, Sumner DR, Hurwitz DE, Block JA. Bone mineral density varies as a function of the rate of joint space narrowing in the hip. *J Rheumatol* 2000;27(3):735-8.
61. Mankin HJ, Dorfman H, Lippiello L, Zarins A. Biochemical and metabolic abnormalities in articular cartilage from osteo-arthritic human hips. II. Correlation of morphology with biochemical and metabolic data. *J Bone Joint Surg [Am]* 1971;53(3):523-37.
62. Ding M, Dalstra M, Linde F, Hvid I. Changes in the stiffness of the human tibial cartilage-bone complex in early-stage osteoarthrosis. *Acta Orthop Scand* 1998;69(4):358-62.
63. Ding M, Odgaard A, Hvid I. Accuracy of cancellous bone volume fraction measured by micro-CT scanning. *J Biomech* 1999;32(3):323-6.
64. Ulrich D, van Rietbergen B, Weinans H, Ruegsegger P. Finite element analysis of trabecular bone structure: a comparison of image-based meshing techniques. *J Biomech* 1998;31(12):1187-92.
65. Zysset PK, Guo XE, Hoffer CE, Moore KE, Goldstein SA. Elastic modulus and hardness of cortical and trabecular bone lamellae measured by nanoindentation in the human femur. *J Biomech* 1999;32(10):1005-12.
66. Turner CH, Rho J, Takano Y, Tsui TY, Pharr GM. The elastic properties of trabecular and cortical bone tissues are similar: results from two microscopic measurement techniques. *J Biomech* 1999;32(4):437-41.
67. Choi K, Kuhn JL, Ciarelli MJ, Goldstein SA. The elastic moduli of human subchondral, trabecular, and cortical bone tissue and the size-dependency of cortical bone modulus. *J Biomech* 1990;23(11):1103-13.
68. Ladd AJ, Kinney JH, Haupt DL, Goldstein SA. Finite-element modeling of trabecular bone: comparison with mechanical testing and determination of tissue modulus. *J Orthop Res* 1998;16(5):622-8.
69. Niebur GL, Yuen JC, Hsia AC, Keaveny TM. Convergence behavior of high-resolution finite element models of trabecular bone. *J Biomech Eng* 1999;121(6):629-35.
70. Keaveny TM, Pinilla TP, Crawford RP, Kopperdahl DL, Lou A. Systematic and random errors in compression testing of trabecular bone. *J Orthop Res* 1997;15(1):101-10.
71. Grynblas MD, Alpert B, Katz I, Lieberman I, Pritzker KP. Subchondral bone in osteoarthritis. *Calcif Tissue Int* 1991;49(1):20-6.
72. Li B, Aspden RM. Composition and mechanical properties of cancellous bone from the femoral head of patients with osteoporosis or osteoarthritis. *J Bone Miner Res* 1997;12(4):641-51.
73. Li B, Aspden RM. Mechanical and material properties of the subchondral bone plate from the femoral head of patients with osteoarthritis or osteoporosis. *Ann Rheum Dis* 1997;56(4):247-54.
74. Mansell JP, Tarlton JF, Bailey AJ. Biochemical evidence for altered subchondral bone collagen metabolism in osteoarthritis of the hip. *Br J Rheumatol* 1997;36(1):16-9.
75. Batra HC, Charnley J. Existence and incidence of osteoid in osteoarthritis femoral heads. A preliminary report. *J Bone Joint Surg [Br]* 1969;51(2):366-71.
76. Fazzalari NL, Forwood MR, Smith K, Manthey BA, Herreen P. Assessment of cancellous bone quality in severe osteoarthrosis: bone mineral density, mechanics, and microdamage. *Bone* 1998;22(4):381-8.
77. Carter DR, Hayes WC. Bone compressive strength: the influence of density and strain rate. *Science* 1976;194(4270):1174-6.
78. Zysset PK, Sonny M, Hayes WC. Morphology-mechanical property relations in trabecular bone of the osteoarthritic proximal tibia. *J Arthroplasty* 1994;9(2):203-16.
79. Li B, Aspden RM. Material properties of bone from the femoral neck and calcar femorale of patients with osteoporosis or osteoarthritis. *Osteoporos Int* 1997;7(5):450-6.
80. Bank RA, Kriikken M, Beekman B, Stoop R, Maroudas A, Lafeber FP, et al. A simplified measurement of degraded collagen in tissues: application in healthy, fibrillated and osteoarthritic cartilage. *Matrix Biol* 1997;16(5):233-43.
81. Bailey AJ. Changes in bone collagen with age and disease. *J Muskuloskel Neuron Interact* 2002;2(6):529-31.
82. Wang X, Li X, Bank RA, Agrawal CM. Effects of collagen unwinding and cleavage on the mechanical integrity of the collagen network in bone. *Calcif Tissue Int* 2002;71(2):186-92.

References

83. Wang X, Bank RA, TeKoppele JM, Agrawal CM. The role of collagen in determining bone mechanical properties. *J Orthop Res* 2001;19(6):1021-6.
84. Bailey AJ, Mansell JP, Sims TJ, Banse X. Biochemical and mechanical properties of subchondral bone in osteoarthritis. *Biorheology* 2004;41(3-4):349-58.
85. Burr DB. The importance of subchondral bone in osteoarthritis. *Curr Opin Rheumatol* 1998;10(3):256-62.
86. Burr DB. Anatomy and physiology of the mineralized tissues: role in the pathogenesis of osteoarthritis. *Osteoarthritis Cartilage* 2004;12 Suppl A:S20-30.
87. van der Harst MR, Brama PA, van de Lest CH, Kiers GH, DeGroot J, van Weeren PR. An integral biochemical analysis of the main constituents of articular cartilage, subchondral and trabecular bone. *Osteoarthritis Cartilage* 2004;12(9):752-61.
88. Burr DB. The importance of subchondral bone in the progression of osteoarthritis. *J Rheumatol Suppl* 2004;70:77-80.
89. Lajeunesse D, Reboul P. Subchondral bone in osteoarthritis: a biologic link with articular cartilage leading to abnormal remodeling. *Curr Opin Rheumatol* 2003;15(5):628-33.
90. Bailey AJ, Sims TJ, Knott L. Phenotypic expression of osteoblast collagen in osteoarthritic bone: production of type I homotrimer. *Int J Biochem Cell Biol* 2002;34(2):176-82.
91. Imhof H, Sulzbacher I, Grapp S, Czerny C, Youssefzadeh S, Kainberger F. Subchondral bone and cartilage disease: a rediscovered functional unit. *Invest Radiol* 2000;35(10):581-8.
92. Burstein D, Velyvis J, Scott KT, Stock KW, Kim YJ, Jaramillo D, et al. Protocol issues for delayed Gd(DTPA)(2-)-enhanced MRI (dGEMRIC) for clinical evaluation of articular cartilage. *Magn Reson Med* 2001;45(1):36-41.
93. Matsui H, Shimizu M, Tsuji H. Cartilage and subchondral bone interaction in osteoarthritis of human knee joint: a histological and histomorphometric study. *Microsc Res Tech* 1997;37(4):333-42.
94. Dieppe P, Cushnaghan J, Young P, Kirwan J. Prediction of the progression of joint space narrowing in osteoarthritis of the knee by bone scintigraphy. *Ann Rheum Dis* 1993;52(8):557-63.
95. Carlson CS, Loeser RF, Jayo MJ, Weaver DS, Adams MR, Jerome CP. Osteoarthritis in cynomolgus macaques: a primate model of naturally occurring disease. *J Orthop Res* 1994;12(3):331-9.
96. Carlson CS, Loeser RF, Purser CB, Gardin JF, Jerome CP. Osteoarthritis in cynomolgus macaques. III: Effects of age, gender, and subchondral bone thickness on the severity of disease. *J Bone Miner Res* 1996;11(9):1209-17.
97. Fazzalari NL, Parkinson IH. Fractal properties of subchondral cancellous bone in severe osteoarthritis of the hip. *J Bone Miner Res* 1997;12(4):632-40.
98. Ding M, Danielsen CC, Hvid I. Bone density does not reflect mechanical properties in early-stage arthrosis. *Acta Orthop Scand* 2001;72(2):181-5.
99. Fazzalari NL, Parkinson IH. Femoral trabecular bone of osteoarthritic and normal subjects in an age and sex matched group. *Osteoarthritis Cartilage* 1998;6(6):377-82.
100. Kamibayashi L, Wyss UP, Cooke TD, Zee B. Trabecular microstructure in the medial condyle of the proximal tibia of patients with knee osteoarthritis. *Bone* 1995;17(1):27-35.
101. Reimann I, Mankin HJ, Trahan C. Quantitative histologic analyses of articular cartilage and subchondral bone from osteoarthritic and normal human hips. *Acta Orthop Scand* 1977;48(1):63-73.
102. Layton MW, Goldstein SA, Goulet RW, Feldkamp LA, Kubinski DJ, Bole GG. Examination of subchondral bone architecture in experimental osteoarthritis by microscopic computed axial tomography. *Arthritis Rheum* 1988;31(11):1400-5.
103. Dequeker J, Mokassa L, Aerssens J. Bone density and osteoarthritis. *J Rheumatol Suppl* 1995;43:98-100.
104. Burger H, van Daele PL, Odding E, Valkenburg HA, Hofman A, Grobbee DE, et al. Association of radiographically evident osteoarthritis with higher bone mineral density and increased bone loss with age. The Rotterdam Study. *Arthritis Rheum* 1996;39(1):81-6.
105. Stewart A, Black A, Robins SP, Reid DM. Bone density and bone turnover in patients with osteoarthritis and osteoporosis. *J Rheumatol* 1999;26(3):622-6.
106. Foss MV, Byers PD. Bone density, osteoarthritis of the hip, and fracture of the upper end of the femur. *Ann Rheum Dis* 1972;31(4):259-64.
107. Hurwitz DE, Sumner DR, Block JA. Bone Density, Dynamic Joint Loading and Joint Degeneration. a review. *Cells Tissues Organs* 2001;169(3):201-9.
108. Bruno RJ, Sauer PA, Rosenberg AG, Block J, Sumner DR. The pattern of bone mineral density in the proximal femur and radiographic signs of early joint degeneration. *J Rheumatol* 1999;26(3):636-40.

109. Pugh JW, Radin EL, Rose RM. Quantitative studies of human subchondral cancellous bone. Its relationship to the state of its overlying cartilage. *J Bone Joint Surg Am* 1974;56(2):313-21.
110. Radin EL, Paul IL, Lowy M. A comparison of the dynamic force transmitting properties of subchondral bone and articular cartilage. *J Bone Joint Surg Am* 1970;52(3):444-56.
111. Yasuda H, Shima N, Nakagawa N, Yamaguchi K, Kinosaki M, Mochizuki S, et al. Osteoclast differentiation factor is a ligand for osteoprotegerin/osteoclastogenesis-inhibitory factor and is identical to TRANCE/RANKL. *Proc Natl Acad Sci* 1998;31(95):3597-602.
112. Rubin J, Murphy TC, Zhu L, Roy E, Nanes MS, Fan X. Mechanical strain differentially regulates endothelial nitric-oxide synthase and receptor activator of nuclear kappa B ligand expression via ERK1/2 MAPK. *J Biol Chem* 2003;278(36):34018-25.
113. Noble BS, Peet N, Stevens HY, Brabbs A, Mosley JR, Reilly GC, et al. Mechanical loading: biphasic osteocyte survival and targeting of osteoclasts for bone destruction in rat cortical bone. *Am J Physiol Cell Physiol* 2003;284(4):C934-43.
114. Carter DR. Mechanical loading history and skeletal biology. *J Biomech* 1987;20(11-12):1095-109.
115. Thi MM, Kojima T, Cowin SC, Weinbaum S, Spray DC. Fluid shear stress remodels expression and function of junctional proteins in cultured bone cells. *Am J Physiol Cell Physiol* 2003;284(2):C389-403.
116. Cowin SC. Wolff's law of trabecular architecture at remodeling equilibrium. *J Biomech Eng* 1986;108(1):83-8.
117. Cowin SC, Moss-Salentijn L, Moss ML. Candidates for the mechanosensory system in bone. *J Biomech Eng* 1991;113(2):191-7.
118. Rubin C, Turner AS, Bain S, Mallinckrodt C, McLeod K. Anabolism. Low mechanical signals strengthen long bones. *Nature* 2001;412(6847):603-4.
119. Parfitt AM. Bone age, mineral density, and fatigue damage. *Calcif Tissue Int* 1993;53 Suppl 1:S82-5; discussion S85-6.
120. Ding M. Age variations in the properties of human tibial trabecular bone and cartilage. *Acta Orthop Scand Suppl* 2000;292:1-45.
121. Graverand MP, Tron AM, Ichou M, Dallard MC, Richard M, Uebelhart D, et al. Assessment of urinary hydroxypyridinium cross-links measurement in osteoarthritis. *Br J Rheumatol* 1996;35(11):1091-5.
122. Thompson PW, Spector TD, James IT, Henderson E, Hart DJ. Urinary collagen crosslinks reflect the radiographic severity of knee osteoarthritis. *Br J Rheumatol* 1992;31(11):759-61.
123. Astbury C, Bird HA, McLaren AM, Robins SP. Urinary excretion of pyridinium crosslinks of collagen correlated with joint damage in arthritis. *Br J Rheumatol* 1994;33(1):11-5.
124. MacDonald AG, McHenry P, Robins SP, Reid DM. Relationship of urinary pyridinium crosslinks to disease extent and activity in osteoarthritis. *Br J Rheumatol* 1994;33(1):16-9.
125. Sinigaglia L, Varenna M, Binelli L, Bartucci F, Arrigoni M, Ferrara R, et al. Urinary and synovial pyridinium crosslink concentrations in patients with rheumatoid arthritis and osteoarthritis. *Ann Rheum Dis* 1995;54(2):144-7.
126. Christensen P, Kjaer J, Melsen F, Nielsen HE, Sneppen O, Vang PS. The subchondral bone of the proximal tibial epiphysis in osteoarthritis of the knee. *Acta Orthop Scand* 1982;53(6):889-95.
127. Mansell JP, Bailey AJ. Abnormal cancellous bone collagen metabolism in osteoarthritis. *J Clin Invest* 1998;101(8):1596-603.
128. Raymaekers G, Aerssens J, Van den Eynde R, Peeters J, Geusens P, Devos P, et al. Alterations of the mineralization profile and osteocalcin concentrations in osteoarthritic cortical iliac crest bone. *Calcif Tissue Int* 1992;51(4):269-75.
129. Banse X, Sims TJ, Bailey AJ. Mechanical properties of adult vertebral cancellous bone: correlation with collagen intermolecular cross-links. *J Bone Miner Res* 2002;17(9):1621-8.
130. McBride DJ, Jr., Shapiro JR, Dunn MG. Bone geometry and strength measurements in aging mice with the oim mutation. *Calcif Tissue Int* 1998;62(2):172-6.
131. Day JD, Manintveld O, Bank RA, Ding M, Sumner DR, Hvid I, et al. Denatured collagen in osteoarthritic bone. In: 49th annual meeting of the Orthopaedic Research Society; 2003; New Orleans, LA; 2003. p. 746.
132. Van der Linden JC, Verhaar JA, Weinans H. A three-dimensional simulation of age-related remodeling in trabecular bone. *J Bone Miner Res* 2001;16(4):688-96.
133. Finlay JB, Bourne RB, Kraemer WJ, Moroz TK, Rorabeck CH. Stiffness of bone underlying the tibial plateaus of osteoarthritic and normal knees. *Clin Orthop* 1989(247):193-201.
134. Fujita T, Fujii Y, Okada SF, Miyauchi A, Takagi Y. Analgesic effect of etidronate on degenerative joint disease. *J Bone Miner Metab* 2001;19(4):251-6.

References

135. Devogelaer JP. Treatment of bone diseases with bisphosphonates, excluding osteoporosis. *Curr Opin Rheumatol* 2000;12(4):331-5.
136. Muehleman C, Green J, Williams JM, Kuettner KE, Thonar EJ, Sumner DR. The effect of bone remodeling inhibition by zoledronic acid in an animal model of cartilage matrix damage. *Osteoarthritis Cartilage* 2002;10(3):226-33.
137. Siris E. Alendronate in the treatment of osteoporosis: a review of the clinical trials. *J Womens Health Gend Based Med* 2000;9(6):599-606.
138. Crandall C. Risedronate: a clinical review. *Arch Intern Med* 2001;161(3):353-60.
139. Rodan GA, Fleisch HA. Bisphosphonates: mechanisms of action. *J Clin Invest* 1996;97(12):2692-6.
140. Russell RG, Rogers MJ. Bisphosphonates: from the laboratory to the clinic and back again. *Bone* 1999;25(1):97-106.
141. Weinstein RS. True strength. *J Bone Miner Res* 2000;15(4):621-5.
142. Delmas PD. How does antiresorptive therapy decrease the risk of fracture in women with osteoporosis? *Bone* 2000;27(1):1-3.
143. Meunier PJ, Boivin G. Bone mineral density reflects bone mass but also the degree of mineralization of bone: therapeutic implications. *Bone* 1997;21(5):373-7.
144. Chavassieux PM, Arlot ME, Reda C, Wei L, Yates AJ, Meunier PJ. Histomorphometric assessment of the long-term effects of alendronate on bone quality and remodeling in patients with osteoporosis. *J Clin Invest* 1997;100(6):1475-80.
145. Monier-Faugere MC, Geng Z, Paschalis EP, Qi Q, Arnala I, Bauss F, et al. Intermittent and continuous administration of the bisphosphonate ibandronate in ovariectomized beagle dogs: effects on bone morphometry and mineral properties. *J Bone Miner Res* 1999;14(10):1768-78.
146. Heaney RP. The bone-remodeling transient: implications for the interpretation of clinical studies of bone mass change. *J Bone Miner Res* 1994;9(10):1515-23.
147. Roschger P, Fratzl P, Klaushofer K, Rodan G. Mineralization of cancellous bone after alendronate and sodium fluoride treatment: a quantitative backscattered electron imaging study on minipig ribs. *Bone* 1997;20(5):393-7.
148. Boivin GY, Chavassieux PM, Santora AC, Yates J, Meunier PJ. Alendronate increases bone strength by increasing the mean degree of mineralization of bone tissue in osteoporotic women. *Bone* 2000;27(5):687-94.
149. Currey JD. Effects of differences in mineralization on the mechanical properties of bone. *Philos Trans R Soc Lond B Biol Sci* 1984;304(1121):509-18.
150. Hirano T, Turner CH, Forwood MR, Johnston CC, Burr DB. Does suppression of bone turnover impair mechanical properties by allowing microdamage accumulation? *Bone* 2000;27(1):13-20.
151. Mashiba T, Hirano T, Turner CH, Forwood MR, Johnston CC, Burr DB. Suppressed bone turnover by bisphosphonates increases microdamage accumulation and reduces some biomechanical properties in dog rib. *J Bone Miner Res* 2000;15(4):613-20.
152. Burr DB, Martin RB, Schaffler MB, Radin EL. Bone remodeling in response to in vivo fatigue microdamage. *J Biomech* 1985;18(3):189-200.
153. Mori S, Burr DB. Increased intracortical remodeling following fatigue damage. *Bone* 1993;14(2):103-9.
154. Burr DB, Turner CH, Naick P, Forwood MR, Ambrosius W, Hasan MS, et al. Does microdamage accumulation affect the mechanical properties of bone? *J Biomech* 1998;31(4):337-45.
155. Van der Linden JC, Birkenhager-Frenkel DH, Verhaar JA, Weinans H. Trabecular bone's mechanical properties are affected by its nonuniform mineral distribution. *J Biomech* 2001;34(12):1573-80.
156. Mashiba T, Turner CH, Hirano T, Forwood MR, Johnston CC, Burr DB. Effects of suppressed bone turnover by bisphosphonates on microdamage accumulation and biomechanical properties in clinically relevant skeletal sites in beagles. *Bone* 2001;28(5):524-31.
157. Ulrich D, Hildebrand T, Van Rietbergen B, Muller R, Ruegsegger P. The quality of trabecular bone evaluated with micro-computed tomography, FEA and mechanical testing. *Stud Health Technol Inform* 1997;40:97-112.
158. Kuhn JL, Goldstein SA, Feldkamp LA, Goulet RW, Jesion G. Evaluation of a microcomputed tomography system to study trabecular bone structure. *J Orthop Res* 1990;8(6):833-42.
159. Rho JY, Roy ME, 2nd, Tsui TY, Pharr GM. Elastic properties of microstructural components of human bone tissue as measured by nanoindentation. *J Biomed Mater Res* 1999;45(1):48-54.
160. McClung MR. Current bone mineral density data on bisphosphonates in postmenopausal osteoporosis. *Bone* 1996;19(5 Suppl):195S-198S.

161. Tonino RP, Meunier PJ, Emkey R, Rodriguez-Portales JA, Menkes CJ, Wasnich RD, et al. Skeletal benefits of alendronate: 7-year treatment of postmenopausal osteoporotic women. Phase III Osteoporosis Treatment Study Group. *J Clin Endocrinol Metab* 2000;85(9):3109-15.
162. Balena R, Toolan BC, Shea M, Markatos A, Myers ER, Lee SC, et al. The effects of 2-year treatment with the aminobisphosphonate alendronate on bone metabolism, bone histomorphometry, and bone strength in ovariectomized nonhuman primates. *J Clin Invest* 1993;92(6):2577-86.
163. Eventov I, Frisch B, Cohen Z, Hammel I. Osteopenia, hematopoiesis, and bone remodelling in iliac crest and femoral biopsies: a prospective study of 102 cases of femoral neck fractures. *Bone* 1991;12(1):1-6.
164. Ding M, Day JS, Burr DB, Mashiba T, Hirano T, Weinans H, et al. Canine Cancellous Bone Microarchitecture after One Year of High-Dose Bisphosphonates. *Calcif Tissue Int*. 2003;In Press.
165. Harris ST, Watts NB, Genant HK, McKeever CD, Hangartner T, Keller M, et al. Effects of risedronate treatment on vertebral and nonvertebral fractures in women with postmenopausal osteoporosis: a randomized controlled trial. Vertebral Efficacy With Risedronate Therapy (VERT) Study Group. *Jama* 1999;282(14):1344-52.
166. Parfitt AM, Drezner MK, Glorieux FH, Kanis JA, Malluche H, Meunier PJ, et al. Bone histomorphometry: standardization of nomenclature, symbols, and units. Report of the ASBMR Histomorphometry Nomenclature Committee. *J Bone Miner Res* 1987;2(6):595-610.
167. Birkenhager-Frenkel DH, Courpron P, Hupscher EA, Clermonts E, Coutinho MF, Schmitz PI, et al. Age-related changes in cancellous bone structure. A two-dimensional study in the transiliac and iliac crest biopsy sites. *Bone Miner* 1988;4(2):197-216.
168. Odgaard A, Andersen K, Melsen F, Gundersen HJ. A direct method for fast three-dimensional serial reconstruction. *J Microsc* 1990;159(Pt 3):335-42.
169. Ruegsegger P, Koller B, Muller R. A microtomographic system for the nondestructive evaluation of bone architecture. *Calcif Tissue Int* 1996;58(1):24-9.
170. Majumdar S. A review of magnetic resonance (MR) imaging of trabecular bone micro-architecture: contribution to the prediction of biomechanical properties and fracture prevalence. *Technol Health Care* 1998;6(5-6):321-7.
171. Ding M, Odgaard A, Danielsen CC, Hvid I. Mutual associations among microstructural, physical and mechanical properties of human cancellous bone. *J Bone Joint Surg Br* 2002;84(6):900-7.
172. Hildebrand T, Laib A, Muller R, Dequeker J, Ruegsegger P. Direct three-dimensional morphometric analysis of human cancellous bone: microstructural data from spine, femur, iliac crest, and calcaneus. *J Bone Miner Res* 1999;14(7):1167-74.
173. Ding M, Odgaard A, Linde F, Hvid I. Age-related variations in the microstructure of human tibial cancellous bone. *J Orthop Res* 2002;20(3):615-21.
174. Kabel J, Odgaard A, van Rietbergen B, Huiskes R. Connectivity and the elastic properties of cancellous bone. *Bone* 1999;24(2):115-20.
175. Kinney JH, Ladd AJ. The relationship between three-dimensional connectivity and the elastic properties of trabecular bone. *J Bone Miner Res* 1998;13(5):839-45.
176. Kinney JH. Connectivity and the elastic properties of cancellous bone [letter]. *Bone* 1999;25(6):741-2.
177. Ciarelli TE, Fyhrie DP, Schaffler MB, Goldstein SA. Variations in three-dimensional cancellous bone architecture of the proximal femur in female hip fractures and in controls. *J Bone Miner Res* 2000;15(1):32-40.
178. Kapadia RD, Stroup GB, Badger AM, Koller B, Levin JM, Coatney RW, et al. Applications of micro-CT and MR microscopy to study pre-clinical models of osteoporosis and osteoarthritis. *Technol Health Care* 1998;6(5-6):361-72.
179. Uchiyama T, Tanizawa T, Muramatsu H, Endo N, Takahashi HE, Hara T. A morphometric comparison of trabecular structure of human ilium between microcomputed tomography and conventional histomorphometry. *Calcif Tissue Int* 1997;61(6):493-8.
180. Uchiyama T, Tanizawa T, Muramatsu H, Endo N, Takahashi HE, Hara T. Three-dimensional microstructural analysis of human trabecular bone in relation to its mechanical properties. *Bone* 1999;25(4):487-91.
181. Garrahan NJ, Mellish RW, Vedi S, Compston JE. Measurement of mean trabecular plate thickness by a new computerized method. *Bone* 1987;8(4):227-30.
182. Mellish RW, Garrahan NJ, Compston JE. Age-related changes in trabecular width and spacing in human iliac crest biopsies. *Bone Miner* 1989;6(3):331-8.

References

183. Parisien MV, McMahon D, Pushparaj N, Dempster DW. Trabecular architecture in iliac crest bone biopsies: infra-individual variability in structural parameters and changes with age. *Bone* 1988;9(5):289-95.
184. Snyder BD, Piazza S, Edwards WT, Hayes WC. Role of trabecular morphology in the etiology of age-related vertebral fractures. *Calcif Tissue Int* 1993;53(Suppl 1):S14-22.
185. Poedenphant J, Nielsen VA, Riis BJ, Gotfredsen A, Christiansen C. Bone mass, bone structure and vertebral fractures in osteoporotic patients. *Bone* 1987;8(3):127-30.
186. Kleerekoper M, Villanueva AR, Stanciu J, Rao DS, Parfitt AM. The role of three-dimensional trabecular microstructure in the pathogenesis of vertebral compression fractures. *Calcif Tissue Int* 1985;37(6):594-7.
187. Gonzalez-Riola J, Pames JA, Hernandez ER, Revilla M, Seco C, Villa LF, et al. Influence of electromagnetic fields on bone mass and growth in developing rats: a morphometric, densitometric, and histomorphometric study. *Calcif Tissue Int* 1997;60(6):533-7.
188. Whitehouse WJ. Errors in area measurement in thick sections, with special reference to trabecular bone. *J Microsc* 1976;107(2):183-7.
189. Ulrich D, van Rietbergen B, Laib A, Ruegsegger P. The ability of three-dimensional structural indices to reflect mechanical aspects of trabecular bone. *Bone* 1999;25(1):55-60.
190. van Rietbergen B, Odgaard A, Kabel J, Huijskes R. Relationships between bone morphology and bone elastic properties can be accurately quantified using high-resolution computer reconstructions. *J Orthop Res* 1998;16(1):23-8.
191. Turner CH, Cowin SC, Rho JY, Ashman RB, Rice JC. The fabric dependence of the orthotropic elastic constants of cancellous bone. *J Biomech* 1990;23(6):549-61.
192. Vesterby A, Mosekilde L, Gundersen HJ, Melsen F, Holme K, Sorensen S. Biologically meaningful determinants of the in vitro strength of lumbar vertebrae. *Bone* 1991;12(3):219-24.
193. Day JS, Ding M, Odgaard A, Sumner DR, Hvid I, Weinans H. Parallel plate model for trabecular bone exhibits volume fraction-dependent bias. *Bone* 2000;27(5):715-20.
194. Hahn M, Vogel M, Pompesius-Kempa M, Delling G. Trabecular bone pattern factor--a new parameter for simple quantification of bone microarchitecture. *Bone* 1992;13(4):327-30.
195. Parkinson IH, Fazzalari NL. Interrelationships between structural parameters of cancellous bone reveal accelerated structural change at low bone volume. *J Bone Miner Res* 2003;18(12):2200-5.
196. Ding M, Hvid I. Quantification of age-related changes in the structure model type and trabecular thickness of human tibial cancellous bone. *Bone* 2000;26(3):291-5.
197. Muehleman C, Bareither D, Huch K, Cole AA, Kuettner KE. Prevalence of degenerative morphological changes in the joints of the lower extremity. *Osteoarthritis Cartilage* 1997;5(1):23-37.
198. Aerssens J, Boonen S, Joly J, Dequeker J. Variations in trabecular bone composition with anatomical site and age: potential implications for bone quality assessment. *J Endocrinol* 1997;155(3):411-21.
199. Thomsen JS, Ebbesen EN, Mosekilde L. Static histomorphometry of human iliac crest and vertebral trabecular bone: a comparative study. *Bone* 2002;30(1):267-74.
200. Goldstein SA, Goulet R, McCubbrey D. Measurement and significance of three-dimensional architecture to the mechanical integrity of trabecular bone. *Calcif Tissue Int* 1993;53(Suppl 1):S127-32; discussion S132-3.
201. Guo XE, Kim CH. Mechanical consequence of trabecular bone loss and its treatment: a three-dimensional model simulation. *Bone* 2002;30(2):404-11.
202. Amling M, Herden S, Posl M, Hahn M, Ritzel H, Delling G. Heterogeneity of the skeleton: comparison of the trabecular microarchitecture of the spine, the iliac crest, the femur, and the calcaneus. *J Bone Miner Res* 1996;11(1):36-45.
203. Koch JC. The laws of bone architecture. *Am J Anatomy* 1917;21:177.
204. Kimmel DB, Jee WS. A quantitative histologic study of bone turnover in young adult beagles. *Anat Rec* 1982;203(1):31-45.
205. Aaron JE, Makins NB, Sagreiya K. The microanatomy of trabecular bone loss in normal aging men and women. *Clin Orthop* 1987(215):260-71.
206. Compston JE, Mellish RW, Garrahan NJ. Age-related changes in iliac crest trabecular microanatomic bone structure in man. *Bone* 1987;8(5):289-92.
207. Seeman E. Pathogenesis of bone fragility in women and men. *Lancet* 2002;359(9320):1841-50.
208. Mosekilde L. The effect of modelling and remodelling on human vertebral body architecture. *Technol Health Care* 1998;6(5-6):287-97.

209. Hordon LD, Raisi M, Aaron JE, Paxton SK, Beneton M, Kanis JA. Trabecular architecture in women and men of similar bone mass with and without vertebral fracture: I. Two-dimensional histology. *Bone* 2000;27(2):271-6.
210. Aaron JE, Shore PA, Shore RC, Beneton M, Kanis JA. Trabecular architecture in women and men of similar bone mass with and without vertebral fracture: II. Three-dimensional histology. *Bone* 2000;27(2):277-82.
211. Thomsen JS, Ebbesen EN, Mosekilde L. A new method of comprehensive static histomorphometry applied on human lumbar vertebral cancellous bone. *Bone* 2000;27(1):129-38.
212. Homminga J, McCreadie BR, Ciarelli TE, Weinans H, Goldstein SA, Huiskes R. Cancellous bone mechanical properties from normals and patients with hip fractures differ on the structure level, not on the bone hard tissue level. *Bone* 2002;30(5):759-64.
213. Ishikawa K, Ohta T, Tahara Y, Suzuki T. The relationship between spinal and appendicular bone mass modified by physical, historical, and lifestyle factors. *J Bone Miner Metab* 2000;18(3):170-5.
214. Mosekilde L. Age-related changes in vertebral trabecular bone architecture--assessed by a new method. *Bone* 1988;9(4):247-50.
215. Kabel J, van Rietbergen B, Odgaard A, Huiskes R. Constitutive relationships of fabric, density, and elastic properties in cancellous bone architecture. *Bone* 1999;25(4):481-6.
216. Majumdar S, Kothari M, Augat P, Newitt DC, Link TM, Lin JC, et al. High-resolution magnetic resonance imaging: three-dimensional trabecular bone architecture and biomechanical properties. *Bone* 1998;22(5):445-54.
217. Yang G, Kabel J, van Rietbergen B, Odgaard A, Huiskes R, Cowin SC. The anisotropic Hooke's law for cancellous bone and wood. *J Elasticity* 1999;53:125-46.
218. Harrigan T, Mann R. Characterization of microstructural anisotropy in orthotropic materials using a second rank tensor. *Journal of Materials Science* 1984;19:761-7.
219. Turner CH, Cowin SC. Dependence of elastic constants of an anisotropic porous material upon porosity and fabric. *Journal of Materials Science* 1987;22:3178-3184.
220. Zysset PK, Goulet RW, Hollister SJ. A global relationship between trabecular bone morphology and homogenized elastic properties. *J Biomech Eng* 1998;120(5):640-6.
221. Zysset PK, Curnier A. An alternative model for anisotropic elasticity based on tensors. *Mechanics of Materials* 1995;21:243-50.
222. Cowin SC, Yang G. Averaging anisotropic elastic constant data. *J Elasticity* 1997;46:151-80.
223. Dequeker J. Assessment of quality of bone in osteoporosis--BIOMED I: fundamental study of relevant bone. *Clin Rheumatol* 1994;13 Suppl 1:7-12.
224. Scheaffer RL, McClave JT. *Probability and Statistics for Engineers*. Boston: Duxbury Press; 1986.
225. Efron B, Tibshirani R. *An introduction to the bootstrap*. New York, London.: Chapman and Hall; 1993.
226. Harrigan T, Jasty M, Mann R, Harris W. Limitations of the continuum assumption in cancellous bone. *J Biomech* 1988;21(4):269-75.
227. Anonymous. Consensus development conference: diagnosis, prophylaxis, and treatment of osteoporosis. *Am J Med* 1993;94(6):646-50.
228. Legrand E, Chappard D, Pascaretti C, Duquenne M, Rohmer V, Basle MF, et al. [Trabecular bone microarchitecture and male osteoporosis] *Microarchitecture osseuse trabeculaire et osteoporose masculine. Morphologie* 1999;83(261):35-40.
229. Recker RR. Architecture and vertebral fracture. *Calcif Tissue Int* 1993;53(Suppl 1):S139-42.
230. Cortet B, Dubois P, Boutry N, Varlet E, Cotten A, Marchandise X. Does high-resolution computed tomography image analysis of the distal radius provide information independent of bone mass? *J Clin Densitom* 2000;3(4):339-51.
231. Daffertshofer A, Lamoth CJ, Meijer OG, Beek PJ. PCA in studying coordination and variability: a tutorial. *Clin Biomech (Bristol, Avon)* 2004;19(4):415-28.
232. Yeni YN, Hou FJ, Vashishth D, Fyhrie DP. Trabecular shear stress in human vertebral cancellous bone: intra- and inter-individual variations. *J Biomech* 2001;34(10):1341-6.
233. van Ruijven LJ, Giesen EB, Farella M, van Eijden TM. Prediction of mechanical properties of the cancellous bone of the mandibular condyle. *J Dent Res* 2003;82(10):819-23.
234. Geraets WG, Van der Stelt PF, Lips P, Van Ginkel FC. The radiographic trabecular pattern of hips in patients with hip fractures and in elderly control subjects. *Bone* 1998;22(2):165-73.
235. Nagele E, Kuhn V, Vogt H, Link TM, Muller R, Lochmuller EM, et al. Technical considerations for microstructural analysis of human trabecular bone from specimens excised from various skeletal sites. *Calcif Tissue Int* 2004;75(1):15-22.

References

236. Rho JY, Tsui TY, Pharr GM. Elastic properties of human cortical and trabecular lamellar bone measured by nanoindentation. *Biomaterials* 1997;18(20):1325-30.
237. Katz JL, Meunier A. Scanning Acoustic Microscopy of human and canine cortical bone microstructure at high frequencies. *Stud Health Technol Inform* 1997;40:123-37.
238. Homminga J, Van-Rietbergen B, Lochmuller EM, Weinans H, Eckstein F, Huiskes R. The osteoporotic vertebral structure is well adapted to the loads of daily life, but not to infrequent "error" loads. *Bone* 2004;34(3):510-6.
239. Luo ZP, An KN. A theoretical model to predict distribution of the fabric tensor and apparent density in cancellous bone. *J Math Biol* 1998;36(6):557-68.
240. Tanck E, Homminga J, van Lenthe GH, Huiskes R. Increase in bone volume fraction precedes architectural adaptation in growing bone. *Bone* 2001;28(6):650-4.
241. Mosekilde L. Sex differences in age-related loss of vertebral trabecular bone mass and structure--biomechanical consequences. *Bone* 1989;10(6):425-32.
242. Weinans H. Is osteoporosis a matter of over-adaptation? *Technol Health Care* 1998;6(5-6):299-306.
243. Ketcham RA, Ryan TM. Quantification and visualization of anisotropy in trabecular bone. *J Microsc* 2004;213(Pt 2):158-71.
244. Flautre B, Hardouin P. Microradiographic aspect on iliac bone tissue in postmenopausal women with and without vertebral crush fractures. *Bone* 1994;15(5):477-81.
245. Compston JE. Connectivity of cancellous bone: assessment and mechanical implications. *Bone* 1994;15(5):463-6.
246. Banse X, Devogelaer JP, Lafosse A, Sims TJ, Grynepas M, Bailey AJ. Cross-link profile of bone collagen correlates with structural organization of trabeculae. *Bone* 2002;31(1):70-6.
247. Garnero P. Markers of bone turnover for the prediction of fracture risk. *Osteoporos Int* 2000;11 Suppl 6:S55-65.
248. Lereim P, Goldie I, Dahlberg E. Hardness of the subchondral bone of the tibial condyles in the normal state and in osteoarthritis and rheumatoid arthritis. *Acta Orthop Scand* 1974;45(4):614-27.
249. Fazzalari NL, Moore RJ, Manthey BA, Vernon-Roberts B. Comparative study of iliac crest and subchondral femoral bone in osteoarthritic patients [published erratum appears in *Bone* 1992;13(6):449]. *Bone* 1992;13(4):331-5.
250. Hu JH, Ding M, Soballe K, Bechtold JE, Danielsen CC, Day JS, et al. Effects of short-term alendronate treatment on the three-dimensional microstructural, physical, and mechanical properties of dog trabecular bone. *Bone* 2002;31(5):591-7.

Acknowledgements

I would like to dedicate this thesis to my parents; to my father who never got to see it and to my mother for always being there. I would also like to acknowledge the generosity of the families and tissue donors who made it possible to perform many of the studies in this thesis.

For my advisors; First, I would like to thank Harrie for being infinitely patient (well, most of the time) and for showing me that you can really do just about anything if you actually believe you can. Keep those bears out of the forest Harrie! Thanks to Jan Verhaar for always managing to bring a bit of the clinic up to the 16th floor. Thanks to Rick for always having time to provide both great advice and mentorship and for making sure that we could actually scan the enormous amount of material in this project. Also, thanks to Gerjo for always bringing the biology across the hall.

In Rotterdam, thanks to my “Paranimfen” Erwin and Holger who made going to work both a great place to learn and talk science (you too Black Jacq and Toonster) while making sure that I never lacked fun or new music. And of course I wouldn’t forget Arely; mmmmm tamales. There’s contender #1 for the title of Grillmeister, Ronald who always throws the BEST parties and contender #2 for Grillmeister, the Holgmeister who always imports the best sausages. I’d love to see the heavyweight title fight grill off, but I don’t think that there’s enough charcoal in Rotterdam. King, I hope that I manage to get you out of the “secure-zone” long enough for a visit but if not, we’ll have to hit the sauna. Migel, I’d love to get some table tennis lessons from you but I’m not sure I could afford the house repairs. At work, thanks to Jarno, Justus, Erik and Elian who inhabit the fun side of the lab. Thanks to Franci and Joopster for the fun on Schiedamseweg. Also from the lab Irene, Nicole, Wendy, Migiel, Olivier, and everybody else; thanks for making Erasmus a great place to work. And of course I wouldn’t forget the ex-pat network; John and Jen, Matt and Joanna and John D (you know who you are).

Thanks to the Aarhus gang: Ming, Ivan, Michel and Anders for getting me back into the field that I love. Also in Aarhus thanks to Annette and Jane for making sure that everything ran well in the lab, to Greg for always having a couch to sleep on and Appleton’s in the fridge (and don’t forget the full selection of videos for Saturday morning viewing), to Anja and Esben for making many dark winter nights hyggelig with red wine, candles and good food, and to Birgitte and Big M for making sure that I never ever left Aarhus without a full belly (full of ris-a-la-mand, ha ha!). Lucas, stay away from the snakes, crocodiles and spiders and close to Belinda.

In Chicago, thanks to Aladino for making sure there was always something to do, Eileen for fostering my latte addiction (look at the card, one more and we get a free one), and Renee for making a great city even better.

Acknowledgements

In Canada I'd like to make sure that my family all know that I love them (bonus points for coming to Legoland, ha ha). James and Ashley, thanks for making your house always feel like home to me, including my own "dirt corner." Thanks to Lorne, Bruce, Mike and Anaud for making sure that Canada was really home and that there is always a good jam to be had.

Publications

1. Hakulinen MA, **Day JS**, Toyras J, Timonen M, Kroger H, Weinans H, Kiviranta I, Jurvelin JS. Prediction of density and mechanical properties of human trabecular bone in vitro by using ultrasound transmission and backscattering measurements at 0.2-6.7 MHz frequency range. *Phys Med Biol* 21;50(8):1629-42 (2005).
2. Sierpowska J, Hakulinen MA, Töyräs J, **Day JS**, Weinans H, Jurvelin JS, Lappalainen R. Prediction of mechanical properties of human trabecular bone by electrical measurements. *Physiological Measurement* 26:S119-S131 (2005).
3. Beumer A, Campo MM, Niesing R, **Day J**, Kleinrensink GJ, Swierstra BA. Screw fixation of the syndesmosis: a cadaver model comparing stainless steel and titanium screws and three and four cortical fixation. *Injury*. 36(1):60-4 (2005).
4. Waarsing JH, **Day JS**, Weinans H. An improved segmentation method for in vivo microCT imaging. *Journal of Bone and Mineral Research* 19(10):1640-50 (2004).
5. **Day JS**, Ding M, Bednarz P, van der Linden JC, Mashiba T, Hirano T, Johnston CC, Burr DB, Hvid I, Sumner DR, Weinans H. Bisphosphonate treatment affects trabecular bone apparent properties through micro-architecture rather than matrix properties. *Journal of Orthopaedic Research* 22(3):465-71 (2004).
6. van der Linden JC, **Day JS**, Verhaar JAN, Weinans H. Altered tissue properties induce changes in cancellous bone architecture in aging and disease. *Journal of Biomechanics* 37(3):367-74 (2004).
7. **Day JS**, van der Linden JC, Bank RA, Ding M, Hvid I, Sumner DR, Weinans H. Adaptation of Subchondral Bone in Osteoarthritis. *Biorheology* 41(3-4):359-68 (2004).
8. Waarsing JH, **Day JS**, van der Linden JC, Ederveen AG, Spanjers C, De Clerck N, Sasov A, Verhaar JAN, Weinans H. Detecting and tracking local changes in the tibiae of individual rats: A novel method to analyse longitudinal in vivo micro-CT data. *Bone* 34(1):163-9 (2004)
9. Ding M, **Day JS**, Burr DB, Mashiba T, Hirano T, Weinans H, Sumner DR, Hvid I. Canine cancellous bone microarchitecture after one year of high-dose bisphosphonates. *Calcified Tissue International* 72(6):737-44 (2003)
10. van der Linden JC, **Day JS**, Verhaar JAN, Weinans H. Combinatie van computersimulaties en experimenten in botonderzoek. *Netherlands Journal for Calcium and Bone Metabolism* 1(2):31-38 (2003).
11. Hu JH, Ding M, Soballe K, Bechtold JE, Danielsen CC, **Day JS**, Hvid I. Effects of short-term alendronate treatment on the three-dimensional microstructural, physical, and mechanical properties of dog trabecular bone. *Bone* 31(5):591-7(2002).
12. Zhao J, **Day J**, Yuan ZF, Gregersen H. Regional arterial stress-strain distributions referenced to the zero-stress state in the rat. *American Journal of Physiology - Heart Circulatory Physiology* 282(2): H622-9(2002).
13. **Day JS**, Ding M, van der Linden, JC, Hvid I, Sumner DR, Weinans H. A decreased subchondral trabecular bone tissue elastic modulus is associated with pre-arthritic cartilage damage. *Journal of Orthopaedic Research* 19(5):914-8(2001).
14. **Day JS**, Ding M, Odgaard A, Sumner DR, Hvid I, Weinans H. Parallel plate model for trabecular bone exhibits a volume fraction-dependant bias. *Bone* 27(5):715-20(2000).
15. **Day JS**, Murdoch DJ, Dumas GA. Calibration of position and angular data from a magnetic tracking device. *Journal of Biomechanics* 33(8):1039-45(2000).
16. **Day JS**, Dumas GA, Murdoch DJ. Evaluation of a long-range transmitter for use with a magnetic tracking device in motion analysis. *Journal of Biomechanics* 31(10):957-61(1998).

Curriculum Vitae

- January 15, 1969 Born in Chatham, Ontario, Canada.
- 1988-1988 Grade 13 High School Diploma, Chatham Colligate Institute.
- 1992-1992 B.Sc., Mining Engineering, Queen's University.
- 1997-1997 M.Sc., Mechanical Engineering, Queen's University
- 2005-2005 Ph.D. Candidate, Erasmus Medical Center, Rotterdam, The Netherlands.
- 1998-1998 Research Assistant, Institute for Experimental Clinical Research, Aarhus, Denmark.
- 1999, 2002, 2003 Visiting Researcher, Department of Orthopedics, Department of Anatomy and Cell Biology, Rush University, Chicago, Illinois, USA.
- 1999, 2000 Visiting Researcher, Orthopaedic Research Laboratory, Aarhus Kommune Hospital, Aarhus, Denmark.
- Present Consulting engineer at Exponent (Failure Analysis Associates), Inc.